FINAL REPORT
AQRP Project 14-007

Analysis of VOC, NO2, SO2 and HCHO data from SOF, mobile DOAS and MW-DOAS during DISCOVER-AQ

Prepared for:

David Sullivan

Texas Air Quality Research Program, The University of Texas at Austin

Prepared by:

John Johansson[1], Johan Mellqvist[1], Pontus Andersson[1]

Barry Lefer[2], James Flynn[2] and Laura Judd[2]

[1] Earth and Space Science Chalmers University of Technology, Hörsalsvägen 11, SE-41296 Göteborg, E-mail: johan.mellqvist@chalmers.se

[2] Department of Earth and Atmospheric Sciences, University of Houston
4800 Calhoun Rd Houston, TX 77204-5007

July 2015

QA Requirements: Audits of Data Quality: 10% Required

Date: 2015-06-30

Title: Analysis of VOC, NO2, SO2 and HCHO data from SOF, mobile DOAS and MW-DOAS during DISCOVER-AQ

Authors: John Johansson, Johan Mellqvist, Pontus Andersson, Barry Lefer, James Flynn and Laura Judd

E-mail: johan.mellqvist@chalmers.se

Executive summary

In a previous project, mobile remote sensing measurements of atmospheric gas column measurements of sulfur dioxide (SO_2), nitrogen dioxide (NO_2), formaldehyde (HCHO) and Volatile Organic Compounds (VOCs) were carried out in a box around the Houston Ship channel (HSC), in parallel with flights by two aircraft from National Aeronautics and Space Administration (NASA). In this project the collected data was reanalyzed, improved and compared to other data, as part of the NASA DISCOVER-AQ (Deriving Information on Surface conditions from Column and Vertically Resolved Observations Relevant to Air Quality) experiment. The data were obtained using mobile optical remote sensing measurements by the Solar Occultation Flux (SOF) and Mobile Differential Optical Absorption Spectroscopy (DOAS) techniques, which were carried out in the Houston area during September 2013.

The DISCOVER-AQ campaign had the objective to demonstrate that geostationary satellites can provide useful environmental data. NASA operated a high altitude aircraft (B200) equipped with optical sensors, measuring columns of SO_2, NO_2, HCHO and aerosol profiles. To validate these measurements they also carried out in situ measurements with a low flying airplane (P3B) that did spirals above two ground stations in the Houston ship channel, equipped with optical (Pandora) and in-situ sensors.

During the 2013 field campaign a new VOC sensor was used to map ratios of the ground concentrations of alkanes and aromatic VOCs downwind of various industries. The sensor is an open path Differential Optical Absorption Spectroscopy (DOAS) system coupled to a custom made multiple-pass cell working in the ultraviolet (UV) region between 250-280 nm. In this project we have refined the spectral analysis for measurements of aromatic VOCs from this sensor and compared its data to parallel data from a proton transfer mass spectrometer (PTRMS) and canister sampling with subsequent Gas Chromatography-Flame Ionization Detector (GC-FID) analysis. The instrument shows a detection limit (1σ) of 0.3-1 ppb of for the Benzene, Toluene, Ethylbenzene and Xylene (BTEX) species. For a number of transects through plumes from real emission sources in the HSC, the ratio of time-integrated benzene concentrations measured by the Mobile White-cell DOAS (MW-DOAS) and a PTRMS operated by Montana State University was 1.00 on average, indicating very good agreement, while for toluene the PTRMS was 11% lower on average. In a corresponding experiment, canister sampling carried out downwind of several refineries in the Middle East and subsequent GC-FID analysis showed 32 % and 43 % lower values, respectively, for the same species compared to MW-DOAS. This will be further investigated. Ground data measured with MW-DOAS, downwind of a Texas City refinery shows that the BTEX to alkane mass rations were 0.10±0.04, corresponding to a mass emission 134 kg/h for the 2013 data. Here it is assumed that the aromatic VOCs and alkanes were well mixed in the emission plume at the measurement position. An additional uncertainty is the few amount of measurements carried out in 2013.

During the campaign, mobile remote sensing by the SOF method and Mobile DOAS were carried out in the Houston area on twenty days in September 2013 together with frequent balloon launches. During ten of these days, column measurements of SO_2, NO_2, HCHO and VOCs in a box around the Houston Ship channel were carried out synchronized with science flights by the NASA aircrafts. During the rest of the days more focused industrial measurements were carried out. The weather during the campaign was relatively poor with 4 good clear days, 10 moderate days and the rest rather cloudy.

A small measurement study was carried out in Sweden in September 2014 to investigate the effects of clouds on the Mobile DOAS measurements. During the course of this study, a so far undetected instrumental effect was discovered which was seen to affect the quality of evaluation negatively. A drift in instrumental lineshape was determined to be the cause of this and a method was developed to compensate for it. This method was successfully applied to the measurements during the DISCOVER-AQ campaign and was seen to improve spectral fit quality and give more stable baselines in some cases.

The measurement study also concluded that the changes in evaluated columns experienced due to clouds are most likely real changes in the actual column due to changes in radiative transfer rather than some form of spectral artifacts. Because of this, development of cloud indicator was determined to be the best way to deal with cloud effects. A cloud indicator based on the principle of a color index, a simple ratio between the spectral intensity at two different wavelengths, was developed and applied to the measurement series in order to allow more data to be used for flux calculations.

Multi-angle Mobile DOAS measurements performed during the last days of the DISCOVER-AQ campaign were evaluated using a new scheme designed to enable absolute columns to be derived. As part of this scheme radiative transfer simulations were performed using in-situ data from the airborne measurements in order to derive direction dependent differential air mass factors needed to convert the evaluated columns to absolute mixing layer columns. After some averaging and filtering, this data could be used to establish an absolute offset for the relative columns from the standard evaluation and control for baseline drift. This gave a better absolute column product that is suited for comparisons with other data from the DISCOVER-AQ campaign.

Table 1 was shows the final emission rates for the 2013 campaign together with corresponding results from previous studies and reported annual routine emissions from the STARS (State of Texas Air Reporting System) emission inventory for 2013.

Table 1 Emission fluxes (kg/h) measured with SOF and Mobile DOAS for different sites, as reported after the measurement campaign. Results from earlier campaigns and Emission inventory data for 2013 [Johansson, 2014b] are also shown.

Area	Species	2006	2009	2011	2013	2013Emission Inventories
HSC	Ethene	878 ± 152	614 ± 284	612 ± 168	475 ± 79	53
	Propene	1511 ± 529	642 ± 108	$563 \pm 294*$	394 ± 245	48
	Alkanes	12276 ± 3491	10522 ± 2032	11569 ± 2598	13934 ± 4321	818
	SO_2	2277 ± 1056	3364 ± 821	2329 ± 466	1683 ± 223	1153
	NO_2	2460 ± 885	-	1830 ± 330	2242 ± 684	1103
Mont Belvieu	Ethene	443 ± 139	444 ± 174	545 ± 284	271 ± 33	29
	Propene	489 ± 231	303 ± 189	$58*$	220 ± 115	21
	Alkanes	874	1575 ± 704	1319 ± 280	$2854 \pm 1212**$	146
	NO_2	-	168 ± 39	305 ± 29	245 ± 102	138
Texas City	Ethene	83 ± 12	122 ± 41	177 ± 48	-	2
	Propene	ND	54 ± 22	$56 \pm 9*$	-	4
	Alkanes	3010 ± 572	2422 ± 288	2342 ± 805	1340 ± 140	276
	SO_2	-	834 ± 298	1285 ± 428	414 ± 172	128
	NO_2	460 ± 150	283 ± 30	492 ± 71	408 ± 93	331

* Propene retrievals were of poor quality throughout much of this campaign

** Only a single day of measurements with variable emissions.

Table of Contents

1. Introduction

A measurement study was carried out in Greater Houston during September 2013, in close coordination with the DISCOVER-AQ mission in Houston, organized by the NASA. The aim was to carry out measurements of columns of VOCs, SO_2, NO_2, and formaldehyde in the Houston Ship channel in parallel with aircraft measurements during DISCOVER-AQ. A second aim was to study direct emissions of the above-mentioned species from refineries and petrochemical industries in the area, to provide support data for ozone modeling. The primary methods used were Solar Occultation Flux (SOF) and Mobile Differential Optical Absorption Spectroscopy (DOAS). As an extra feature two additional instruments, i.e. Mobile extractive Fourier-Transfer Infra-Red spectrometry (meFTIR) and Mobile White-cell Differential Optical Absorption Spectroscopy (MW-DOAS), mapping ground concentrations of alkanes and aromatic VOCs, were added to the project.

The background to study VOC emissions in this project is that earlier measurements in the TexAQS 2006 campaign [Mellqvist 2007, 2008b, 2010; Rappenglück 2008a, 2008b; De Gouw 2009; Wert 2003; Ryerson 2003] showed high alkene and alkane emissions from the industrial areas in the vicinity of Houston as well occasional large plumes of formaldehyde [Rivera 2009a, 2009b; Rappenglück 2008a; Buhr 2006]. The VOC measurements were 5–10 times higher than inventory values and studies show that this has impact on the tropospheric ozone production. Similar discrepancies, between inventories and were again found during the 2009 FLAIR (Formaldehyde and alkenes from Large Industrial Releases) study [Mellqvist 2009] and in a 2011 AQRP study [Johansson 2011, Johansson 2014b].

During the NASA DISCOVER-AQ campaign, column measurements of VOCs, NO_2, SO_2 and HCHO were carried out in a box around the Houston Ship channel with SOF and Mobile DOAS during 10 days in parallel with flight measurements from two aircraft. On non-flight days SOF and Mobile DOAS measurements were carried out to study industrial emissions for instance in Mt Belvieu and Texas City.

The DISCOVER-AQ (Deriving Information on Surface conditions from Column and Vertically Resolved Observations Relevant to Air Quality) campaign has the objective to demonstrate that geostationary satellites can provide useful environmental data. DISCOVER-AQ will seek answers to three major research questions: 1) how well the column and surface observations O_3, NO_2 and HCHO correlate and on what spatial scale information about these variables is needed to interpret column measurements 2) how do column and surface observations differ in their diurnal variation? 3) What are typical gradients in key variables at scales finer than current satellite and model resolutions?

The Mobile DOAS and SOF data accumulated in this study in particular will help in task 1 and 3.

2. Methods

The main methods used in this project were the two optical remote sensing methods, i.e. the SOF to measure emissions of VOCs (alkenes and alkanes) and Mobile DOAS to measure formaldehyde, NO_2 and SO_2. In addition a Mobile extractive FTIR (MeFTIR) system was used together with an experimental Mobile White cell DOAS (MW-DOAS) to try to quantify aromatic-to-alkane ratios in VOC plumes. Meteorological measurements were obtained from Global Positioning System (GPS) sondes and Continuous Air Monitoring Stations (CAMS) operated by TCEQ (Texas Commission on Environmental Quality). The instruments were operated from the bed and backseat of a van powered by a small diesel generator. The instruments were cooled by an air conditioner, Figure 1.
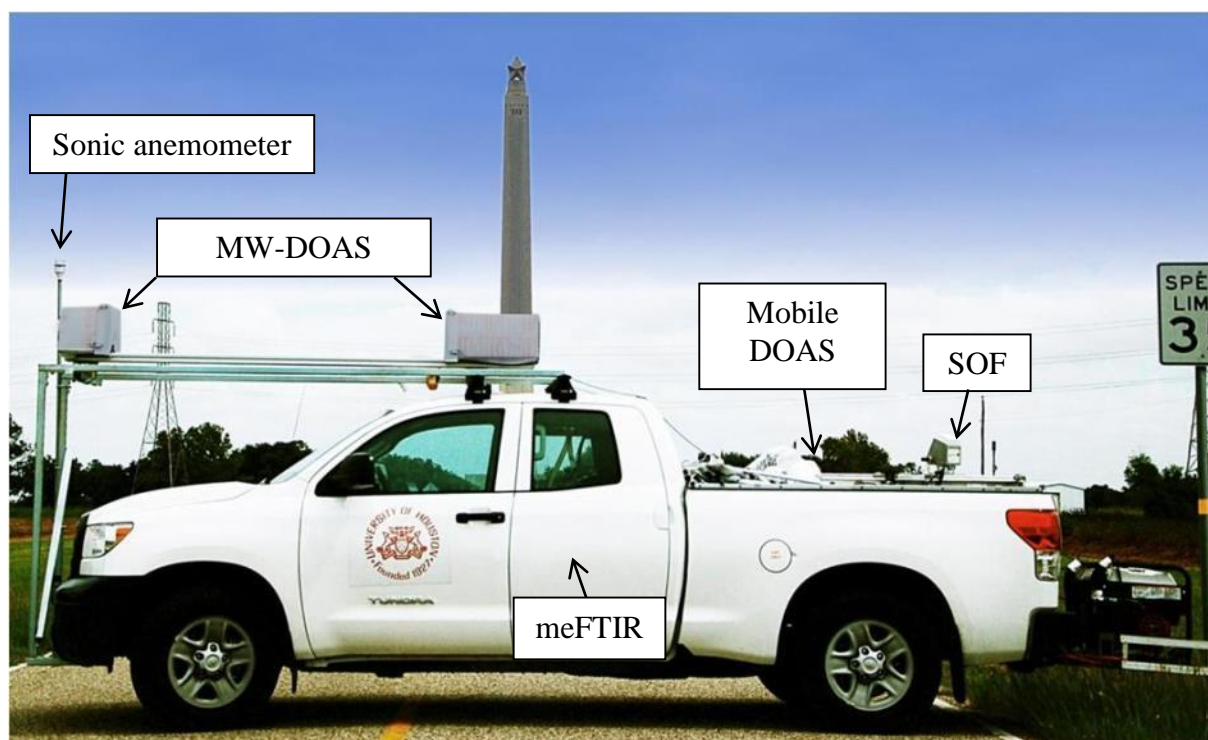

Figure 1 The measurements vehicle used.

Figure 2 The SOF system. The solar tracker (front left) transmits the solar light into the infrared spectrometer (mid right with a GPS on top) independent of the vehicle's position.

2.1 The SOF method

2.1.1 General

The Solar Occultation Flux (SOF) method was developed from a number of different research projects in the end of 1990's [Mellqvist 1999a, 1999b; Galle 1999]. The method utilizes the sun as the light source and gas species that absorb in the infrared portion of the solar spectrum are measured from a mobile platform.

The method is today used to screen and quantify VOC emissions from industrial conglomerates down to sub-areas in individual plants.

The SOF method has been applied in several larger campaigns in both Europe and the US and in more than 45 individual plant surveys over the last 7 years. In the various campaign studies it has been found that the measured emissions obtained with SOF are 5–10 times higher than the reported emission obtained by calculations. For instance in a recent study in Houston, TexAQS 2006, it was shown that the industrial releases of alkenes for the Houston Galveston area, on average, were 10 times higher than what was reported [Mellqvist 2010]. These results were supported by airborne measurements [De Gouw 2009]. For alkanes the discrepancy factor was about 8 [Mellqvist 2007]. In a similar study for the conglomerate of refineries and oil storage in the Rotterdam harbor during 2008 [Mellqvist 2009a], a discrepancy factor of 4.4 was found between the alkane measurements and the reported VOC emission values, with individual sites varying between a factor of 2–14. A SOF study was also carried out in France during 2008 for which large discrepancies were obtained. Also for Swedish refineries the emissions can be considerably higher than calculations and the measurements show that the VOC emissions typically correspond to 0.03–0.09 % of their throughput of oil, with more than half of the emissions originating from oil and product storage [Kihlman 2005a, 2005b].

2.1.2 Details of the method

The SOF method is based on the recording of broadband infrared spectra of the sun with a Fourier transform infrared spectrometer (FTIR) that is connected to a solar tracker. The latter is a telescope that tracks the sun and reflects the light into the spectrometer independent of its position. From the solar spectra it is possible to retrieve the path-integrated concentration (column, see Eq. 1) in the unit mg/m^2 of various species between the sun and the spectrometer. In Figure 1 a measurement system is shown built into a van. The system consists of a custom built solar tracker, transfer optics and a Bruker EM27 FTIR spectrometer with a spectral resolution of 0.5 cm^{-1}, equipped with a combined MCT (mercury cadmium telluride) detector or an InSb (indium antimonide) detector. Optical filters were used to reduce the bandwidth when conducting alkene and alkane measurements.
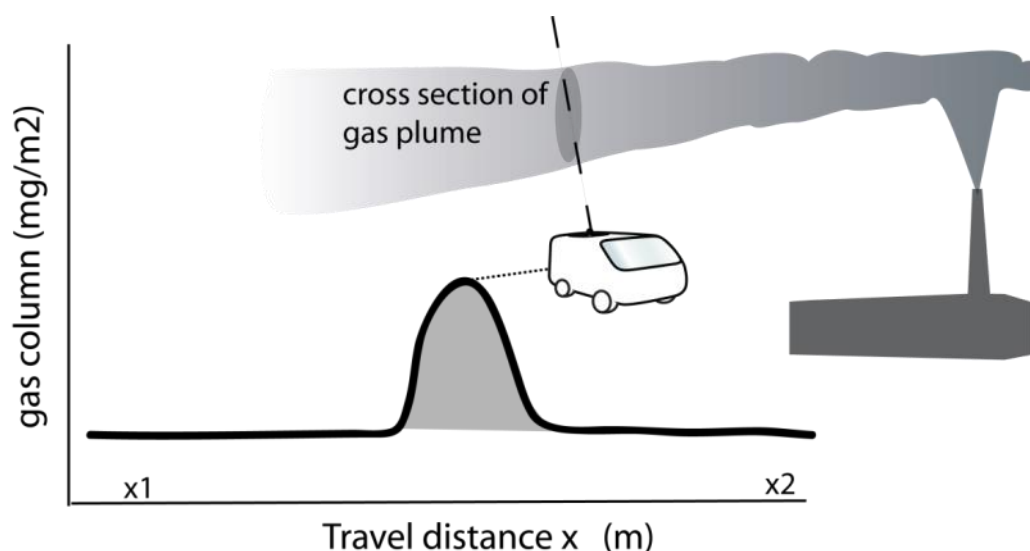
Figure 3 Illustration of the SOF measurements.

To obtain the gas emission from a source, the car is driven in such way that the detected solar light cuts through the emission plume. This is illustrated in Figure 3 To calculate the gas emission the wind direction and speed is also required and these parameters are usually measured from high masts and towers.

The spectral retrieval is performed by a custom software, QESOF [Kihlman 2005b], in which calibration spectra are fitted to the measured spectra using a nonlinear multivariate fitting routine. Calibration data from the High-resolution Transmission molecular absorption database (HITRAN)[Rothman 2003] are used to simulate absorption spectra for atmospheric background species at the actual pressure, temperature and instrumental resolution of the measurements. The same approach is applied for several retrieval codes for high resolution solar spectroscopy [Rinsland 1991; Griffith 1996] and QESOF has been tested against these with good results. For the retrievals, high resolution spectra of ethene, propene, propane, n-butane, n-octane and other VOCs (e.g. isobutene, 1,3-butadiene) were obtained from the PNL (Pacific Northwest Laboratory) database [Sharpe 2004]. These are degraded to the spectral resolution of the instrument by convolution with the instrument lineshape. The uncertainty in the absorption strength of the calibration spectra is about 3.5 % for the five species.

During the campaign the SOF system was operated in two parallel optical modes, one for alkenes and one for alkanes. The former mode was specifically targeted at ethene and propene and these species were retrieved simultaneously in the wavelength region between 900 and 1000 cm^{-1}, taking into account the interfering species water, carbon dioxide (CO_2) and ammonia. Ethene is also evaluated separately from propene over a shorter wave number interval. In Figure 4 solar spectra corresponding to a measurement downwind of an industrial facility in Longview are shown. The solar spectra were measured both outside and inside the emission plume. In addition spectral fits of ethene and propene are shown obtained using the QESOF spectral retrieval algorithm. The fit shown here was evaluated between 900 cm^{-1} and 1000 cm^{-1} to show both ethene and propene.

The alkane optical mode corresponds to measurements in the infrared region between 3.3–3.7 µm (2700–3005 cm^{-1}), using the vibration transition in the carbon and hydrogen bond (CH-stretch). The absorption features of the different alkanes are similar and interfere with each

other, but since the number of absorbing C-H-bonds is directly related to the molecule mass, the total alkane mass can be retrieved despite the interference. In the analysis we therefore use calibration spectra of propane, n-butane, and n-octane and fit these to the recorded spectra, using a resolution of 8 cm^{-1}. Aromatics and alkenes also have absorption features in the CH-stretch region, but mainly below 3.33 μm for the most abundant species. A sensitivity study of the SOF alkane retrieval was made for the TexAQS 2006 [Mellqvist 2007], taking into account the typical matrix of VOCs, and this study showed that total alkane mass obtained by the SOF was overestimated by 6.6 %. Here we assume the same uncertainty.
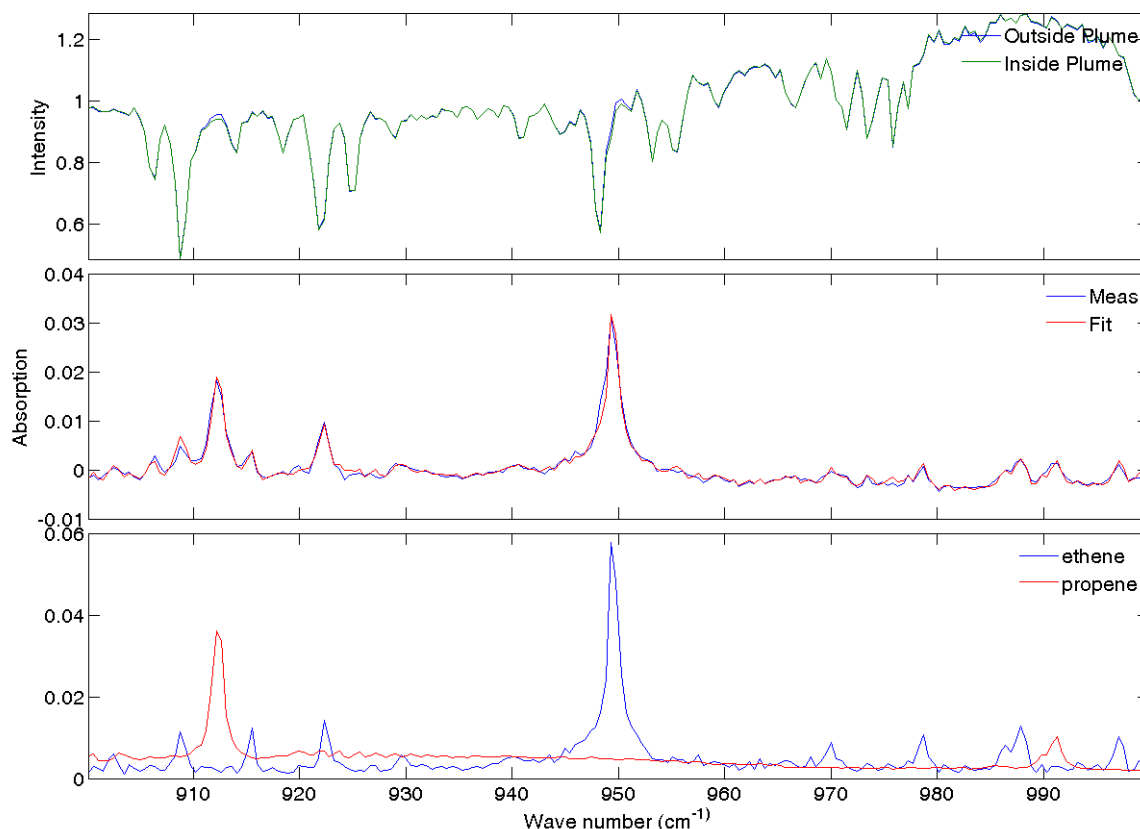

Figure 4 Solar spectra measured outside and inside the emission plume of an industrial plant in arbitrary intensity units (upper). Measured and fitted spectral evaluation for ethene and propene (calibrated spectra, lower) using the QESOF spectral retrieval algorithm is also shown (middle).

2.1.3 Flux calculation

To obtain the gas emission from a target source, SOF transects, measuring vertically integrated species concentrations, are conducted along roads oriented crosswind and close downwind (0.5–3 km) of the target source so that the detected solar light cuts through the emission plume as illustrated in Figure 2. The gas flux is obtained first by adding the column measurements and hence the integrated mass of the key species across the plume is obtained. To obtain the flux this value is then multiplied by the mass average wind speed of the plume, u'_{mw}. The flux calculation is shown in Eq. 1. Here, **x** corresponds to the travel direction, **z** to the height direction, **u'** to the wind speed orthogonal to the travel direction (x), **u'$_{mw}$** to the mass weighted average wind speed and **H$_{mix}$** to the mixing layer height. The slant angle of the sun is compensated for, by multiplying the concentration with the cosine factor of the solar zenith angle.

$$flux = \int_{x1}^{x2}\left(\int_{0}^{Hmix} conc(z) \cdot u'(z) \cdot dz \right) dx = u'_{mw} \int_{x1}^{x2} column(x) \qquad \text{(Eq. 1)}$$

$$\text{where} \quad u'_{mw} = \frac{\int^{Hmix} conc(z)u'(z) \cdot dz}{\int_{o}^{Hmix} conc(z)dz} \quad \text{and} \quad column = \int_{0}^{Hmix} conc(z) \cdot dz$$

The wind is not straightforward to obtain since it is usually complex close to the ground and increases with the height. The situation is helped by the fact that SOF measurements can only be done in sunny conditions. This is advantageous since it corresponds to *unstable meteorological conditions* for which wind gradients are smoothed out by convection. Over relatively flat terrain with turbulence inducing structures the mean wind varies less than 20 % between 20 and 100 m height using standard calculations of logarithmic wind. This is illustrated for the harbor of Göteborg in Figure 5. Here the average daytime wind velocity and wind direction profile for all sunny days during August of 2004 have been simulated [Kihlman 2005a] using a meteorological flow model denoted TAPM [Hurley 2005].

In addition, for meteorological conditions with considerable convection, the emission plume from an industry mixes rather quickly vertically giving a more or less homogeneous distribution of the pollutant versus height through the mixing layer even a few kilometers downwind. In addition to the atmospheric mixing, the plumes from process industries exhibit an initial lift since they are usually hotter than the surrounding air.

The rapid well-mixed assumption agrees with results from airborne measurements made by NOAA (National Oceanic and Atmospheric Administration) [De Gouw 2009] and Baylor University [Buhr 2006] during the TexAQS 2006 in which also SOF measurements were conducted [Mellqvist 2010]. The NOAA measurements indicate that the gas plumes from the measured industries mix evenly from the ground to 1000 m altitude, i.e. throughout the entire mixing layer, within 1000–2000 s (~25 min) transport time downwind the industrial plants. This indicates a vertical mixing speed of the plume between 0.5 to 1 m/s. This is further supported by Doppler LIDAR (Light Detection And Ranging) measurements by NOAA showing typical daytime vertical mixing speeds of ±(0.5–1.5) m/s [Tucker 2007].
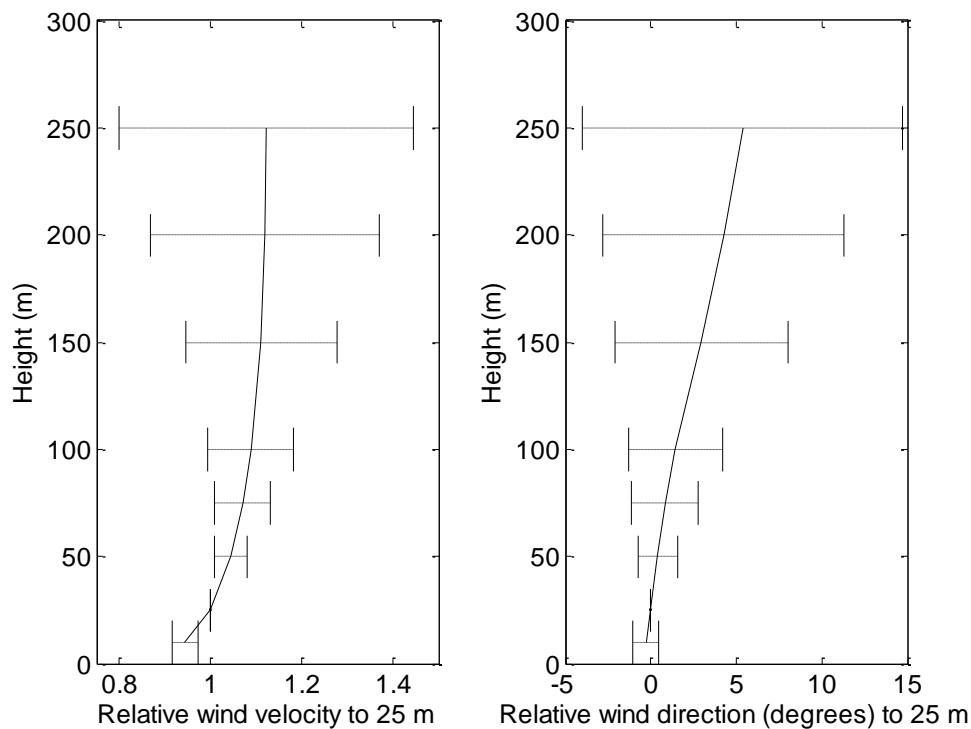
Figure 5 Average daytime wind velocity and wind direction profile retrieved by simulation above Göteborg harbor area averaged over all sunny days during a month with a wind-speed of 3–6 m/s at ground. The error bars indicate standard deviation between daily averages [Kihlman 2005a].

In this study, the measurements were conducted downwind of the industries at a typical plume transport time of 100–1000 s. According to the discussion above this means that the emission plumes have had time to mix up to heights of several hundred meters above the ground, above the first 50–100 m where the wind is usually disturbed due to various structures. For this reason we have used the average wind from 0 to 500 m height in the flux calculations. In this study the wind was obtained from wind profiles measured by radar profiler at the La Porte airport, GPS balloon sondes from Lynchburg ferry crossing in the HSC. Additionally, we used wind data from three TCEQ CAMS sites near the study areas, adjusted to be comparable to the GPS wind balloons, since the wind measurements close to the ground are systematically lower. Note that it only affects the wind speed very little if the 0–100, 0–200 or 0–500 m wind is chosen.

Figure 6 shows a real measurement example illustrating the principle for the SOF and Mobile DOAS measurements. Here a measurement of alkanes, a transect across the plume downwind of a refinery, is shown. The measured gas column of alkanes in the unit mass/area (mg/m2), as measured by the SOF in the solar light, is plotted versus distance across the plume. The wind was measured simultaneously by a Global Positioning System (GPS) tracking weather balloon, in the vicinity of the measurement as shown in Figure 7 and the 0–200 m value corresponds to 7.9 m/s, while the 0–500 value corresponds to 8.4 m/s. In the flux calculation the columns are integrated across the transect, whereby the integrated mass in unit mass per length unit in the plume (mg/m) is obtained. This value corresponds to an average column value of 48 mg/m2 across the whole transect, over 1300 m. This mass value is then multiplied by the wind speed, to obtain mg/s.
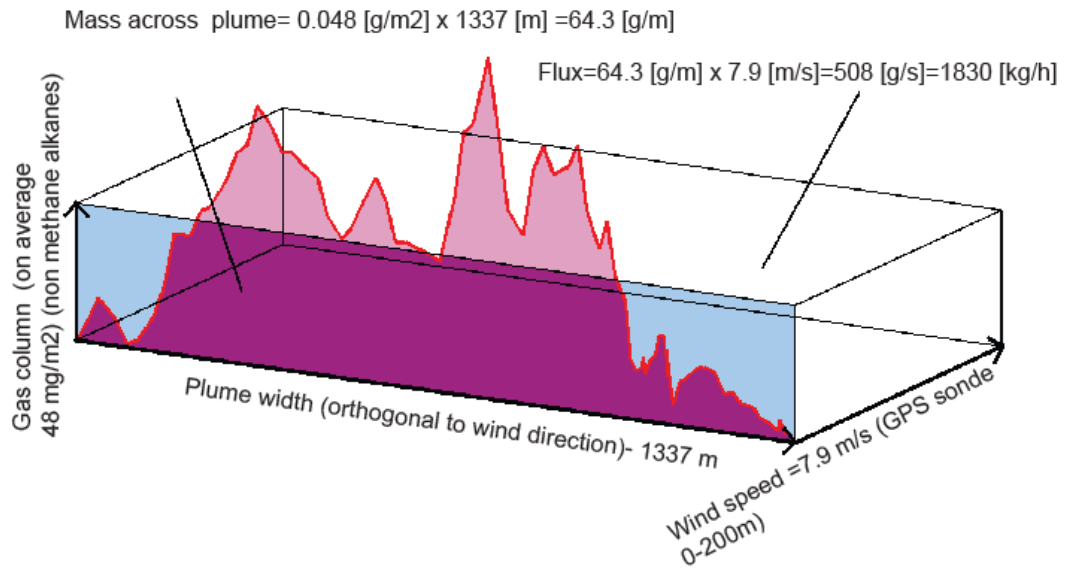
Figure 6 Illustration of the flux calculation in the SOF method for a measurement of alkanes conducted downwind of a refinery. The gas column of alkanes, retrieved from the spectra, is plotted versus distance. In the flux calculation the gas columns are integrated along the measurement transect, corresponding to the lilac area. This area, which is the integrated mass of the plume, corresponds to the same mass as an average column of 48 mg/m^2 integrated along the transect of 1337 m. The integrated mass is then multiplied with the wind speed yielding the flux in mass per seconds. Here an average wind speed from ground to 200 m was used corresponding to 7.9 m/s obtained from the GPS sonde in Figure 7.
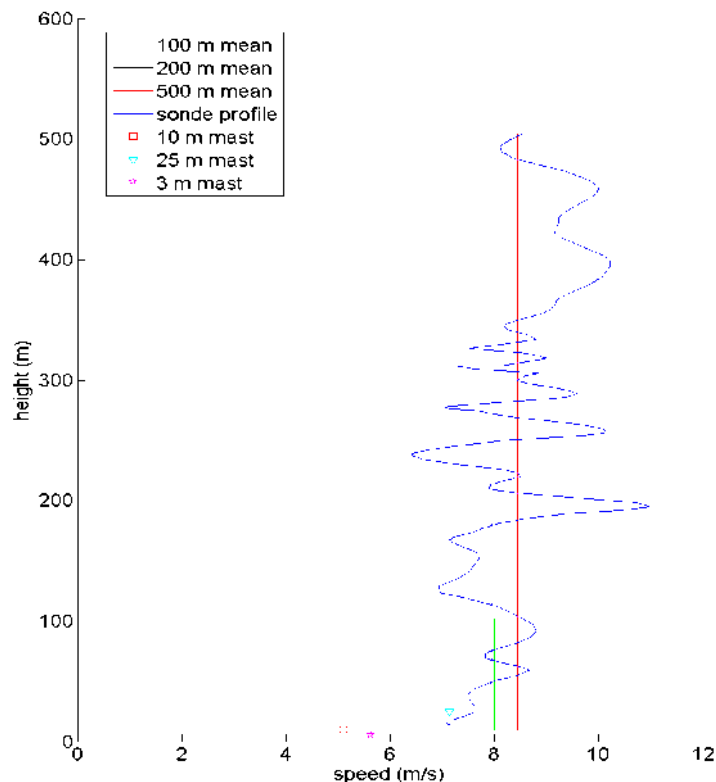

Figure 7 Wind profile measured with a GPS sonde less than ten minutes after the alkane transect shown in Figure 6 above. The wind speed versus height is shown for the balloon measurements in addition to the 0–500 and the 0–200 m average values, and values for several masts at the refinery.

To verify that a measured flux is originating from a specific area upwind of where the emission was detected, another measurement transect needs to be performed upwind of that

area to make sure that the emission is not coming from another source further away. If no significant flux is detected on the upwind side, this measurement does not need to be repeated for every downwind transect. If a smaller flux is measured on the upwind side than on the downwind side, the emission from the area in between is the difference between these fluxes. In this case the upwind transect needs to be repeated with every downwind transect. This type of emission measurements is preferably avoided since it might increase the uncertainty. Upwind measurements were performed for all areas during the study, but they are not presented in the result chapter.

2.2 Mobile DOAS

2.2.1 General

Mobile DOAS (Differential Optical Absorption Spectroscopy) measurements of scattered solar light in zenith direction were carried out in parallel with the SOF measurements, from the same vehicle, in order to measure formaldehyde, NO_2 and SO_2. DOAS works in the UV and visible wavelength region while SOF works in the infrared region and hence there are large differences in spectroscopy and in the used spectrum evaluation methods. However, both methods measure vertical columns which are integrated along measurement transects and multiplied by the wind to obtain the flux. The principle of flux-measurements using Mobile DOAS is hence the same as for SOF, section 2.1.3, although it is not necessary to compensate for any slant angle observations since the telescope is always pointing towards zenith. The DOAS system also works under cloudy conditions in contrast to SOF, although the most precise measurements are conducted in clear sky.

The DOAS method was introduced in the 1970's [Platt 1979] and has since then become an increasingly important tool in atmospheric research and monitoring both with artificial light sources and in passive mode utilizing the scattered solar light. In recent time the multi axis DOAS method (scanning passive DOAS) has been applied in tropospheric research for instance measuring formaldehyde [Heckel 2005]. Passive DOAS spectroscopy from mobile platforms has also been quite extensively applied in volcanic gas monitoring [Galle et al., 2002] for SO_2 flux measurements and for mapping of formaldehyde flux measurements in megacities [Johansson 2009]. Mobile DOAS has only been used to a limited extent for measurements of industries; Rivera et al. [2009b] did SO_2 measurements on a power plant in Spain for validation purposes, showing agreement with continuous emission measurements within 7% on average for 47 flux measurements over 3 days. They also made measurements at an industrial conglomerate in Tula in Mexico [Rivera 2009c] and measurements of SO_2, NO_2 and HCHO during the TexAQS 2006 campaign [Rivera 2010]. There are also groups in both China and Spain working with mobile mini DOAS.

2.2.2 Details of the method

The Mobile DOAS system used in this project, shown in Figure 8 and Figure 9, has been developed for airborne surveillance of SO_2 in ship plumes [Mellqvist 2008a, Johansson 2014a] but has for this project been modified to also measure HCHO and NO_2. It consists of a UV spectrometer (ANDOR Shamrock 303i spectrometer, 303 mm focal length, 300 μm slit) equipped with a CCD (charge-coupled device) detector (Newton DU920N-BU2, 1024 by 255 pixels, thermoelectrically cooled -70ºC). The spectrometer has wavelength coverage of 309 to 351 nm and a spectral resolution of 0.63 nm (1800 grooves/mm holographic grating). The spectrometer is connected to a quartz telescope (20 mrad field of view, diameter 7.5 cm) via

an optical fiber (liquid guide, diameter 3 mm). An optical band pass filter (Hoya) is used to prevent stray light in the spectrometer by blocking wavelengths longer than 380 nm.
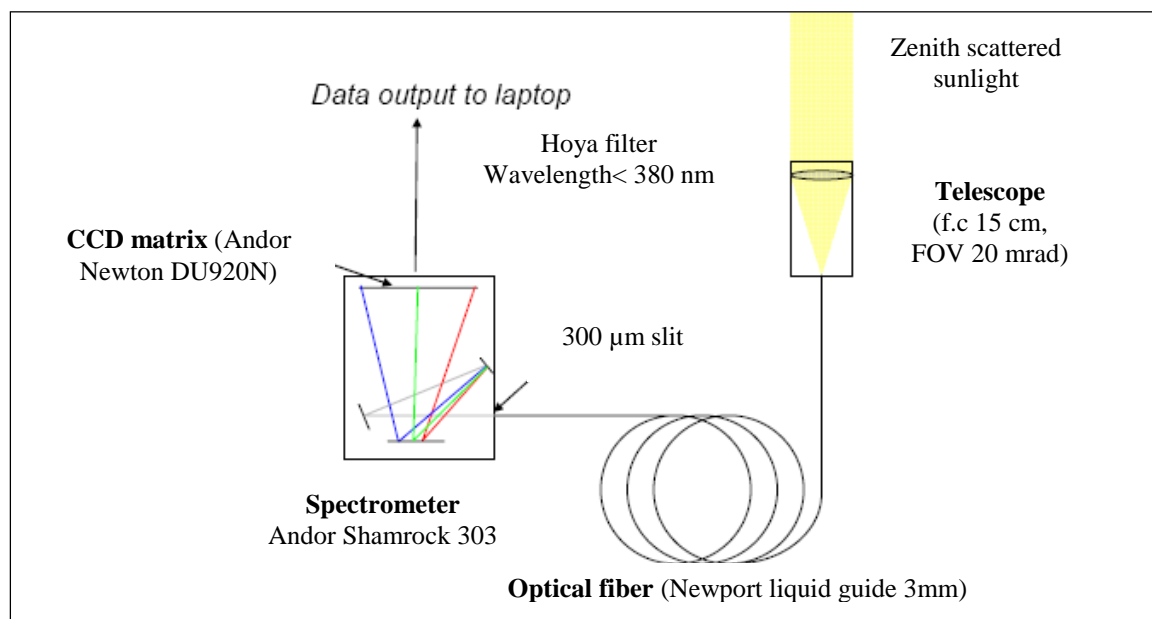

Figure 8 Overview of the Mobile DOAS system used. Scattered solar light is transmitted through a telescope, and an optical fiber to a UV/visible spectrometer. From the measured spectra the amount of HCHO, NO_2 and SO_2 in the solar light can be retrieved.

The DOAS system measures ultraviolet spectra in the 308–352 nm spectral region from which total columns of HCHO, NO_2 and SO_2 can be retrieved, Figure 10. HCHO and NO_2 are retrieved between 324 to 350 nm, together with the interfering species O_3, O_4 and SO_2. SO_2 and O_3 is then retrieved between 310 to 324 nm together with the NO_2 and HCHO columns obtained from the previous retrieval at 324–350 nm, Figure 11.

In the spectral evaluation the recorded spectra along the measurement transect are first normalized against a reference spectrum recorded upwind of the industry of interest. In this way most of the absorption features of the atmospheric background and the inherent structure of the sun is eliminated. Ideally the reference spectrum is expected not to include any concentration above ambient of the trace species of interest, however in urban and industrial areas this is difficult to achieve, and therefore our measurement in this case will produce the difference in vertical columns between the reference spectrum and all measured spectra across the plume for every measurement series. The normalized spectra are further high pass filtered according the algorithms proposed by Platt and Perner [1979], and then calibration spectra are scaled to the measured ones by multivariate fitting. Here we have used a software package denoted QDOAS [Van Roozendael 2001] developed at the Belgian Institute for Space Aeronomy (BIRA/IASB) in Brussels.

The calibration spectra used here for the various gases are obtained from the following: HCHO [Cantrell 1990], NO_2 [Vandaele 1998], SO_2 [Bogumil 2003], O_3 [Burrows 1999] and O_4 [Hermans 1999]. In addition to these calibration spectra it is also necessary to fit a so called Ring spectrum, correcting for spectral structures arising from inelastic atmospheric scattering [Fish 1995]. The Ring spectra used have been synthesized with a component of the QDOAS software, which uses a high resolution solar spectrum to calculate the spectrum of Raman scattered light from atmospheric nitrogen and oxygen, convolves this spectrum and the high resolution solar spectrum with the instrument lineshape and calculate the ratio

between them. One problem with the acquired spectra is the fact that the wavelength scale of the spectrometer was variable with shifts in the wavelength scale for the individual spectra. Even though these shifts were minute, within 0.02 nm, they still cause large residuals when normalizing the spectra to the reference spectrum. To overcome this we have used the QDOAS program, to characterize the wavelength calibration of the spectra by comparing the positions of the solar absorption lines with a high-resolved solar spectrum. This improved the results quite considerably. An example of a fit can be seen in Figure 10 in which a calibration spectrum of formaldehyde has been fitted to the measured differential absorbance. This differential spectrum corresponds to a high pass filtered atmospheric spectrum with the features of ozone, NO_2 and spectrum of inelastic atmospheric scattering removed. This spectrum was measured south west of the HSC and corresponds to $3.8 \cdot 10^{16}$ molecules/cm^2 as can be seen in Figure 10.
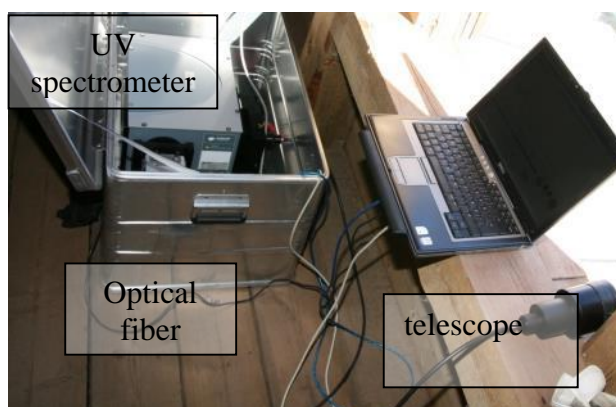
Figure 9 The Mobile DOAS system consisting of a UV spectrometer, optical fiber and UV telescope.
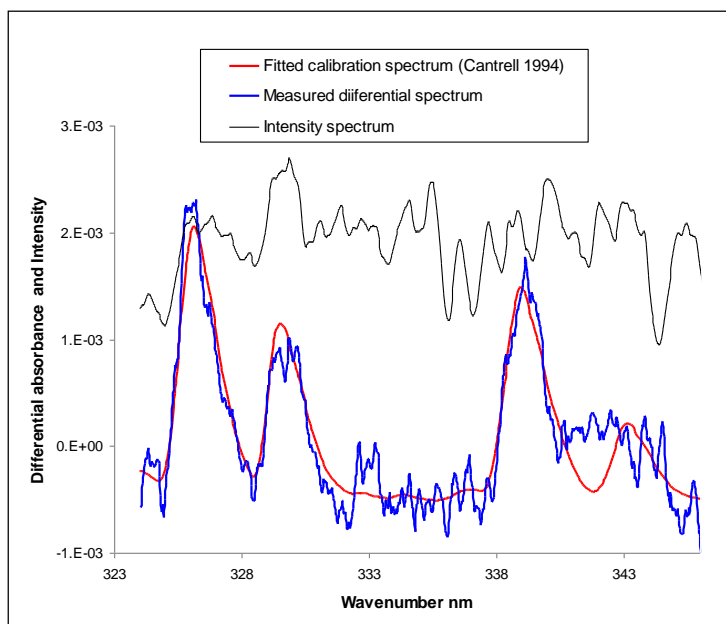
Figure 10 Ultraviolet spectrum (Intensity counts versus wavelength) measured south west of HSC by the Mobile DOAS system on May 20 2009, 10:40, adapted from Mellqvist 2010. From this spectrum a formaldehyde column of $3.8 \cdot 10^{16}$ molecules/cm^2 was derived by fitting a calibration spectrum to the measured high pass filtered absorbance (after subtraction of ozone, NO_2 and inelastic atmospheric scattering).
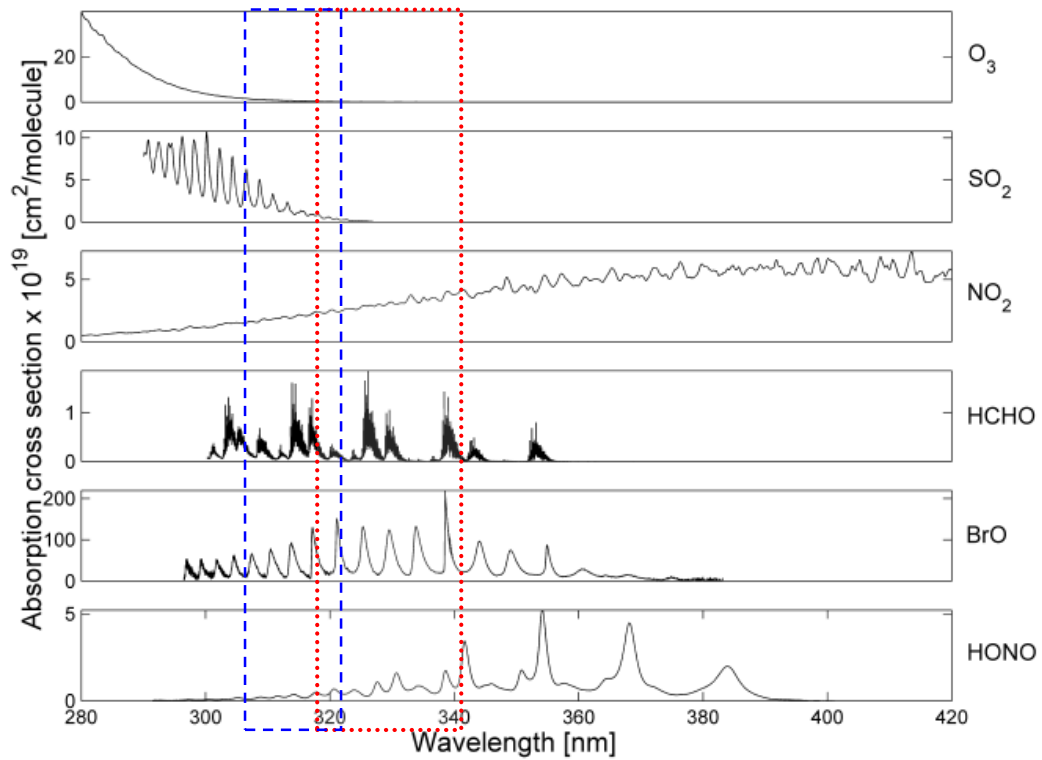
Figure 11 Absorption features of formaldehyde and some other interfering species of relevance are shown. The two wavelength regions applied for the retrieval of HCHO (red) and NO₂ (red) and SO₂ (blue), respectively, indicated by the colored rectangles. The above species were retrieved simultaneously, together with oxygen dimer (O₄) and a zenith sky spectrum and a so called ring spectrum.

2.3 Mobile extractive FTIR

In addition to the SOF and Mobile DOAS measurements, a Mobile extractive FTIR (MeFTIR) system, [Samuelsson 2005a; Galle 2001], was used together with the MW-DOAS described below measuring ground concentrations of mainly ethene, propene, alkanes, and methane. In contrast to the line integrating methods SOF and DOAS, MeFTIR measures the concentration in one mobile point. The meFTIR was not included in the main project and only a few results will be presented.

The extractive FTIR system contains a spectrometer of the same type used for the SOF system, Bruker IRCube, but utilizes an internal glow bar as an infrared radiation source instead of the sun, and transmits this light through a measurement cell. The spectrometer was connected to an optical multi-pass cell (Infrared Analysis Inc.) operated at 40 m path-length, and the transmitted light was detected simultaneously with an InSb-detector (indium antimonide) in the 2.5–5.5 μm (1800–4000 cm^{-1}) region and a MCT (mercury cadmium telluride) detector in the 8.3–14.3 μm (700–1200 cm^{-1}) region . Temperature and pressure averages in the cell were integrated over the cycle of each spectrum. Atmospheric air was continuously pumped with high flow through the optical cell from the outside, taking the air in from the roof of the van through a Teflon tube. A high flow pump was used to ensure that the gas volume in the cell was fully replaced within a few seconds. Spectra were subsequently recorded with an integration time of typically 10 seconds. A GPS-receiver was used to register the position of the van every second. The concentration in the spectra was analyzed online, fitting a set of calibration spectra based on the Hitran2000 infrared database (updated to the 2007 edition) [Rothman et al. 2003] and the PNL database [Sharpe 2004] in a least-squares fitting routine [Griffith 1996]. Since the MeFTIR system was an add-on and not included in the project only a few examples are shown here.

The MeFTIR system is used in the emission plume together with tracer gas releases at the emission source, in order to quantify the emission. This way, emissions for a total tank filling cycle or ship loading procedure can be determined. The method has also been deployed for flare efficiency analysis and methane emissions

Figure 12 The MeFTIR instrument used in parallel with the SOF system during the campaign. The gas is extracted into the White-cell where it is analyzed by infrared absorption measurements. The residence time in the gas cell, and hence the measurements time resolution, is a few seconds.

2.4 Mobile White Cell DOAS (MW-DOAS)

Measurements of aromatic VOCs were carried using a custom built multi-reflection cell (so called White cell) connected to an ultraviolet (UV) lamp (Xe) and a grating spectrometer (Andor) using optical fibers. The White cell is shown in Figure 13 and Figure 1 . The open White Cell a is based upon an optical configuration described by [Doussin, 1999] and a total of 84 reflections with 2.5 m basepath are obtained yielding a total light path of 210 m. The mirrors are coated with high reflective coating (r>99.7%). Wavelength calibration was carried out using a hollow cathode lead (Pb) lamp. The measurements are carried out in the wavelength region 250-285 nm and analyzed using the DOAS (Differential Optical Absorption Spectroscopy) retrieval principle using custom software and QDOAS. Several aromatic compounds exhibit strong absorption lines in the measured wavelength region. The calibration cross sections for benzene, toluene and p-xylene were from Fally [2009] and the cross sections for styrene and trimethylbenzene were from Etzkorn [1999].
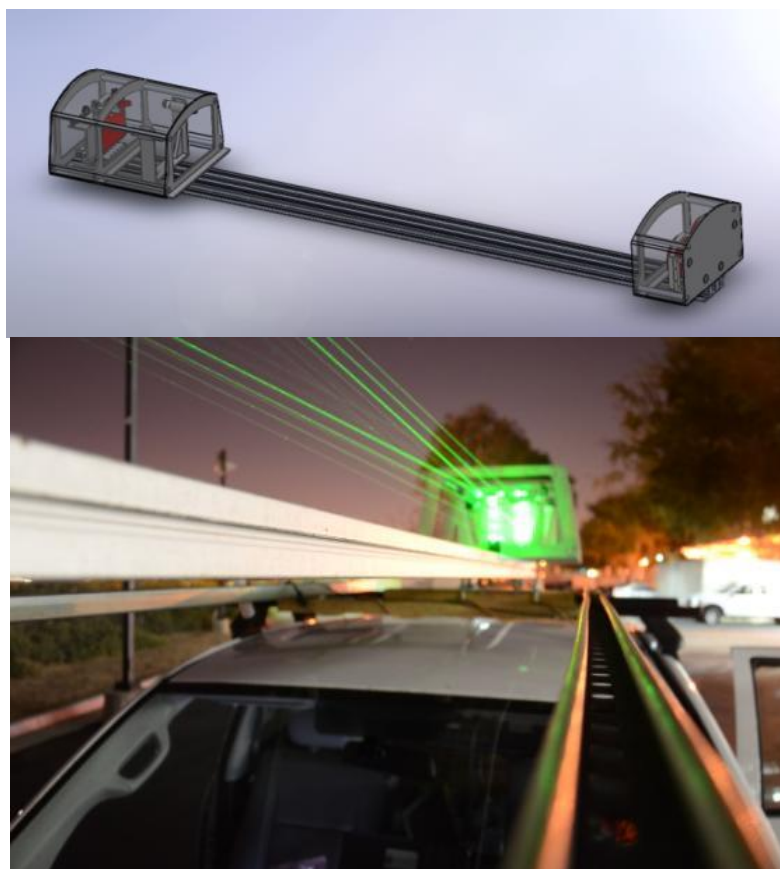
Figure 13 Measurements of aromatic VOCs were carried using a UV multi-reflection cell (White cell) connected to a DOAS spectrometer (MW-DOAS).

3. Measurements

The first objective of this study was to carry out column measurements of NO_2, SO_2, HCHO and VOCs around the Houston ship channel during the NASA DISCOVER-AQ aircraft flights. The second objective was to carry out more detailed emission measurements on specific industries, with the mentioned species above.

The campaign period was dominated by cloudy weather and prevailing easterly wind. A frontal passage at the later part of the campaign brought improved weather conditions with mostly clear skies. Out of twenty measurement days, 4 had good conditions (clear), 10 moderate conditions (partly cloudy) and the rest rather poor, (cloudy with patches of sun), as shown in Table 2. These weather conditions made SOF and Mobile DOAS measurements difficult.
The two objectives of the campaign were conflicting for easterly winds, i.e. coordinated column measurements with NASA in the large SOF box around HSC and industrial emission measurements of VOCs and other species. On flight days, which had the best weather, the first objective was prioritized and few good days were therefore available for the second objective. The reason why it is difficult to carry out emission measurements in easterly wind is the fact that most industries lie on the south side of HSC, in a row stretching from east to west. In northerly wind (Northwest to Northeast) it is easy to identify the industries and obtain the emissions, since the measurements on Highway 225 are relatively close to the sources (1-2 km). In easterly wind most of the emissions are detected on the I-610 bridge. Since it is around 20 km to many of the large alkene sources, the VOCs have typically traveled more than one hour, and a large fraction of the highly reactive ones are then degraded. In comparison to previous studies the SOF measurement in the alkene channel (900-1000 cm^{-1}) was rather noisy in the first part of the campaign, but getting better in the second half. This appears to have been caused by strong absorption by water vapor due to high humidity.

Table 2 Measurement table and activity.

Date	DISCOVER-AQ flight day	Independent SOF day	Weather conditions
Sep 3		X	Moderate
Sep 4	X		Poor
Sep 6	X		Poor
Sep 8		X (afternoon)	Moderate
Sep 9		X	Moderate
Sep 10		X	Poor
Sep 11	X		Moderate
Sep 12	X		Moderate/good
Sep 13	X		Moderate/poor
Sep 14	X		Poor
Sep 15		X	Poor
Sep 16		X	Poor
Sep 18		X	Moderate
Sep 22		X	Moderate
Sep 23		X (afternoon)	Moderate
Sep 24	X		Moderate/good
Sep 25	X		Good

Sep 26	X		Good
Sep 27	X		Poor
Sep 28		X	Poor

3.1 Column measurements

The NASA DISCOVER-AQ has the objective to demonstrate that geostationary satellites can provide useful environmental data. In September 2013, during 10 mission days, NASA flew high altitude aircraft (B200) equipped with optical sensors, measuring columns of SO_2, NO_2, HCHO and aerosol profiles (LIDAR). To validate these measurements they carried out in situ measurements with a low flying airplane (P-3B) that also carried out spirals above two ground stations in the Houston ship channel, Figure 14 and Figure 15. On the ground station a column measuring Pandora, was used to measure columns of SO_2, NO_2 and HCHO, using direct sun and multi axis absorption measurements in the UV region. As already described in section 1 the data in the DISCOVER-AQ will be used to (1) Relate column observations to surface conditions for aerosols and key trace gases O_3, NO_2, and HCHO, (2) Characterize differences in diurnal variation of surface and column observations for key trace gases and aerosols and (3) Examine horizontal scales of variability affecting satellites and model calculations.

Ten days of column measurements of NO_2, SO_2, HCHO and VOCs (alkanes or alkenes) were carried out around the Houston ship channel during the NASA DISCOVER-AQ aircraft flights. A map with the measurement routes for the SOF vehicle and the two aircraft is shown in Figure 15. Four of these days were clear while six were partially cloudy. The measurements from both SOF and DOAS correspond to relative measurements from a reference point along the measurements transects or box. However during the last 4 flights, from September 22 and onwards, the Mobile DOAS measurements were carried out in two angles, zenith and $\pm30^o$ and from these measurements it is actually possible to calculate the total tropospheric column. This was outside the scope of the original project and given the short time between end of campaign and writing of the final report these data will be made available at a later stage. For partly cloudy conditions the spectral retrieval and interpretation of column results from the zenith sky measurements by the Mobile DOAS is challenging. The clouds scatter the light and the optical path through the atmosphere of the observed light is hence changed causing variations in the measured columns. In addition there may be optical interference effects. Hence column measurements of for instance NO_2 carried out around the Houston ship channel over 1 hour in partly cloudy conditions will have a variability (baseline drift) caused by this effect. Unfortunately, due to time constraints the data given here are not compensated for this effect. Note that the data that is based on multiple angles will make the cloud effect smaller.

The NO_2, SO_2 and HCHO column data from the Mobile DOAS system should be similar to the corresponding data from the high altitude NASA B200 airplane since the measurements are based on the same principles (vertical open path DOAS). The two data sets can therefore be compared directly for various locations around the HSC. Compared to the airborne measurements the ground based measurements should have higher spatial resolution, lower detection limits (more light) and potentially better accuracy (better understanding of the optical path through the lower mixing layer).
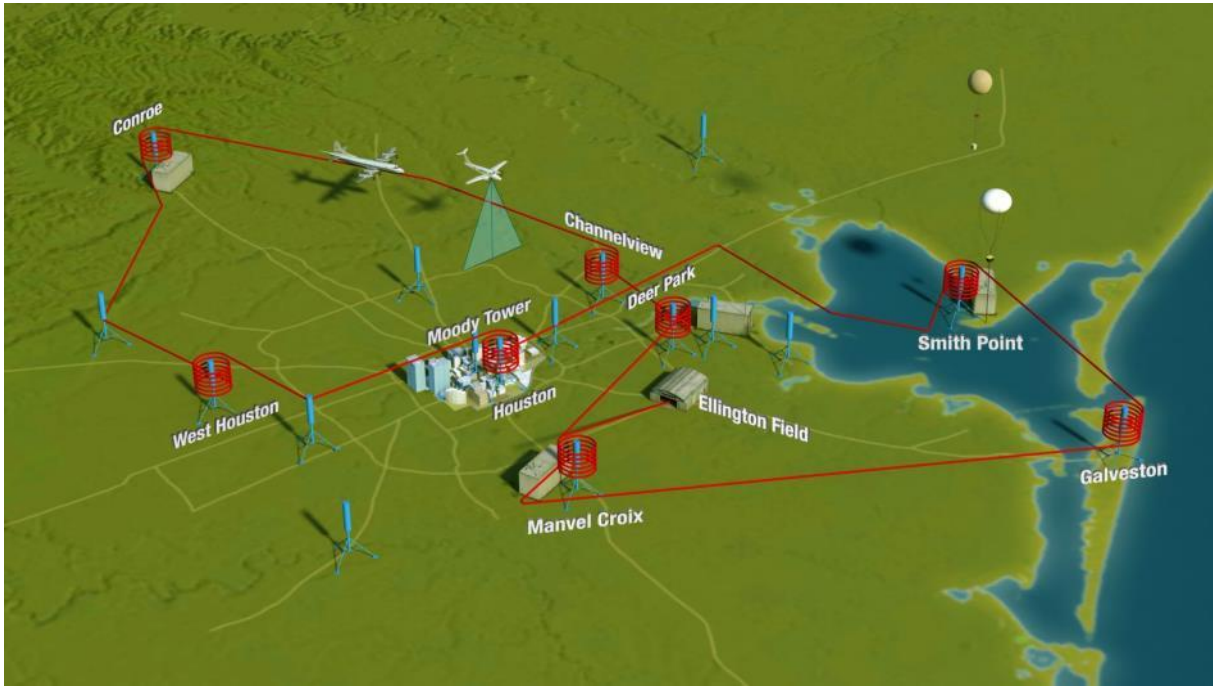
Figure 14 The DISCOVER-AQ airborne flight campaign is illustrated here. A low flying P 3-B aircraft, equipped with in-situ measurement equipment, flew following the red lines, measuring height profiles by circling around the ground sites. A high flying King Air aircraft flew at 26000 feet doing NADIR scanning UV measurements. Adopted from NASA
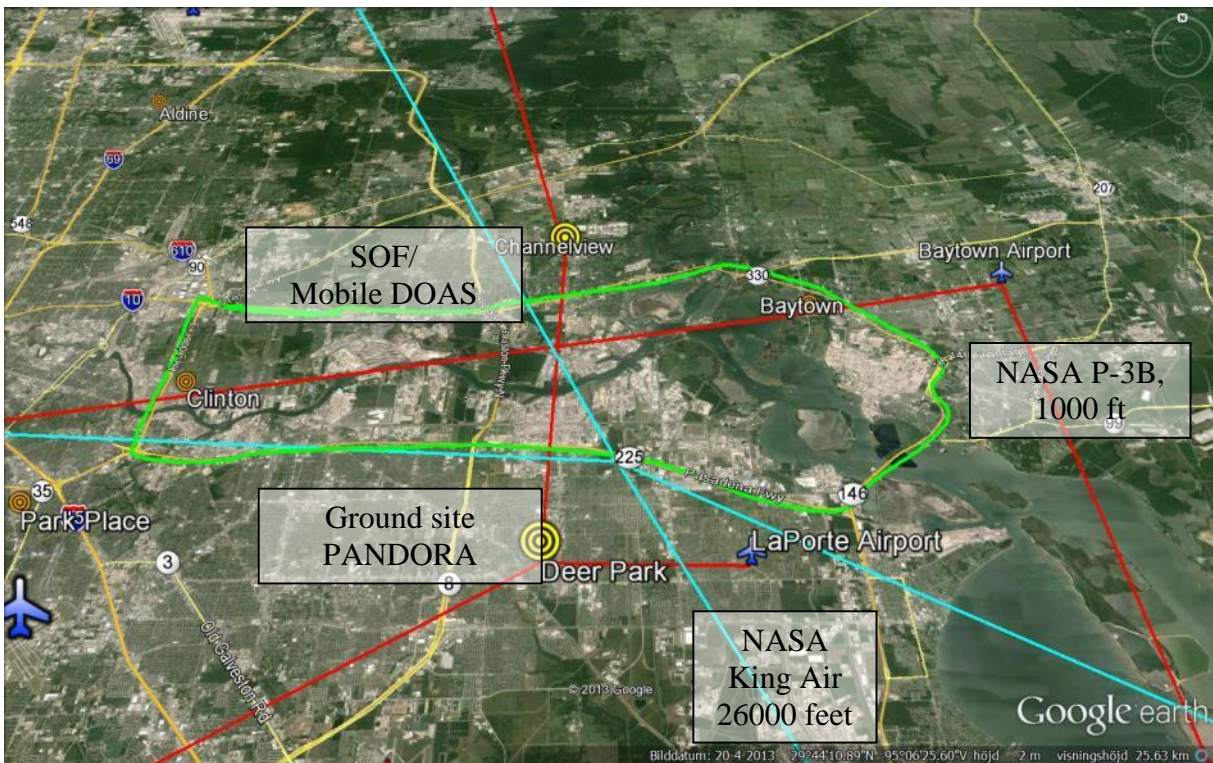

Figure 15 SOF box measurements around Houston Ship Channel (Hwy 225, I 610, I610) were carried out on all 10 flight days of NASA DISCOVER-AQ, following the indicated path in light green. Also shown is the flight path of the low altitude aircraft, P-3B (red), and the NASA King Air (Cyan).

3.2 Wind measurements

During the campaign, 22 weather balloons with GPS-tracking radiosondes were launched to probe the local height profile for the wind. A majority of the radiosondes were launched during the period September 22-27 when the weather was most favorable for the SOF and Mobile DOAS measurements. A site near the San Jacinto battleground monument in the middle of Houston Ship Channel was used to launch most of the radiosondes, although other sites nearby were also used occasionally. Figure 16 shows the launch of one of the weather balloons and the wind profile measured by a radiosonde launched on September 26.
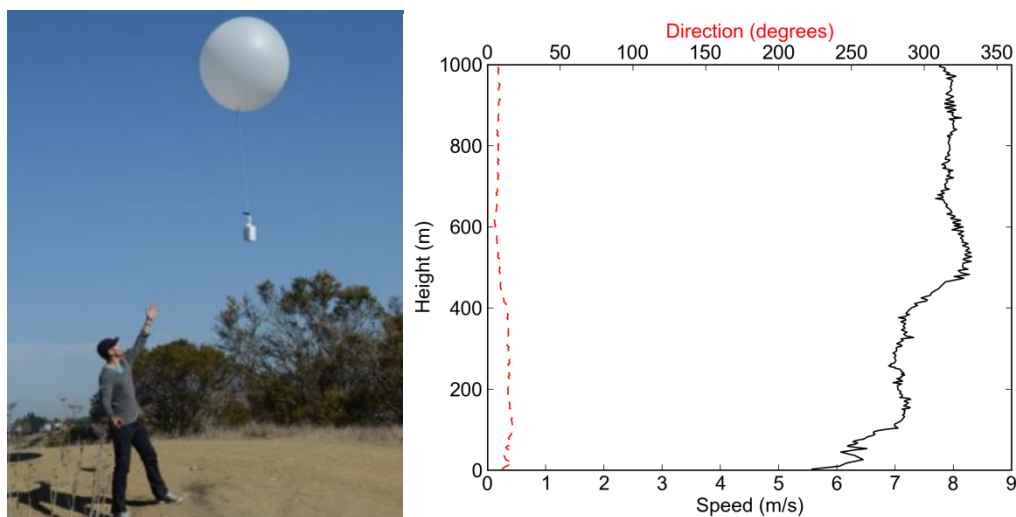
Figure 16 The launch of a weather balloon carrying a radiosonde and the wind profile measured by a radiosonde launched from the San Jacinto battleground monument at 17:54 on September 24. The black line is the speed profile and the dashed red line is the direction profile.

Radiosonde wind profiles were used for flux calculations when available sufficiently close in time, typically within an hour, to a measurement transect. The wind profiles were averaged over a height interval deemed representative for the plumes measured, typically 0 to 350 meters, and then used for flux calculations. For measurement transects with no suitable radiosonde wind profile available, ground based wind measurements were used for the flux calculations. The best alternative available in HSC was the TCEQ operated radar wind profiler in La Porte, just south of State Highway 225. This profiler gives a wind profile every 30 minutes with a height resolution of 57 meters. Each radiosonde wind profile was compared to the radar wind profile closest in time and they generally showed good agreement. One such comparison is shown in Figure 17. Scatter plots of 0-500 m averages of the two types of profiles are shown in Figure 18 for both wind speeds and wind directions. With the exceptions of the wind directions of three profiles, this confirms the good agreement. These three outliers in the wind direction scatter plot are all from the same day, September 25, and the radiosonde profiles seem to be the correct ones. This shows that the radar profiler can occasionally have larger direction errors. This type of large wind direction errors can, however, typically be avoided from geometrical constraints, i.e. an approximate true wind direction can be inferred by the locations of the observed plumes in relation to their sources.
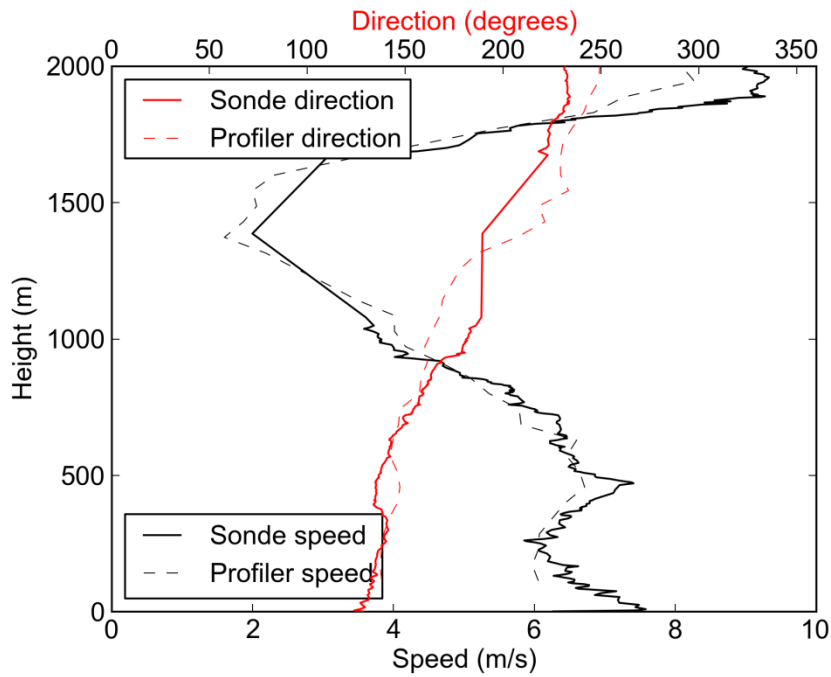
Figure 17 Comparison between a wind profile measured by a radiosonde launched at 14:19, September 26 and the wind profile measured at the same time by the radar wind profiler at La Porte.
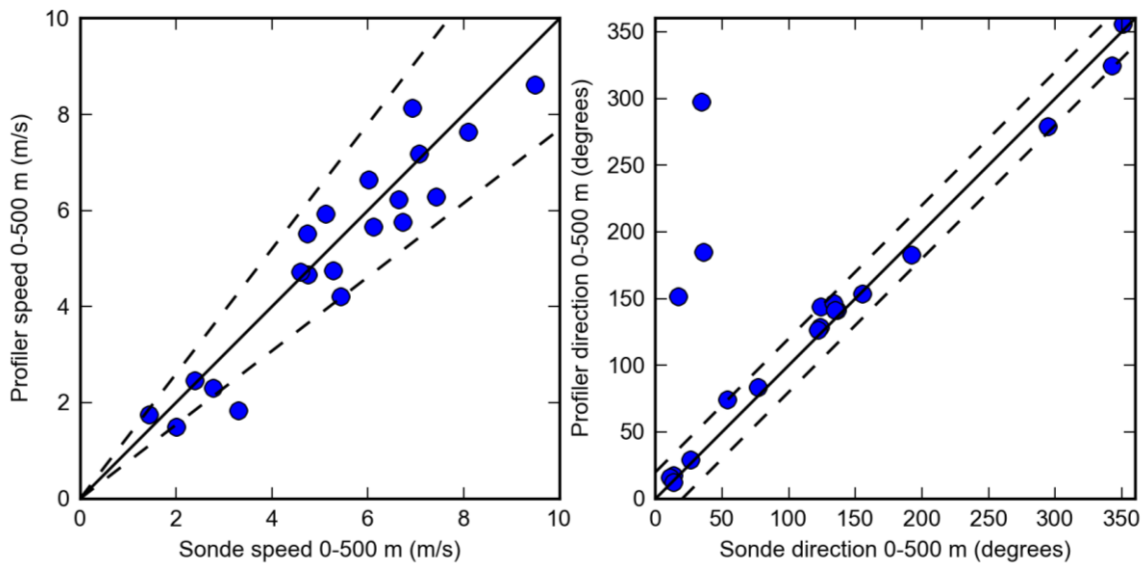

Figure 18 Scatter plots of 0-500 m averages of all radiosonde profiles and 0-500 m averages of simultaneous radar profiles. Wind speeds in the left plot and wind directions in the right plot. Dashed lines show ±30% for wind speeds and ±20° for wind directions.

Complementary wind data from ground masts at six different CAMS sites were used when the wind direction from the radar profiler did not match geometrical constraints, especially for measurements outside the HSC area. Wind speeds from CAMS sites were rescaled to match 0-500 m averages of sonde profiles on average. Figure 46 shows scatter plots of the 0-500 m averages of the radiosondes and the rescaled simultaneous CAMs site winds. It should be noted that the sites C620 and C1022 are located in Texas City and C617 between Baytown and Mont Belvieu, which explains their larger deviations from the profiles measured in HSC.
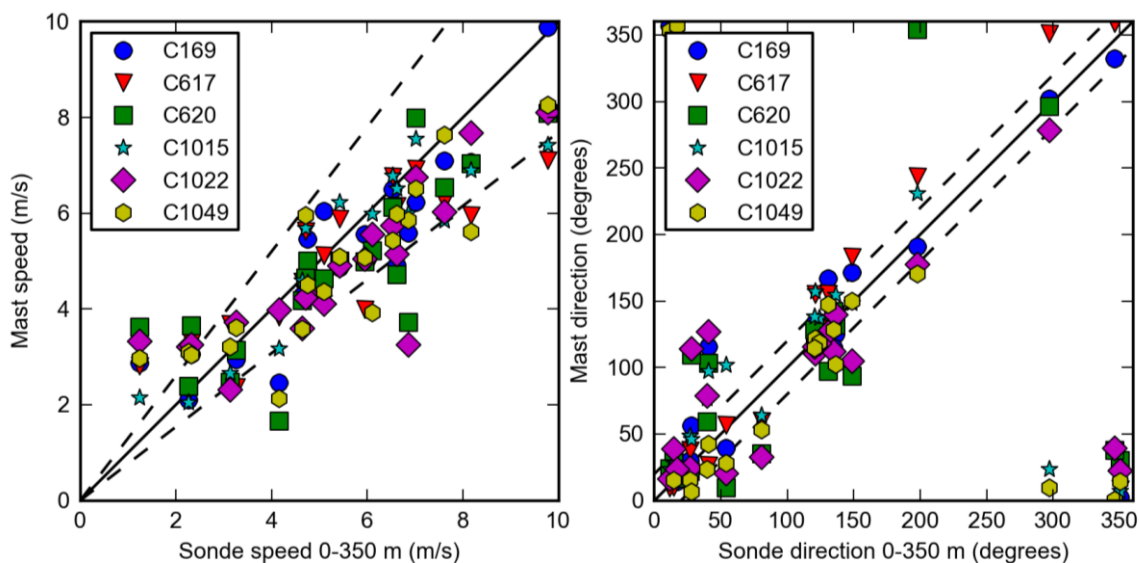
Figure 19 Scatter plots of 0-500 m averages of all radiosonde profiles and the simultaneous rescaled winds from six different CAMS sites. Wind speeds in the left plot and wind directions in the right plot. Dashed lines show ±30% for wind speeds and ±20° for wind directions.

3.3 Emission measurements

As shown in the measurement activity table, Table 2, the days with the clearest weather were focused on carrying out column measurements in the box around the HSC to support the DISCOVER-AQ campaign, as shown Figure 15. The dominating wind directions, northeasterly to southeasterly, combined with the measurement route prescribed for the column measurements were generally not optimal for flux measurements. This was because they often resulted in intercepting emission plumes relatively far downwind from their sources and at steep angles. The dominating wind directions also made it difficult to separate measurements into the sectors used for HSC in previous campaigns (see Figure 20). However, during some of these days it was still possible to also derive emission fluxes. Two days (September 24 and 25) of northerly winds toward the end of the campaign and occasional deviations from the prescribed measurement route were of great value for this. For these reasons, it was still possible to get some emission fluxes for the sectors used in the 2006, 2009 and 2011 campaigns, allowing more detailed comparisons. The number of measurements for each sector was, however, in many cases lower than in previous campaigns. Since the wind was rarely straight northerly, neither in this campaign nor in the previous ones, separating these sectors is inherently imprecise and will not always include the emissions from exact same sources in every a particular sector. Measurements for which the emissions from the different sectors could not be separated has in some cases been used to estimate the total emissions from two or three adjacent sectors.

In addition to the HSC measurements, most non-flight days were used to measure emissions from the refineries in Texas City and the petrochemical industries in Mont Belvieu. However, due to the poor weather during the campaign and the fact that the days with better weather was usually flight days, many non-flight days did not produce much of value. For this reason, the number of measurements is also limited for these areas.

Figure 20 SOF sectors in the Houston ship channel into which the emissions were divided for analysis. The sectors are named: 1. Allen Genoa Rd, 2. Jefferson Rd (Davison in Mellqvist 2007), 3. Deer Park, 4. Battleground Rd, 5. Miller Cutoff Rd, 6. Sens Rd, 7. Baytown.

3.4 Concentrations measurements of aromatic and alkanes

During the measurement campaign the MW-DOAS was mounted on the roof of the measurements van (Toyota Tundra) with the aid of roof racks and a special constructed frame, Figure 1. Five evening/nighttime measurements were carried out mapping aromatic emissions in the HSC area and Texas City. An intercomparison was carried out on September 17 between the MW-DOAS and a PTR-MS operated by Berk Knighton, (University of Montana) and installed in a van run by the research company Aerodyne. The measurements were carried out while driving downwind of various sources in Channelview and Baytown, HSC-. The PTR-MS instrument is a modified version of an early instrument by the company Ionicon with a quadropole mass spectrometer and a detection limit of (1.9 ppb) [Rogers, 2006].

As described in section 3.4 an intercomparison exercise was carried out on September 17, 2013 comparing the MW-DOAS on the SOF van with a PTR-MS instrument. The Mobile labs were driven in a caravan downwind of several known emission sites to perform almost simultaneous measurements. The time difference between the measurements varied between 10-60 s, depending on the driving speed

Figure 21 A measurement intercomparison of aromatic VOCs were carried out, comparing the MW-DOAS in the SOF van (middle) to a PTR-MS instrument in the Aerodyne truck, (right). The figure also shows the NASA van and all crews.

The MW-DOAS measurements of aromatic VOC concentration were accompanied by simultaneous meFTIR measurements of alkanes, with the aim to measure the ratio of aromatic to alkanes downwind of industrial site. Since the SOF measures emissions of alkanes downwind of industries, the aromatic emissions can be inferred by multiplying the SOF values with the aromatic to alkane mass ratio, assuming that the ratio measurements are representative for the whole emission plume.

The MW-DOAS and meFTIR were added as an extra, non-funded, activity to the project and therefore only few results will be given.

4. Measurement uncertainty and quality assurance

4.1 Measurement uncertainty SOF and Mobile DOAS

The main uncertainty for the flux measurements in the SOF and Mobile DOAS measurements comes from the uncertainty in the wind field. Since a detailed wind analysis has not been performed yet, the uncertainty in flux calculations cannot be estimated. Instead Table 3 shows the estimated uncertainties for the flux measurements during the 2011 SOF campaign in Houston. For the final report a similar estimation will be made for the 2013 campaign.

Table 3 Uncertainty estimation of the flux measurements (the variability of the sources not taken into account).

	Wind Speed [a]	Wind Direct [b]	Spectroscopy (cross sections) [c]	Retrieval error [d]	Composite flux measurement uncertainty [e]
Alkanes	16–30 %	6–9 %	3.5 %	12 %	21–34 %
Ethene	16–30 %	6–9 %	3.5 %	10 %	20–33 %
Propene	16–30 %	6–9 %	3.5 %	20 %	27–37 %
HCHO	16–30 %	6–9 %	3 %	10 %	20–33 %
SO$_2$	16–30 %	6–9 %	2.8 %	10 %	20–33 %
NO$_2$	16–30 %	6–9 %	4 %	10 %	20–33 %

a) Comparing mast wind averages with the 0–500 m GPS sonde averages, the max data spreads 16–30 % (1σ, 30 %)
b) The 1σ deviation among the wind data compared to the 0–500 m sonde is 18°. For a plume transect orthogonal to the wind direction, which is always the aim, this would give a 6 % error. For a measurement in 75° angle the error is 9 %.
c) Includes systematic and random errors in the cross section database.
d) The combined effects of instrumentation and retrieval stability on the retrieved total columns during the course of a plume transect and error of the SOF alkane mass retrieval. Estimated for SOF.
e) The composite square root sum of squares uncertainty

4.2 Validation and comparisons

The performance of the SOF method has been tested by comparing it to other methods and tracer gas release experiments. In one experiment, tracer gas (SF$_6$) was released from a 17 m high mast on a wide parking lot. The emission rate was then quantified by SOF measurements 50–100 m downwind the source, yielding a 10 % accuracy for these measurements when averaging 5–10 transects [Kihlman 2005b].

More difficult measurement geometries have also been tested by conducting tracer gas releases of SF$_6$ from the top of crude oil tanks. For instance, in an experiment at Nynas refinery in Sweden tracer gas was released from a crude oil tank. In this case, for close by measurements in the disturbed wind field at a downwind distance of about 5 tank heights, the overestimation was 30 %, applying wind data from a high mast [Kihlman 2005a; Samuelsson 2005b].

The SOF method has also been compared against other methods. In another experiment at the Nynas refinery a fan was mounted outside the ventilation pipe, sucking out a controlled VOC flow from the tank. The pipe flow was measured using a so called pitot pipe and the concentration was analyzed by FID (Flame ionization detector) which made it possible to calculate the VOC emission rate, which was 12 kg/h. In parallel, SOF measurements were carried out at a distance corresponding to a few tank heights, yielding an emission rate of 9 kg/h, a 26 % underestimation in this case. Similar measurements from a joint ventilation pipe

from several Bitumen cisterns yielded a FID value of 7 kg/h and only 1 % higher emission from the SOF measurements [Samuelsson 2005b].

During the TexAQS 2006 the SOF method was used in parallel to airborne measurements of ethene fluxes from a petrochemical industrial area in Mont Belvieu [De Gouw 2009]. The agreement was here within 50 % and in this case most of the uncertainties were in the airborne measurements. The SOF method has not been directly compared to the laser based DIAL method (Differential Absorption LIDAR) [Walmsley 1998] which is commonly used for VOC measurements. Nevertheless, measurements at the same plant in Sweden (Preem refinery) yield very similar results when measuring at different years. Differences have been seen for bitumen refineries however [Samuelsson 2005b]. Rivera et al. [2009] did Mobile DOAS measurements of SO_2 on a power plant in Spain and the average determined flux with the DOAS came within 7 % of the values monitored at the plant measurements. All in all the experiment described above is consistent with an uncertainty budget of 20–30 %.

4.3 Quality assurance

A formalized QA/QC protocol has not yet been adopted for the SOF method or for Mobile DOAS. However, the spectroscopic column concentration measurements is basically the same as a long path FTIR measurement through the atmosphere corresponding to an effective path length of about 5 km for atmospheric background constituents. For such measurements, there is an EPA guidance document (FTIR Open-Path Monitoring Guidance Document," EPA-600/R-96/040, April 1996).
In addition the US-EPA has developed a test method (OTM 10, Optical Remote Sensing for Emission Characterization from Non-Point Sources), [Thoma 2009] for fugitive emission of methane from landfills. This method is based on measuring the gas flux by integrating the mass across the plume and then multiplying with the wind speed. The mass is here measured by long path FTIR or tuneable diode lasers. The OTM 10 is hence quite similar to the SOF method, since it uses long path FTIR but more importantly since it determines the flux in the same principal manner. The spectral retrieval code used in the SOF method (QESOF) [Kihlman 2005a] relies on principles adopted by the Network for the Detection of Atmospheric Composition Change (NDACC www.ndsc.ncep.noaa.gov), which is a global scientific community in which precise solar FTIR measurements are conducted to investigate the gas composition changes of the atmosphere. Chalmers University is a partner of this community and has operated a solar FTIR in Norway since 1994. The QESOF code has been evaluated against several published codes developed within NDACC with good agreement, better than 3 %.

Even though a formalized QA/QC protocol is missing there are several QA procedures carried out prior to conducting the SOF measurements. This includes checking the instrumental spectral response (usually done by measuring solar spectra and investigating the width and line position of these) and investigating that the instruments measures in the same manner, independent of the direction of the instrument relative to the sun. Usually the instrument is aligned to have the same light response in all directions.

The FTIR instrument, used in SOF, is not calibrated prior to measurements but one instead relies on calibration data from the scientific literature. This is appropriate as long as the instrument is well aligned, and whether the alignment has been sufficient can actually be checked afterwards by investigating the widths and shape of the absorption lines in the

measured solar spectra. Noteworthy is the fact that the spectra are stored in a computer and that the spectral analysis is conducted afterwards which makes it possible to conduct quality control on the data. From this analysis the individual statistical error is obtained for each measurement. Quality control is also conducted by filtering out spectra of lower quality (determined in the Fourier-transform algorithm).

For open path DOAS standardization work is carried out which is very similar to this application from a spectroscopic point of view. For instance the US EPA has tested several long path instruments within their environmental technology verification program with good results.

The spectral evaluation used in this study is similar to many other studies since we rely on a software package widely used by the DOAS community (QDOAS) and we use published calibration reference data. The most important issue when it comes to quality assurance is to investigate the lineshape of the spectrometer and the wavelength calibration. During the campaign this was done by regular measurement with a low pressure Hg calibration lamp. The wavelength calibration was also corrected afterwards by comparing the measured spectra to a solar spectrum, and then shifting them accordingly to the difference. The quality of the data is also maintained by ensuring a low root-mean-square error (RMSE) in the spectral fit.

4.3.1 10% Audit of Data Quality

To satisfy the 10% data quality audit requirements, the following steps were taken:
   a. All time series graphs and tables were reviewed the Principal Investigator and two other researchers.
   b. All standard operating procedures were followed during the measurement phase, and this was double checked during the current project by review of the trip logs and calibration data.

5. Results

5.1 Data analysis of DOAS measurements

During the measurements in Houston, clouds have been seen to affect the evaluated columns substantially, making it hard to distinguish real emission plumes and establish consistent baselines for flux calculations during cloudy and partly cloudy conditions. For this reason, measurements in these conditions have been mostly excluded during the after analysis. The change in evaluated column due to clouds could be an effect of spectral features caused by the clouds that the retrieval model cannot account for, or it could be that the clouds change the pathways of the measured light, increasing or decreasing its path through ambient concentrations of the measured species. Depending on which of these effects it is, there might be different options to improve the data. If it is mainly a matter of unaccounted spectral effects, it might be possible to account for these or at least make the spectral retrieval less sensitive to them. However, if the evaluated columns are real, but corresponding to changes in the pathways of the measured light, the problem cannot be fixed on the spectral retrieval side. In principle it might be possible to model the radiative transfer in the clouds to determine the pathways of the measured light, but this would most likely require detailed information about the cloud properties and this type of data is not available. In this case it may, however, still be possible to use measurements from partly cloudy days after employing some kind of cloud filter to sort out the measurements affected by clouds.

In order to investigate the influence of clouds on the Mobile DOAS spectroscopic retrieval a small measurement study was conducted in relatively unpolluted locations in Sweden. A number of long stationary measurement series were performed in rural locations without any major potential emissions sources upwind. During the course of the measurements notes were made of any clouds occurring and photographs of the sky was taken regularly. During the evaluation of these measurement series, certain instrumental effects were detected and since these could also be important error sources, they were investigated further.

5.1.1 Correction for instrumental drift

Figure 22, Figure 23, Figure 24 and Figure 26 show time series of the root-mean-square (RMS) error of the spectral fit (blue line) for four different long measurement series on different days. They also show the theoretical RMS error (red line) for the same measurement series due to photon noise and readout noise. This is basically a function of the light intensity; high intensity gives low RMS error, while low intensity gives high RMS error. If the spectral retrieval algorithm can properly account for all spectral variations, the RMS error of the fit should only be due to noise and the two lines should follow each other fairly closely. Hence any clear deviation of the blue line from the red line is a sign that the spectral retrieval algorithm cannot account for all the spectral variation.
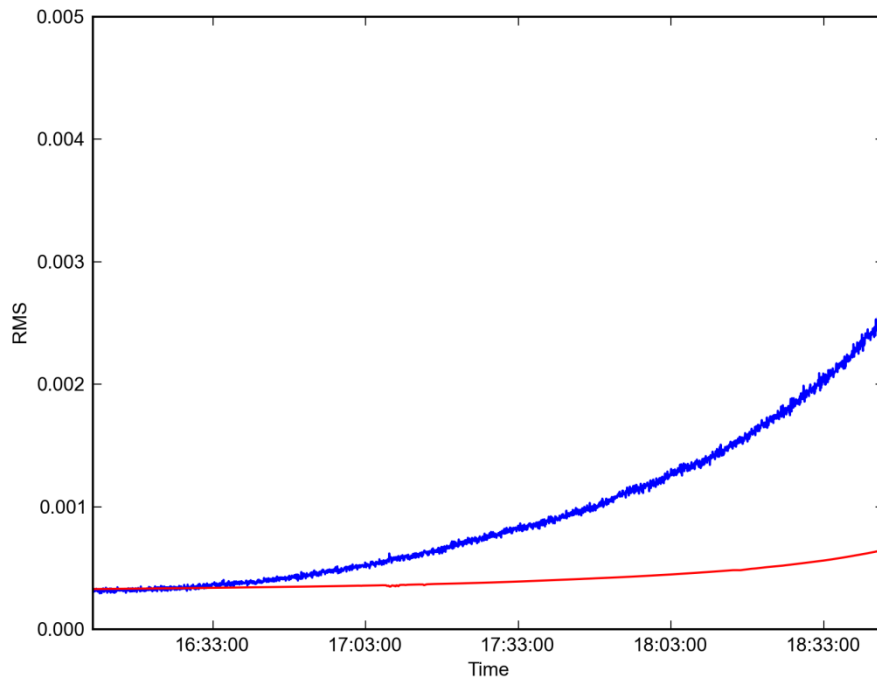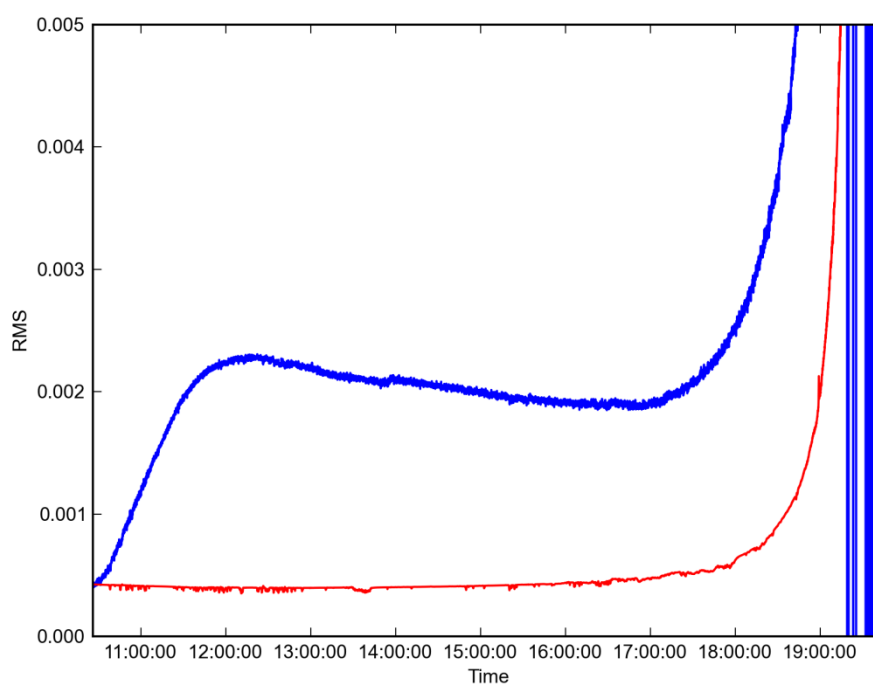
Figure 22 Root-mean-square (RMS) error in spectral retrieval (blue line) of stationary zenith sky DOAS measurements on September 17, 2014 together with theoretical root-mean-square of the statistical noise (red line) calculated based on the measured light intensity.
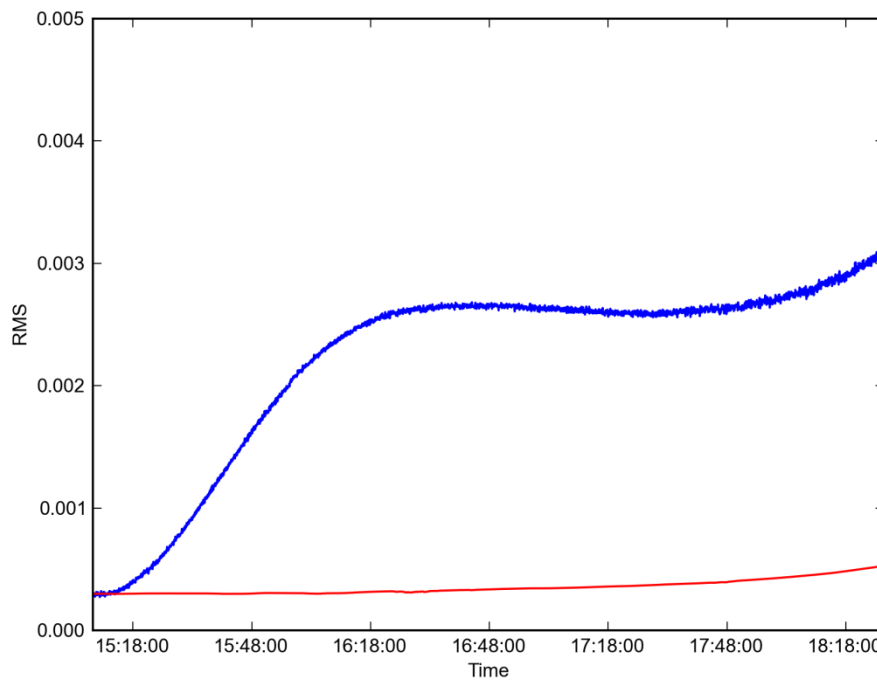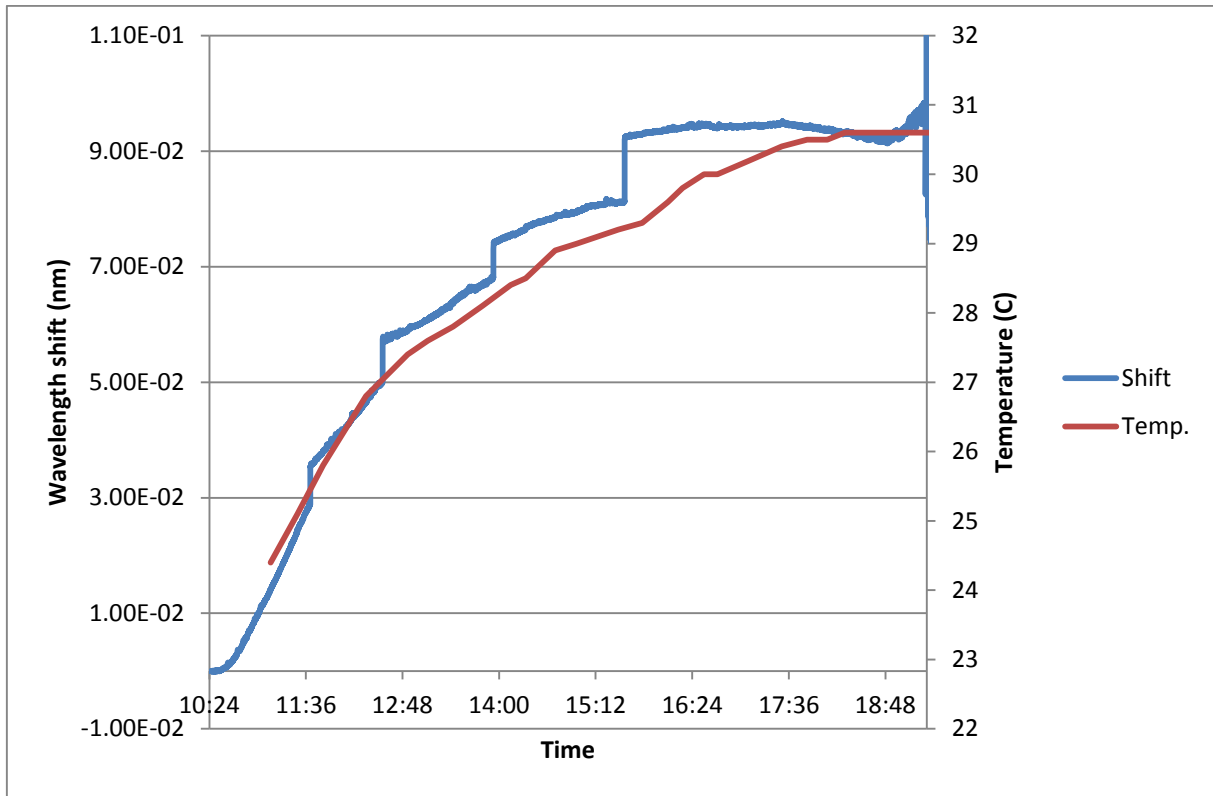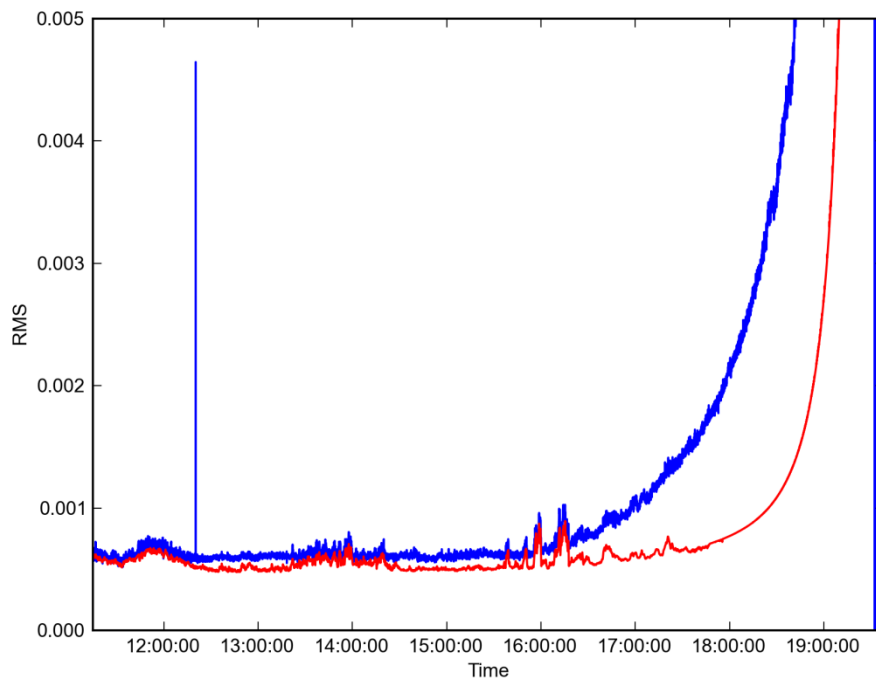

Figure 23 Root-mean-square (RMS) error in spectral retrieval (blue line) of stationary zenith sky DOAS measurements on September 18, 2014 together with theoretical root-mean-square of the statistical noise (red line) calculated based on the measured light intensity.

Two different effects not related to clouds became apparent in this study. One of them was a reoccurring increase in fit RMS in the afternoon/evening. This effect can be seen in all of these measurement series, but most clearly in Figure 22 and Figure 26 where there are no other big effects at the same time. This effect is most likely due to the fact that the absorption signal, primarily that of O_3, becomes larger at this time due to the long atmospheric path at high solar zenith angles (SZA). The larger the O_3 absorption, the higher the necessity to be able to represent this absorption with high accuracy in the spectral fitting algorithm. In these measurement series the fit RMS generally started rising at about 16:30 (UTC+2), which corresponds to a SZA of approximately 72°. The last measurements in the DISCOVER-AQ campaign in Houston were done in the end of September. During this time the SZA is lower than 72° from about 8:45 to about 17:45. Most measurements of any interest during the campaign were made within this time frame and hence this effect should not be expected to be a significant problem in those measurements. For measurements outside this time frame the situation can be improved by using a wavelength window with weaker O_3 absorption for the spectral retrieval. An example of this is shown in Figure 27, where the same RMS time series as in Figure 26 are shown but for the wavelength window 336-359 nm instead of 324-350 nm used for the other figures.
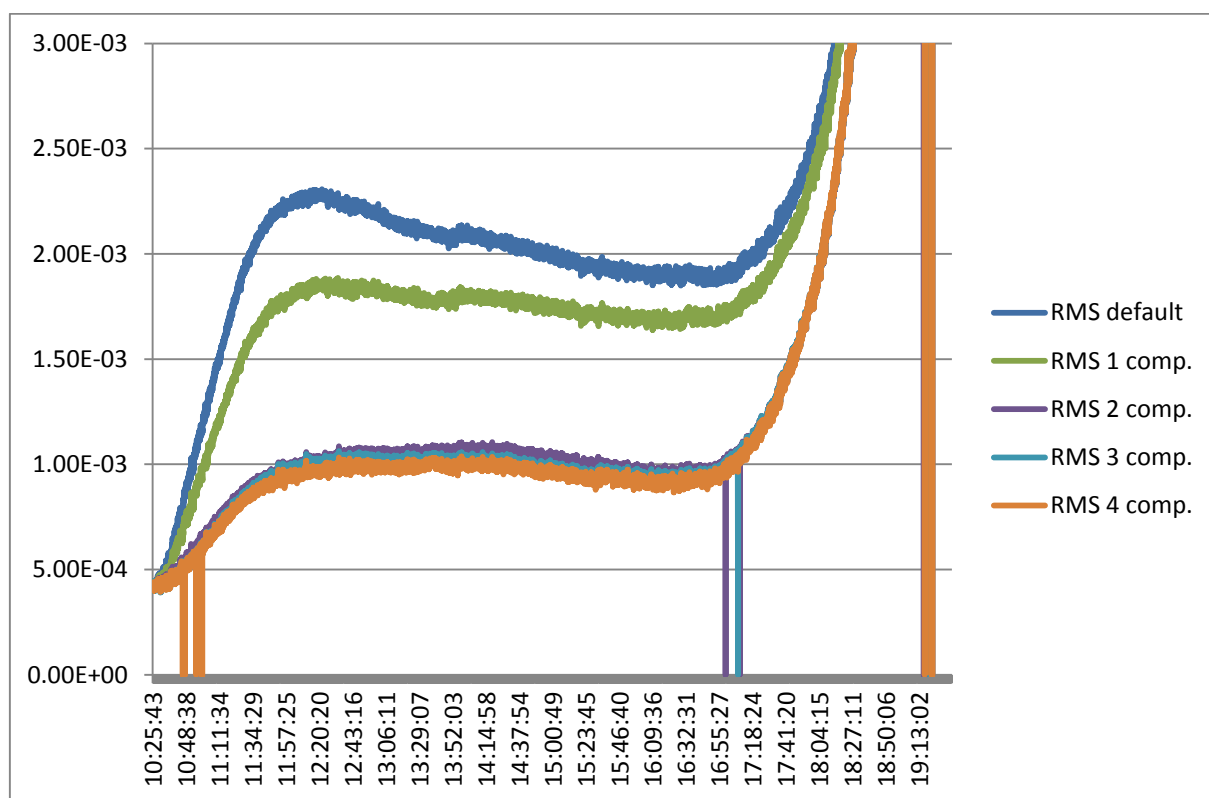

Figure 24 Root-mean-square (RMS) error in spectral retrieval (blue line) of stationary zenith sky DOAS measurements on September 25, 2014 together with theoretical root-mean-square of the statistical noise (red line) calculated based on the measured light intensity.

Figure 25 Wavelength shift fitted by the spectral retrieval algorithm (blue line) together with the temperature (red line) measured inside the spectrometer box.

Figure 26 Root-mean-square (RMS) error in spectral retrieval (blue line) of stationary zenith sky DOAS measurements on September 26, 2014 together with theoretical root-mean-square of the statistical noise (red line) calculated based on the measured light intensity.

The second effect is one that seems to be associated with the startup of the spectrometer. This can be clearly seen in Figure 23 and Figure 24. These measurement series were started right after the spectrometer startup and in both series the fit RMS increases rapidly during a period of roughly an hour. Another interesting feature to note during these series is the wavelength shift between the evaluated spectrum and the reference spectrum taken at the start as determined by the spectral fitting algorithm. Figure 25 shows this wavelength shift together with the temperature logged inside the spectrometer protection box for the same measurement series as in Figure 24.
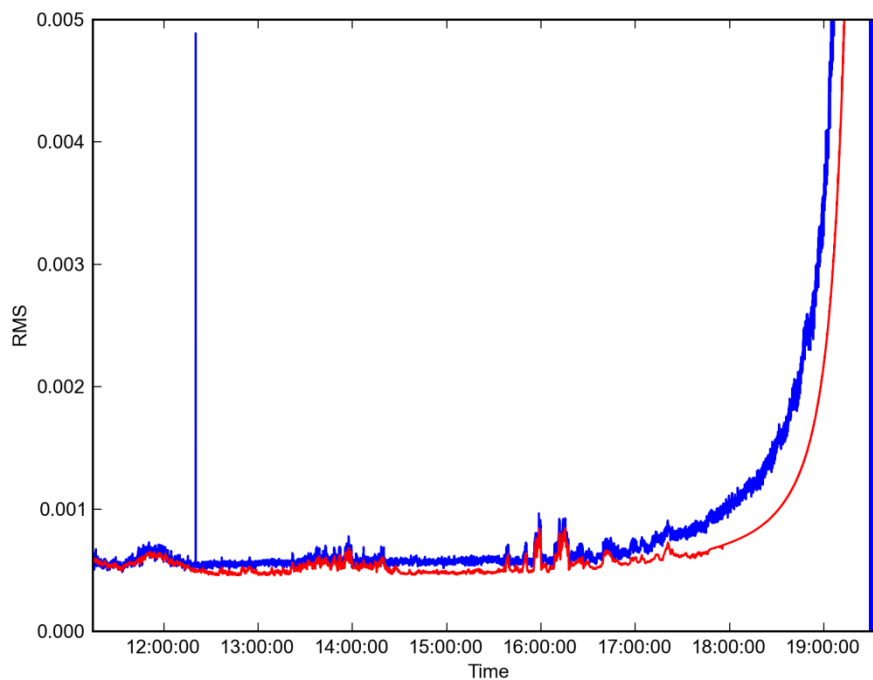
Figure 27 The same RMS time series as in Figure 26 but using the wavelength window 336-359 nm instead of 324-350 nm.

The spectral retrieval is designed to be able to handle spectral shifts such as this and the fact that the RMS time series does not exhibit the same clear discontinuous jumps as the wavelength shift is a clear sign that the bad fit is not directly caused by the wavelengths shift, though they could have an indirect relation. Another sign of this is the fact that the RMS increase happens on a shorter time scale than the wavelength shift. It was hypothesized that the increase in RMS error was caused by small changes in the spectrometer lineshape (also referred to as the instrumental function) which due to the Fraunhofer lines in the measured spectrum could give rise to significant artificial structures in the calculated absorbance. To investigate this further, a mercury lamp spectrum was measured continuously for several hours in a similar fashion to a normal measurement series. The lineshape of a particular mercury emission line was recovered from each spectrum and a synthetic spectrum was produced by convolving a high resolution solar spectrum with this lineshape. This way the artificial absorbance features caused by the changing lineshape could be reconstructed isolated from the atmospheric effects that would be present in a real zenith sky spectrum. To find the most significant spectral features, singular value decomposition (SVD) was applied to the time series of absorbance features in the synthesized spectra. The four most significant

components were extracted and spectral retrievals with 1-4 of these components included as pseudo-absorbers were tested on the real measurement series on September 25.

The RMS error time series from these retrievals as well as the normal one is shown in Figure 28. Here it is clearly shown that the first two components make a significant difference in RMS error, but adding further components after the two first does not appear to make much difference. Figure 29 and Figure 30 show the corresponding time series for evaluated HCHO columns and Ring effect components respectively. These also support the notion that adding the first two SVD components as pseudo-absorbers improve the spectral retrieval considerably, but that further components do not add much. With two or more SVD components, the HCHO time series is fairly constant throughout the day, which should be expected in a unpolluted location, while the normal evaluation had shown a significant decrease on the same time scale as the rapid increase in RMS error. Similarly, the Ring effect time series for evaluations with two SVD components or more shows the expected diurnal behavior due to changing solar zenith angle, with a maximum around solar noon, while the normal evaluation once again shows a significant deviation on the time scale of the rapid increase in RMS error. The Ring effect time series also shown a number rapid variations caused by passing clouds. These are however the same for all evaluations. Similarly, the HCHO time series shows a short deviation around 13:40 which seem to have been due to a thicker cloud than the rest during this day.

Figure 28 Root-mean-square (RMS) error in variations of spectral retrieval of stationary zenith sky DOAS measurements on September 25, 2014.
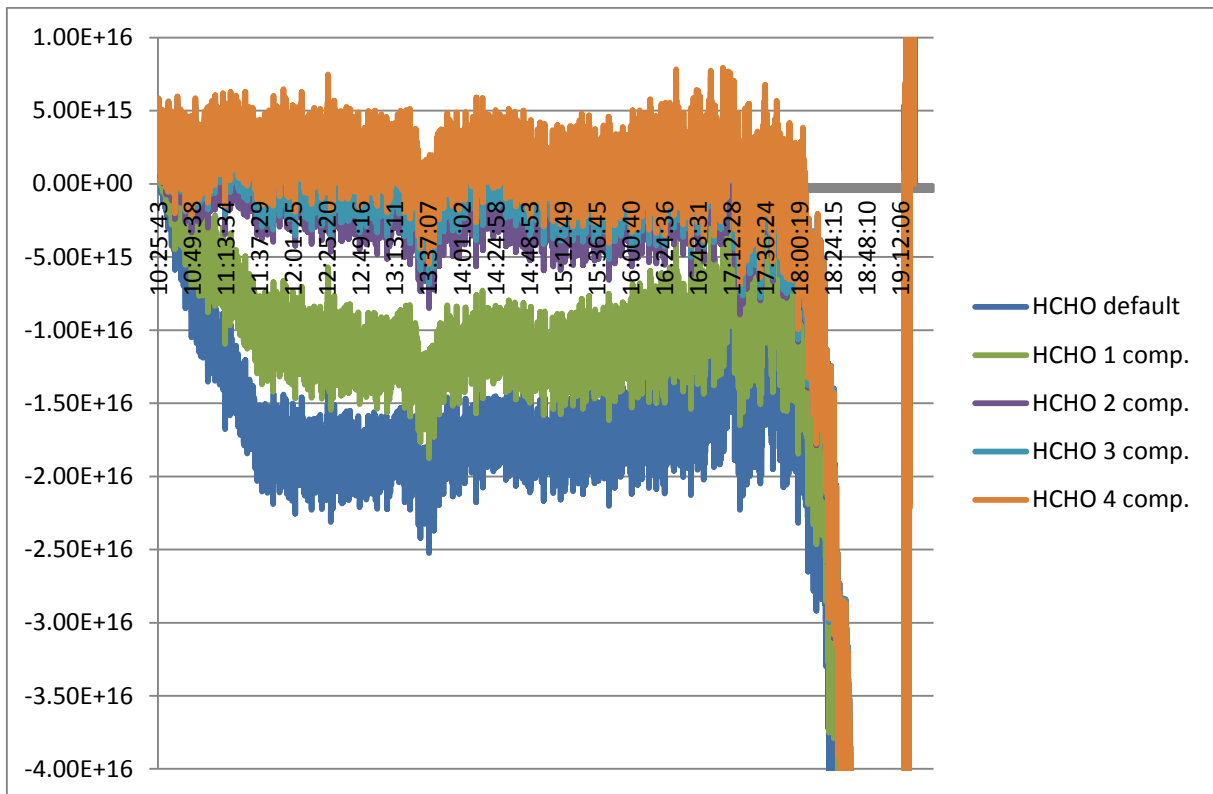
Figure 29 Evaluated HCHO column in variations of spectral retrieval of stationary zenith sky DOAS measurements on September 25, 2014.
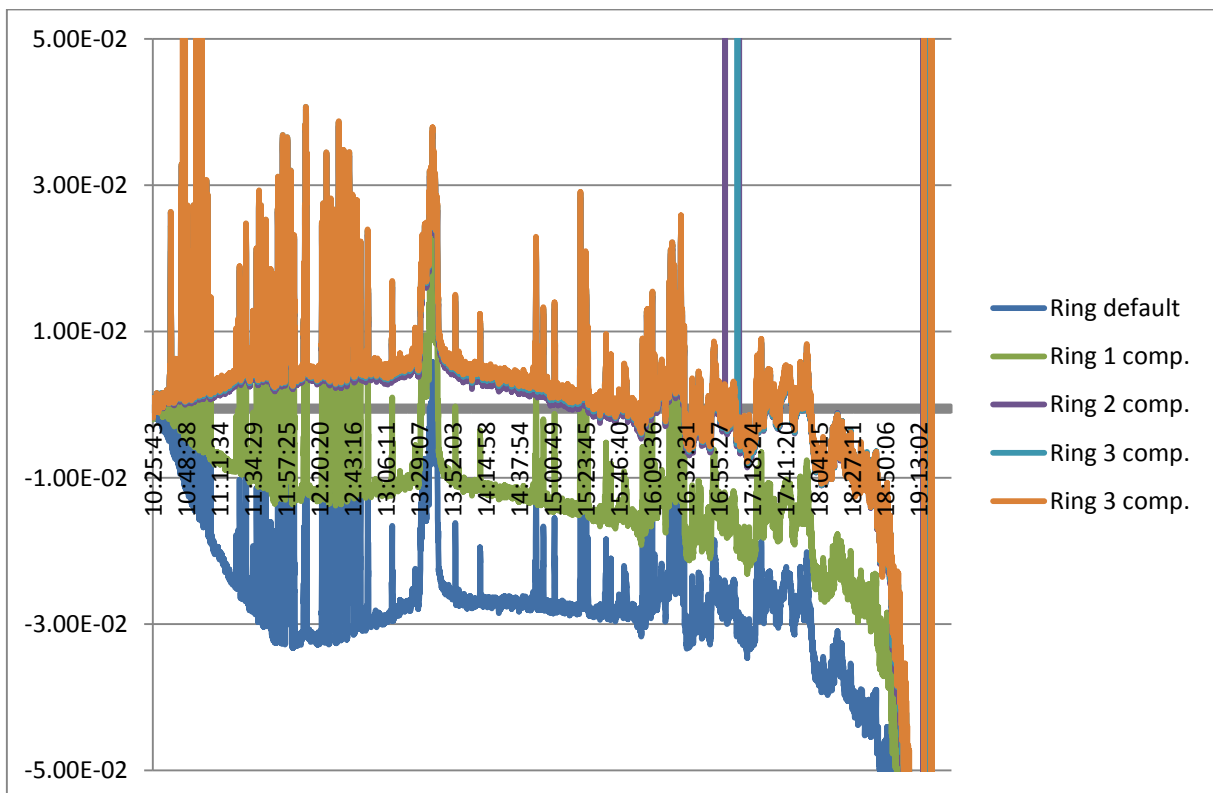
Figure 30 Evaluated Ring effect component in variations of spectral retrieval of stationary zenith sky DOAS measurements on September 25, 2014.

Although adding two of these pseudo-absorbers seem to decrease the RMS error significantly, it is still larger than what would be expected due to only photon noise. One obvious reason for this is that the lineshape variations used to produce the pseudo-absorbers were all from a single mercury line. The lineshape should, however, be expected to vary slightly with wavelength, and thereby the variations in lineshape should also be expected to be slightly different for different wavelengths. These variations could, however, not be taken into account in the method used here. The remaining RMS error elevation, however, does not appear to be associated with a significant effect on the evaluated columns of interest, as shown in Figure 29. Hence this method was determined to be sufficient to account for the variations in lineshape in the spectral retrieval. The retrieval with two pseudo-absorbers was applied to the DOAS measurements during the DISCOVER-AQ campaign and were seen to produce similar improvements in the RMS error and the evaluated columns.

5.1.3 Investigation of cloud effects

The main purpose of the small measurement study was to investigate cloud effects. Plenty of clouds were interfering with the measurements on these days, but they seemed to have little effect on the quality of the spectral fits. This is perhaps most evident in the RMS error time series from September 26 shown in Figure 26, which showed little instrumental effects. This was a day with overcast throughout the day with varying thickness of the cloud cover. This time series does indeed show some rapid variations in RMS error caused by the clouds, but these are also seen in the theoretical RMS series, indicating that these are due to the variations in light intensity, rather than any spectral features caused by the clouds. The same pattern is seen throughout the measurement study. The clouds seem to have some effects on evaluated components of Ring effect, O_2 collision complex (O_4), NO_2 and occasionally on HCHO, but these does not seem to be associated with elevations in RMS error that cannot be explained by decrease in light intensity. Hence these effects are assumed to be due to changes in radiative transfer, i.e. the paths taken by the measured light, rather than spectral artifacts not accounted for by the spectral retrieval. This is also supported by the fact that evaluated columns, such as O_4 and NO_2, typically either both increase or decrease when they are both affected by a cloud. If this was due to interference from an unknown spectral artifact it would be just as likely that they change in opposite directions. Since the effects of clouds on evaluated columns does not appear to be due to spectral artifacts, they cannot be eliminated by changes to the spectral retrieval. Hence the best option is to try to filter out the measurements affected by clouds.

5.1.4 Implementation of cloud indicator

In order to better be able to determine which measurements were seriously cloud affected, a cloud indicator was developed. The cloud indicator was based on calculating a color index in a similar fashion as in [Wagner 2014]. The color index was calculated as the ratio of spectral intensities at 324 nm and 350 nm. This was compared to the same ratio as calculated for spectra modeled using the radiative transfer modeling software SCIATRAN. Two scenarios were modeled; one with no aerosols and one with high aerosol loadings. The model was run for a range of solar zenith angles and the color index of each measured spectrum was compared to the modeled color indices for the same solar zenith angle as the spectrum was measured with.
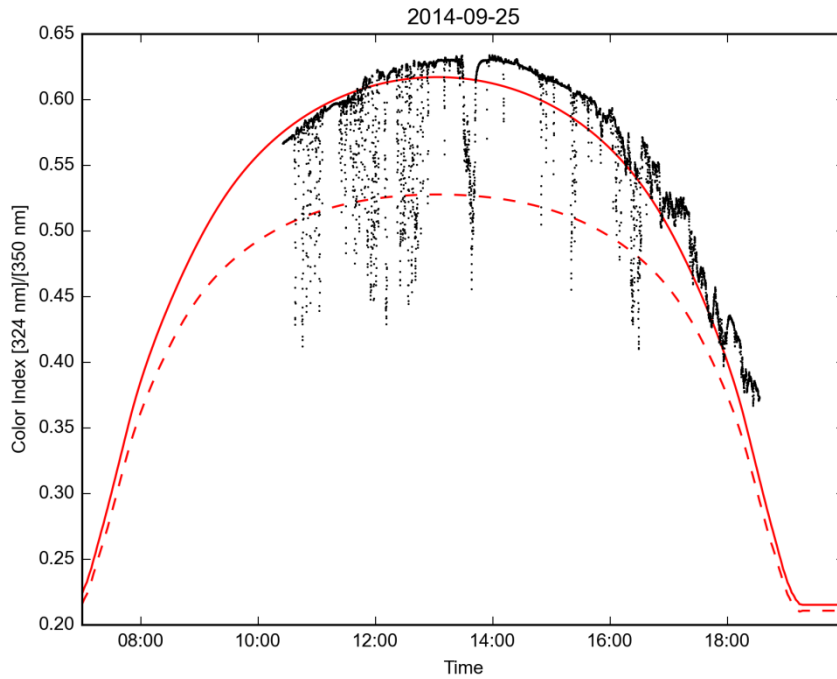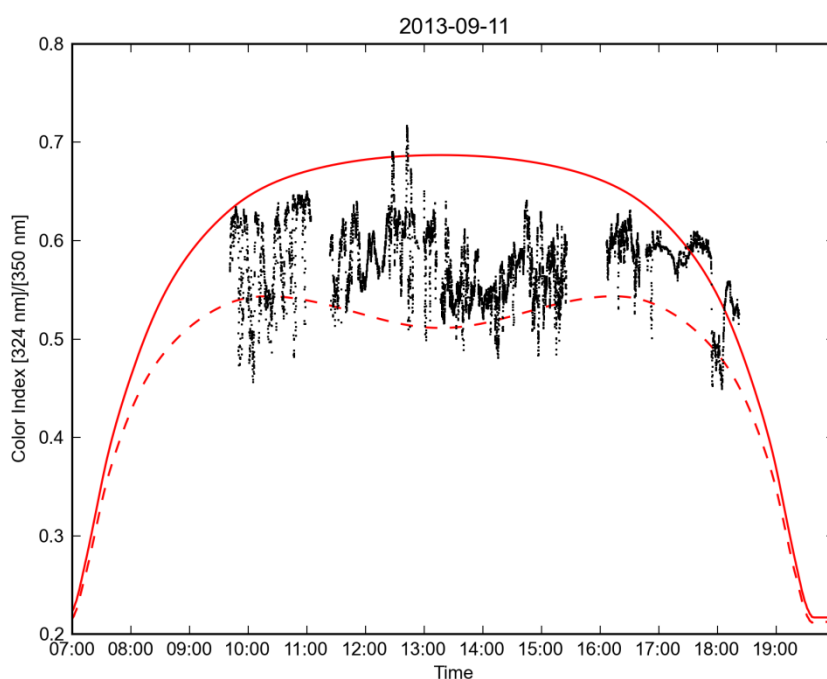
Figure 31 Color index for sky measurements on September 25, 2014. Black dots represent the measured spectra and the red lines represent model values for a scenario with no aerosols (solid line) and a scenario with high aerosol loadings (dashed line).
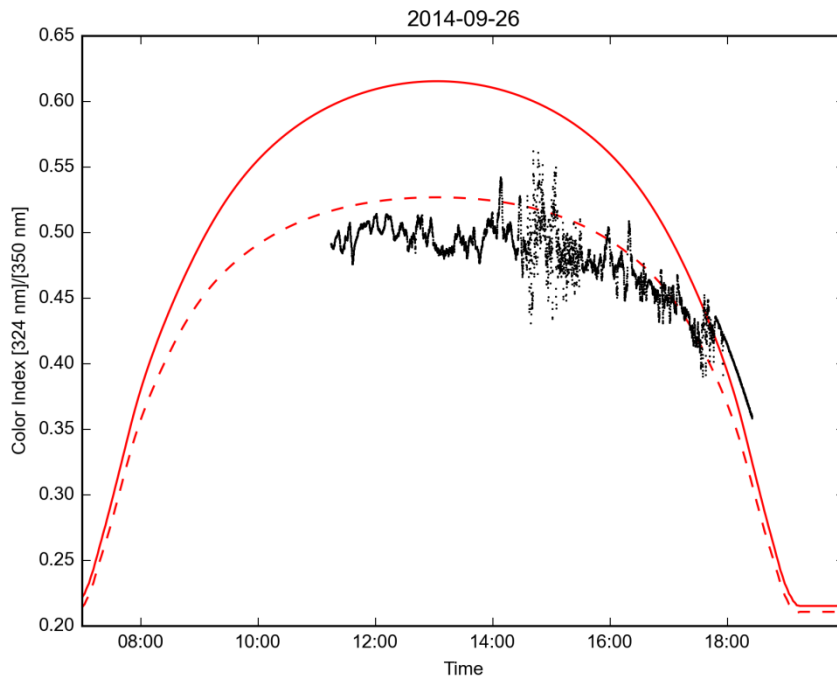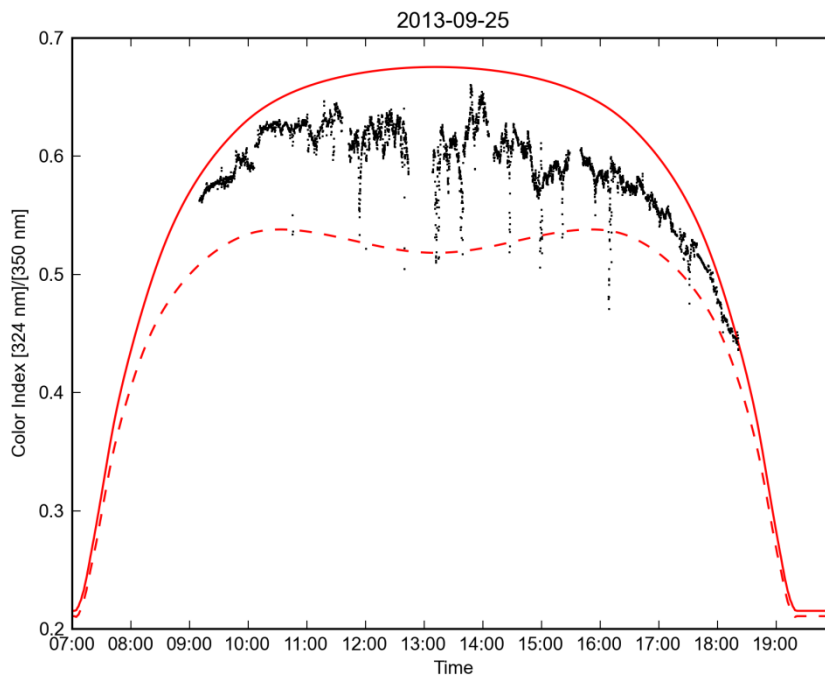

Figure 32 Color index for sky measurements on September 26, 2014. Black dots represent the measured spectra and the red lines represent model values for a scenario with no aerosols (solid line) and a scenario with high aerosol loadings (dashed line).

Figure 31 shows the time series of both measured and modeled color indices for the test measurements on September 25, 2014. This was a partly cloudy day with scattered clouds. Most of the time, the measured color index is close to that of the model scenario with no aerosols, but there are numerous short periods when the color index dives to values closer to the high aerosol scenario. These periods all correspond to scattered clouds passing the field of view of the DOAS system. For comparison, Figure 32 shows the corresponding time series for the test measurements on September 26, 2014. This was a day with complete overcast the whole day. This is consistent with the color index staying close to the high aerosol model scenario the whole day.
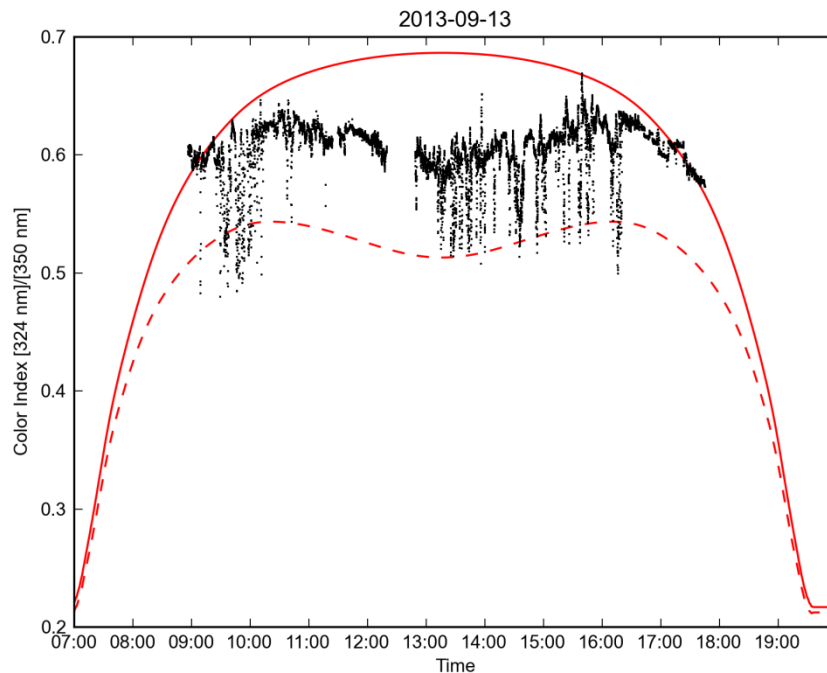
Figure 33 Color index for Mobile DOAS measurements on September 13, 2013. Black dots represent the measured spectra and the red lines represent model values for a scenario with no aerosols (solid line) and a scenario with high aerosol loadings (dashed line).

The color index has been calculated for all of the Mobile DOAS measurement series during the DISCOVER-AQ campaign. Figure 33 shows the results for September 13, 2013, which is an example of a day where the presence of small scattered clouds is easy to detect from the rapid variations in color index. This was a partly cloudy day with many clouds but also a lot of clear skies that can be easily distinguished from this figure. By contrast, the results for September 11, 2013, shown in Figure 34, indicate that it might not always be easy to distinguish between clear sky and clouds. This was a partly cloudy day with fewer clear patches and for much of the day the color index stays somewhere in the middle rather than rapidly jumping between two extremes. Finally, Figure 35 shows the results for September 25, 2013, which was pretty clear all day long. Even though it was clear, the color index was still fairly low for much of the time, especially in the afternoon. This is because the color index is also affected by aerosol loadings and September 25 was the most intense smog episode during the campaign. Together these examples illustrate that the application of the color index as a cloud indicator is not entirely straightforward. Initially, it was attempted to filter out measurements affected by clouds by setting some type of threshold for the color index, but this proved to be difficult due to changing aerosol conditions. Additionally, not all

measurements affected by clouds needs to be filtered out, since it is primarily the changes in radiative transfer caused by drastic variations in cloud types and thickness that causes problems. Instead the color index was used as a tool to manually determine which measurements were too much negatively impacted by clouds to be used for flux calculations. Too make the color index more comparable between different parts of the day, it was normalized using the radiative transfer model values for the corresponding solar zenith angle. The cloud indicator used was calculated using the formula:

$$I = \frac{CI_M - CI_1}{CI_0 - CI_1}$$

where CI_M is the measured color index and CI_0 and CI_1 are the modeled color indices for the cases with zero and high aerosol loadings respectively.

Figure 34 Color index for Mobile DOAS measurements on September 11, 2013. Black dots represent the measured spectra and the red lines represent model values for a scenario with no aerosols (solid line) and a scenario with high aerosol loadings (dashed line).

Figure 35 Color index for Mobile DOAS measurements on September 25, 2013. Black dots represent the measured spectra and the red lines represent model values for a scenario with no aerosols (solid line) and a scenario with high aerosol loadings (dashed line).

5.1.5 Evaluation of multi-angle measurements

During the end of the DISCOVER-AQ campaign the Mobile DOAS system was operated in an experimental scanning mode. In this mode the DOAS telescope was pointing to a mirror attached to a motor, allowing the field of view to be tilted sideways during the measurements. During these days the viewing direction was sequentially changed according to the pattern: ZENITH -> 30° LEFT -> ZENITH -> 30° RIGHT -> … with one spectrum recorded between every change. The purpose of this scheme was to try to determine absolute column, as opposed to the relative columns retrieved from the normal Mobile DOAS measurements, by evaluating the 30° tilted measurements with the almost simultaneous zenith measurement as reference. To be able to get anything meaningful out of this type of evaluation, radiative transfer simulations was needed to determine how the different measurement directions would be impacted by the same air masses.

Radiative transfer modeling
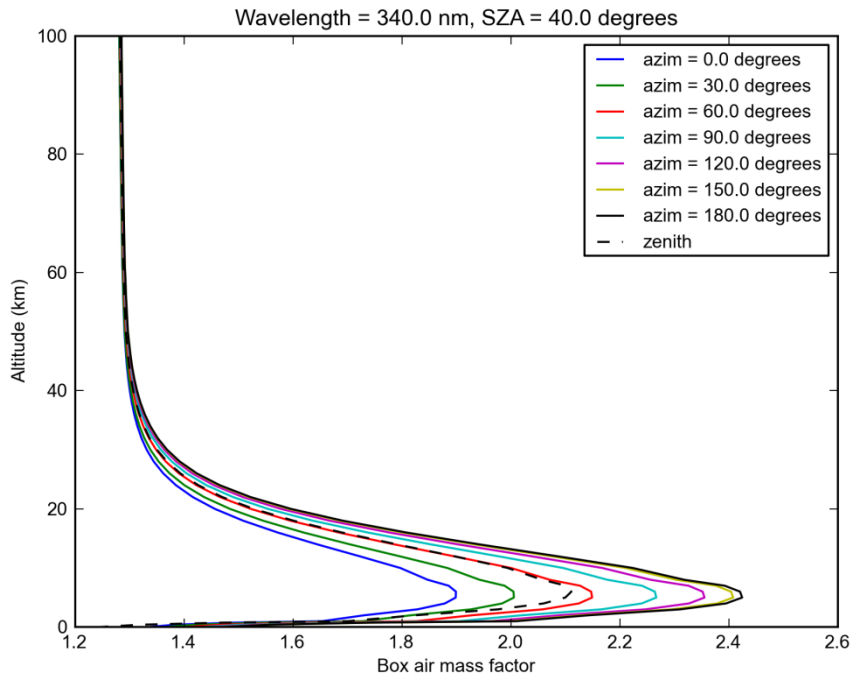
Figure 36 Box air mass factor profiles from radiative transfer simulations with 40° solar zenith angle. The solid lines show box air mass factors for 30° off-zenith viewing direction for different azimuth directions relative to the sun while the dashed black line show the box air mass factors for zenith viewing direction.

To be able to interpret the multi-angle DOAS measurements a number of radiative transfer simulations were performed using the SCIATRAN radiative transfer modeling software. As input for the simulations, profiles of trace gas concentrations and aerosol extinction coefficients were taken from in-situ measurements from the spiral flights made by the P3B aircraft. Simulations were run for both zenith and 30° off-zenith viewing directions, and with both solar zenith angle and relative azimuthal angle varied in 2° steps. The output produced by the simulations was so called box air mass factors. These are defined as the ratio between the average path length of the measured light through a certain height layer and the thickness of that layer. Figure 36 shows a few examples of these box air mass factor profiles for 40° solar zenith angle and a few different relative azimuth angles for the 30° off-zenith viewing direction as well as for the zenith viewing direction (which of course has no azimuth angle dependence). If the box air mass factor profile for the zenith viewing direction is subtracted from those for the 30° off-zenith directions, a set of differential box air mass factor profiles is produced. Figure 37 show the differential box air mass factors calculated from the profiles in Figure 36. Under the assumption that the profiles of the measured species and the parameters determining radiative transfer do not have large horizontal variations on a local scale, the resulting column from a DOAS evaluation of a 30° off-zenith spectrum with a zenith spectrum measured close in time as reference should be the height integration of the profile of the species multiplied by the corresponding differential box air mass factor profile.
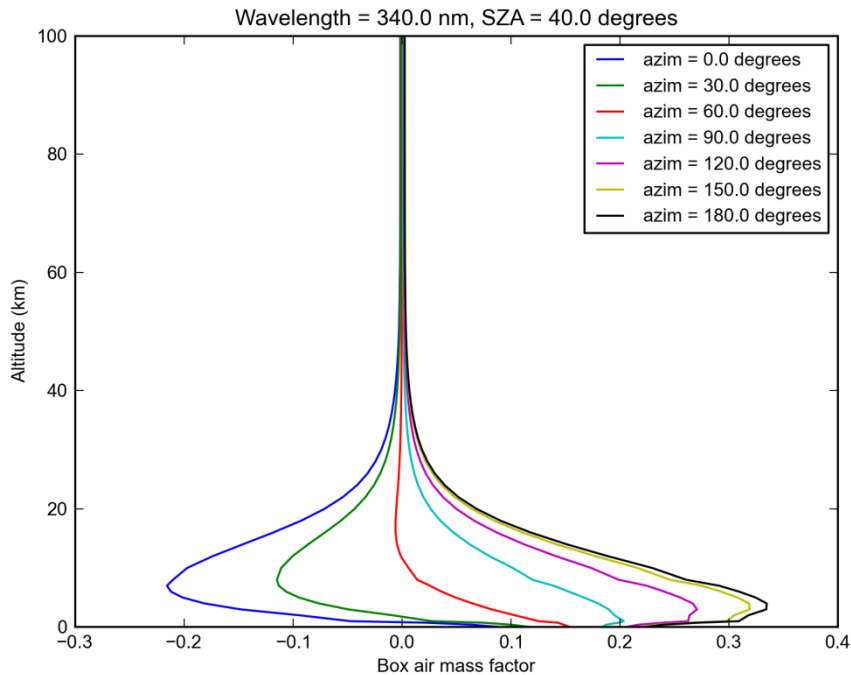
Figure 37 Differential box air mass factors between 30° off-zenith viewing direction and zenith viewing direction for solar zenith angle 40° and a range of relative azimuth angles.

If the concentrations of the species evaluated are assumed to be constant throughout the mixing layer and zero above, an average of the differential box air mass factor profile can be calculated for this layer and the evaluated column should be expected to be this averaged value multiplied with the vertical column in the mixing layer. Figure 38 shows the dependence of this average calculated for a boundary layer height of 2.5 km, referred to as the mixing layer air mass factor, on solar zenith angle and relative azimuth angle. Here it can be seen that the mixing layer column should have its biggest impact on the evaluated columns in viewing directions opposite to the sun, while for viewing directions close to the sun, the air mass factor can even go negative.

In reality the concentration profiles will of course not be zero above the mixing layer. A contribution to the evaluated columns from the atmosphere above the mixing layer can be calculated based on the differential box air mass factor profiles and an a priori concentration profile for this layer. This contribution was determined to be small for realistic concentration profiles for all species examined except for ozone.
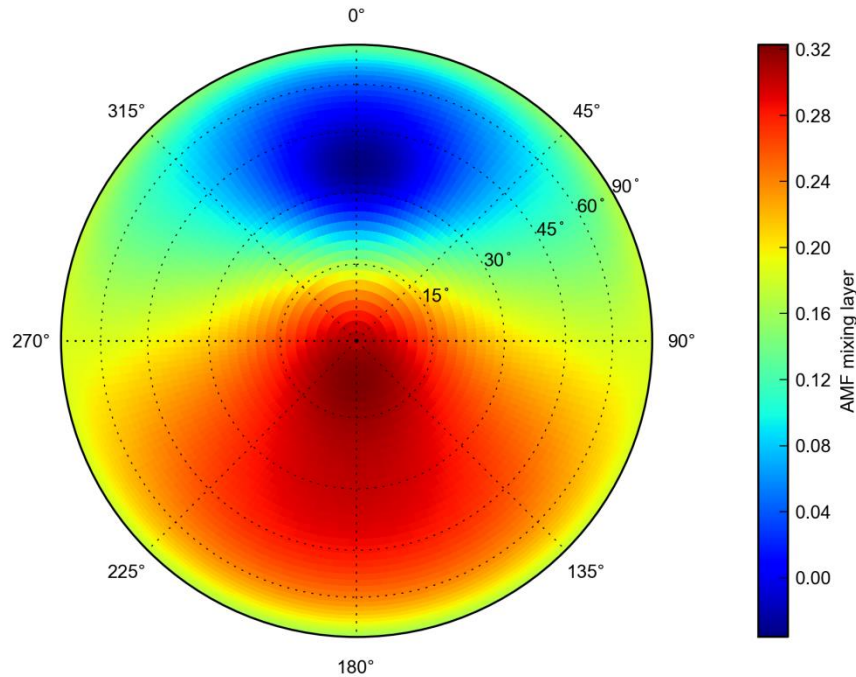
Figure 38 Mixing layer air mass factor for 30° off-zenith spectra evaluated with a zenith spectrum as reference, as a function of solar zenith angle (radial axis) and relative azimuth angle (azimuth axis).

Interpretation of results

In order to apply the results from the radiative transfer simulations, the geometry for each spectrum must be known. The solar zenith and azimuthal direction can easily be calculated based on the date and time and the latitude and longitude. To get the measurement azimuthal angle relative to the sun, the orientation of the measurement vehicle must be known. This was determined based on the driving direction calculated from the GPS data. Figure 39 shows the driving speed and driving direction as calculated from the GPS data for September 25. The azimuth angle for the left or right angle was calculated by subtracting or adding 90° to the driving direction. Based on the solar zenith angle and the relative azimuth angle, a value for the mixing layer air mass factor could be interpolated from the data in Figure 38 for each measured off-zenith spectrum. Similarly, an effective column for the atmosphere above the mixing layer could be calculated as discussed above. The mixing layer column could then be calculated by subtracting the calculated column from the upper atmosphere from the evaluated column and dividing by the mixing layer air mass factor. To reduce noise, a moving average of 4 subsequent off-zenith spectra was used and evaluated with a reference of 8 averaged zenith spectra covering approximately the same period. The computed values for the mixing layer air mass factor and the upper atmosphere column were also averaged for the corresponding time periods. In this scheme, each evaluated spectrum would represent a time period of approximately 40 seconds. Additionally, it was found that for small values of the mixing layer air mass factor, which typically correspond to measurements with relative azimuth angle less than 90°,the results often became very chaotic. This can be understood for a number of reasons. Firstly, dividing by a small value will of course always amplify noise. Secondly, for a small angle between the measurement direction and the sun, the correctness of the radiative transfer simulations will be more dependent on properly accounting for forward scattering of aerosols, which may require detailed knowledge of the aerosol scattering phase function. Thirdly, as seen in Figure 37, the differential box air mass factor profiles for small

relative azimuth angles show much larger variation within the lowest layers. This means that any deviations from the assumption of a constant profile within the mixing layer will give rise to larger errors for these directions. Because of all this, measurements with mixing layer air mass factor below 0.15 were filtered out. This meant that for most times left and right results are not available simultaneously.
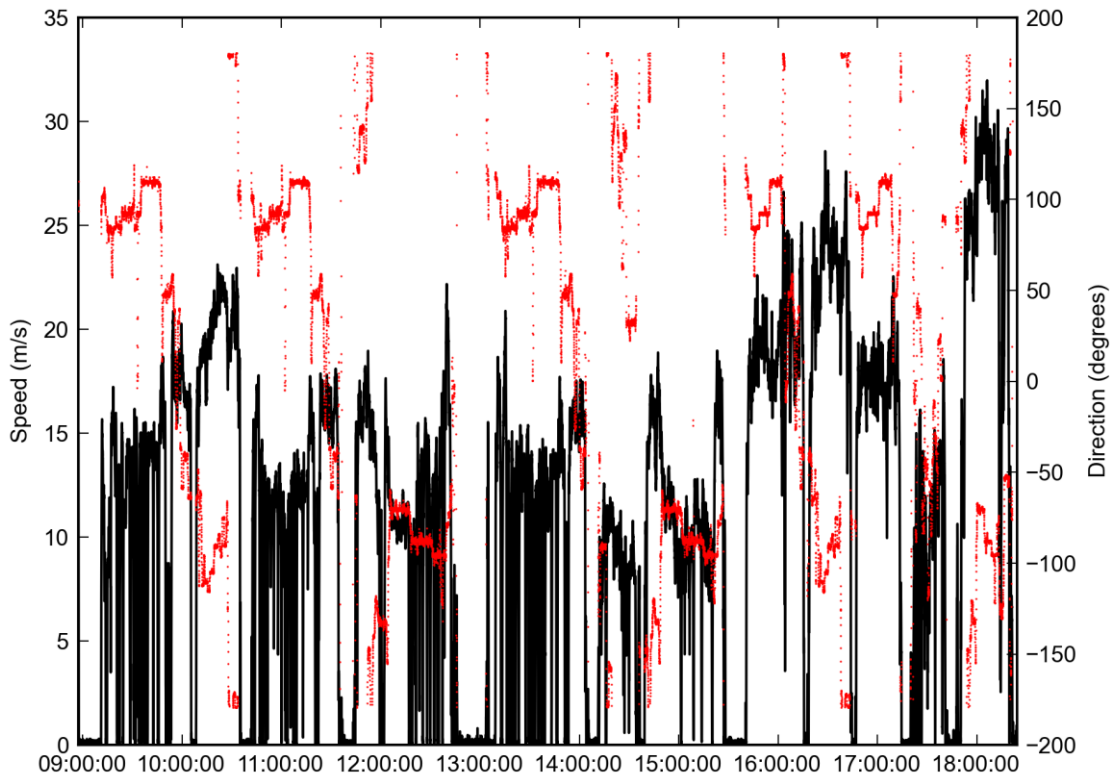
Figure 39 Driving speed (black line) and direction (red dots) calculated based on GPS data for September 25, 2013.

Figure 40 shows an example of the results for HCHO from September 25. Here the calculated mixing layer columns are shown together with the normal relative column evaluation series for the entire day. The relative column series has been offset to match the absolute columns on average. The absolute column time series is obviously still more noisy than the relative column one, but this is not unexpected since the assumption of no large horizontal variations in the atmosphere will certainly not hold true everywhere. This is confirmed by the observation that the absolute columns time series seem to be more stable when there are no large variations in the relative column time series, which is typically when driving on the upwind side of the Ship Channel. Instead the absolute columns are least stable when the relative columns indicate that the vehicle is passing a large plume, which would be a very clear violation of the assumption of little horizontal variation. Figure 41 shows the corresponding results for NO_2 for the same day. Comparing Figure 40 and Figure 41 illustrates that the background concentration of HCHO is much larger than for NO_2, while the local variations are much larger for NO_2.

The absolute and relative column time series complement each other. The relative column time series is much less noisy but lacks information about absolute columns and could be prone to baseline drifts. The absolute column time can be used to determine an offset for the relative column time series and provides some checks against baseline drift. This way an absolute column time series with the same noise level as for the relative column time series. This merged data product is better suited for comparing to other measurements in the DISCOVER-AQ campaign and for examining large scale plumes.
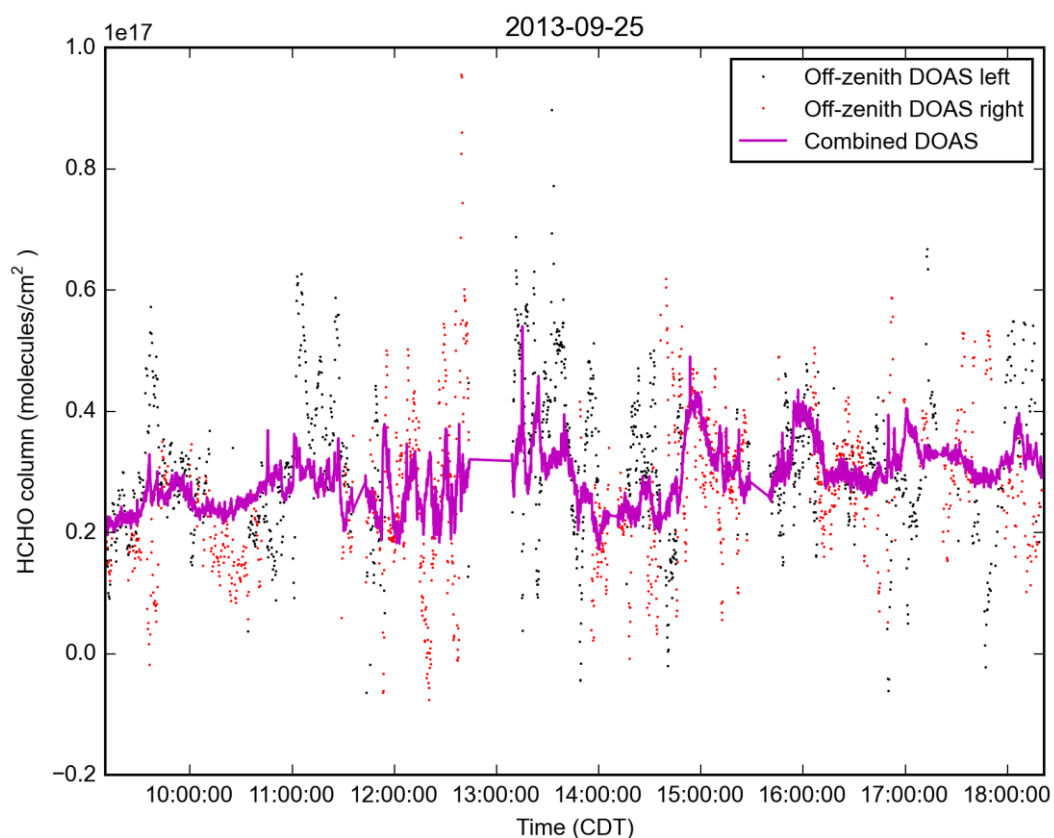
Figure 40 Evaluated absolute HCHO columns for the off-zenith measurements (black dots – left side tilt, red dots – right side tilt) together with relative HCHO columns evaluated with standard evaluation. The relative column time series has been offset to match the absolute columns on average.
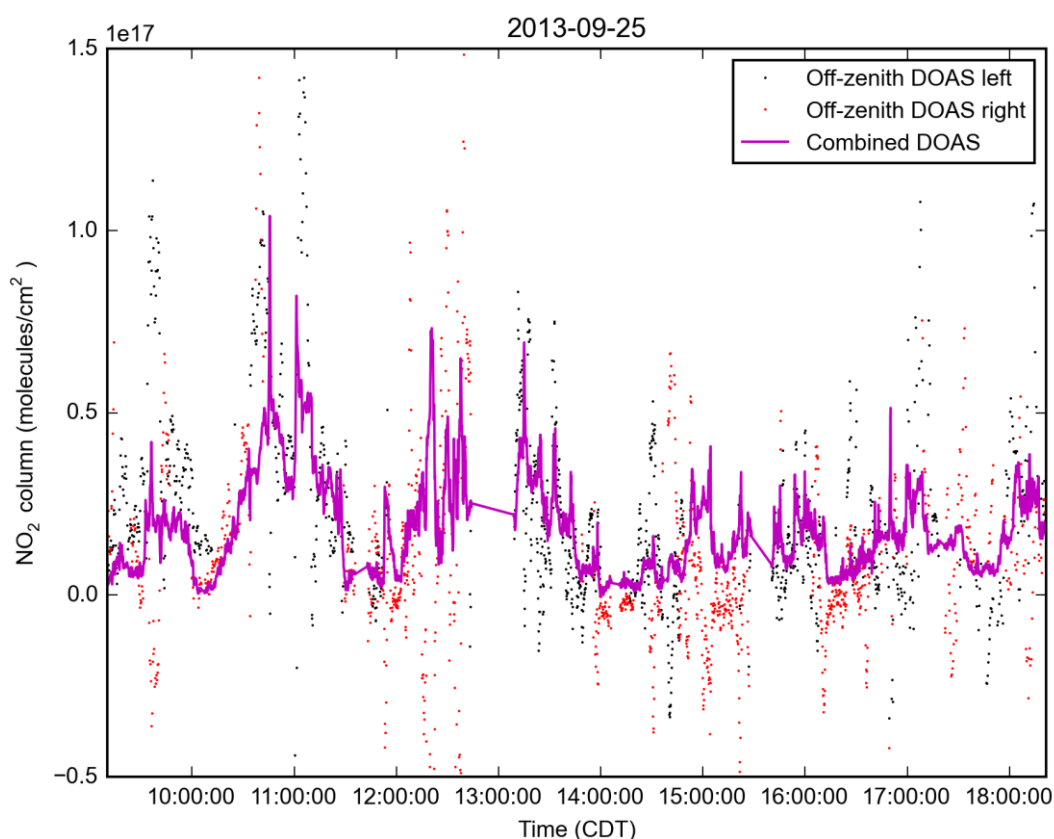
Figure 41 Evaluated absolute NO$_2$ columns for the off-zenith measurements (black dots – left side tilt, red dots – right side tilt) together with relative NO$_2$ columns evaluated with standard evaluation. The relative column time series has been offset to match the absolute columns on average.

5.2 New retrievals and flux calculations

For the DOAS measurements the new spectral retrieval with pseudo-absorbers to compensate for changes in instrumental lineshape was applied to all measurement series and the cloud indicator was calculated for each measured spectrum. Additionally absolute column time series were derived based on off-zenith measurements for September 25 and 26. The methods for these procedures are described in previous sections.

Based on this new dataset, flux calculations were remade for SO$_2$, NO$_2$ and formaldehyde. These are presented together with original flux calculations for alkanes, ethene and propene in section 5.4. In this process, the cloud indicator was used to better determine which measurements to include in the flux calculations. This resulted in the inclusion of some measurements originally not used as well as the exclusion of some measurements previously determined as not significantly affected by clouds. Figure 42 shows an example of an NO$_2$ measurement originally used for flux calculations at Baytown (sector HSC 7). The plot below the map shows the evaluated NO$_2$ columns (black line) as well as the cloud indicator (green dots). The significant drop in the cloud indicator value seen repeatedly in the plume indicates the interference of scattered clouds. The decrease in the cloud indicator seems to be partly correlated with increases in NO$_2$ column. This indicates that these elevated NO$_2$ columns may be at least partly due to changes in radiative transfer and hence an NO$_2$ flux calculated based on this measurement may give a significant overestimation.

Figure 42 Mobile DOAS measurement of NO₂ northwest of Baytown (HSC 7) affected by clouds on September 8, 2013, 16:55–17:00. Each measured spectrum is represented with a point, which color and size indicate the evaluated integrated vertical NO₂ column. The NO₂ column by distance driven through the plume is also shown in the lower part of the figure together with the cloud indicator (green). A line from each point indicates the direction from which the wind is blowing.

5.3 Comparison to data from DISCOVER-AQ

The Mobile DOAS absolute column datasets for NO₂ and HCHO, as described in Section 5.1.5, have been compared with three other datasets from the DISCOVER-AQ campaign: stationary PANDORA measurements, in-situ measurements from the low altitude P-3B aircraft, and ACAM measurements from the high altitude B200 aircraft. PANDORA is a stationary solar tracking DOAS instrument which provided direct sun measurements from a number of different sites in the Greater Houston area during the 2013 DISCVOER-AQ campaign. Three of these sites, Deer Park, Moody Tower and Channelview, were close enough to the typical measurement route of the SOF vehicle to be interesting for comparisons with the Mobile DOAS data set. The locations of these sites as well as the measurement route for the SOF vehicle are shown in Figure 43. Since the ground sites were also used for flying in spirals with the P-3B aircraft and for the B200 aircraft to fly over, all comparisons were based on these three sites. Continuous PANDORA measurements of vertical NO₂ columns are available from these sites for most of the time, but unfortunately no HCHO data has been released. For the Mobile DOAS measurements a section of the measurement route was chosen to be most representative of the measurements for each of the ground sites. These sections are marked with beige arrows in Figure 43. Each time the SOF vehicle traversed one of these sections provided one comparison opportunity. For each such opportunity the mean of all column measurements within the section was calculated, as well as the 5 and 95 percentiles to illustrate the variability. The P-3B aircraft flew a route which included spirals up or down through the boundary layer over each of the ground sites. This flight route is shown in cyan in Figure 43. From the aircraft in-situ measurements of NO₂ were made using the NCAR 4-channel chemiluminescence instrument and of HCHO with the NCAR Difference Frequency Generation Absorption Spectrometer (DFGAS). Each spiral was divided into 100 meter bins

and an average concentration was calculated for all measurements in each bin. These profiles were integrated to produce total boundary layer columns. Concentrations for bins with no measurements were assigned by extrapolation in some cases. Each column calculated this way provided one comparison data point. The B200 aircraft flew a measurement route that regularly passed over each of the ground sites. A typical measurement route is shown in green and red in Figure 43. From this aircraft the Airborne Compact Atmospheric Mapper (ACAM) instrument performed downward-looking DOAS measurements of NO_2 and HCHO. The instrument was equipped with a cross-track scanner to provide a swath of measurements along the track, but only the nadir measurements were used for these comparisons. The data available from these measurements are only slant columns since no inversion to vertical columns has been made. For this reason these measurements should not necessarily be expected to be directly comparable to vertical columns provided by the other methods. For each pass over one of the sites the mean of all nadir measurements within an area roughly corresponding to the horizontal extent of the P-3B spirals was calculated, as well as the 5 and 95 percentiles to illustrate the variability.
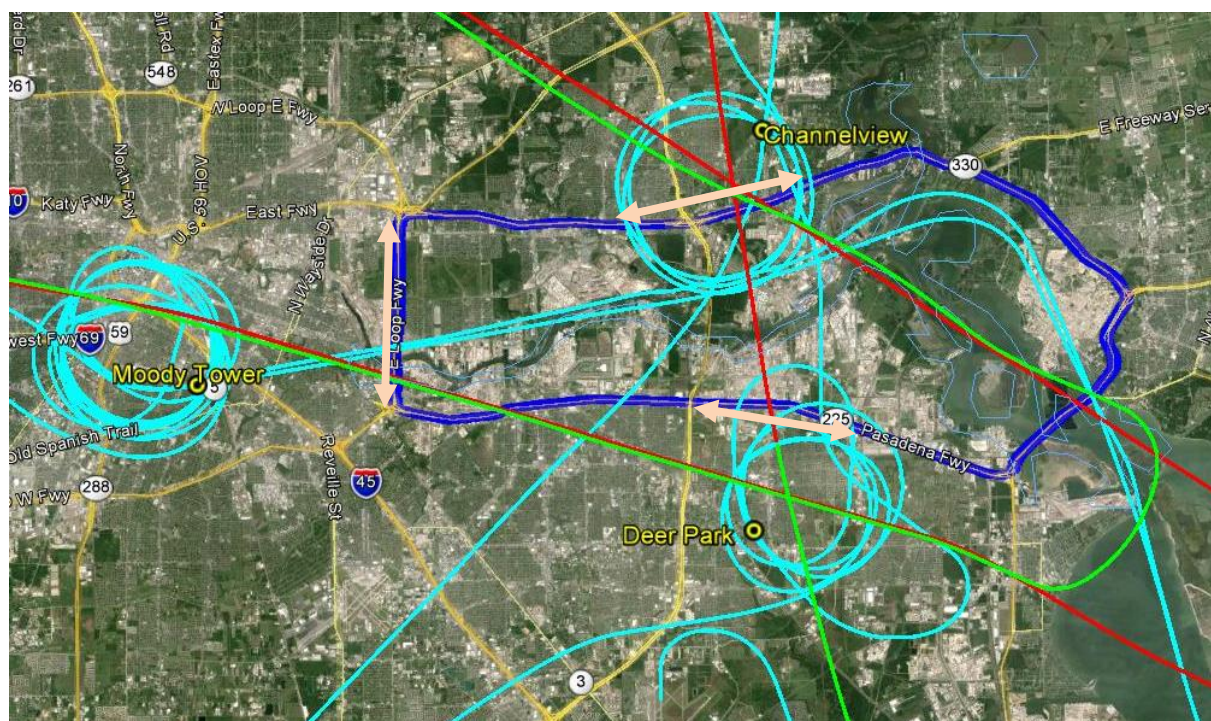
Figure 43 Map of the area around Houston Ship Channel showing the location of the different measurements compared. Yellow markers show the three ground sites where stationary PANDORA measurements were performed: Deer Park, Moody Tower and Channelview. The flight route of the low altitude P-3B aircraft with its spirals above the three ground sites is shown in cyan. The typical measurement path of the Mobile DOAS vehicle is shown in blue and the flight path of high altitude B200 aircraft is shown in green and red. Beige arrows shows the sections of the Mobile DOAS route used for comparison with the three sites.

Figure 44 shows a comparison of all the measurements of NO_2 by the different methods at the three sites on September 25 plotted as a function of time. For the Deer Park site a relatively high level of agreement is seen. All measurements in an episode from approximately 10:30 to 12:00 show highly elevated NO_2 levels. Although there seems to be some disagreement between the different methods, the Mobile DOAS measurements indicate that there is also large local variability. Since the different methods are sampling slightly different air masses, it is not surprising to find this level of disagreement in such variable conditions. Later in the day the spiral measurement seems to indicate higher NO_2 columns than the PANDORA, but

the variability within Mobile DOAS measurements seem to approximately bridge this gap with the mean values somewhere in between. For the Moody Tower site, there seems to be fairly good agreement between spirals, PANDORA and Mobile DOAS, although the Mobile DOAS columns seem to be a bit high at times. This discrepancy is somewhat understandable, since Moody Tower is the site that is furthest from the Mobile DOAS measurement route and the NO_2 concentration might be expected to be higher closer to the Ship Channel. For the Channelview site, the spirals once again show slightly higher values than the PANDORA in the afternoon, but for this site the Mobile DOAS agrees better with the PANDORA.
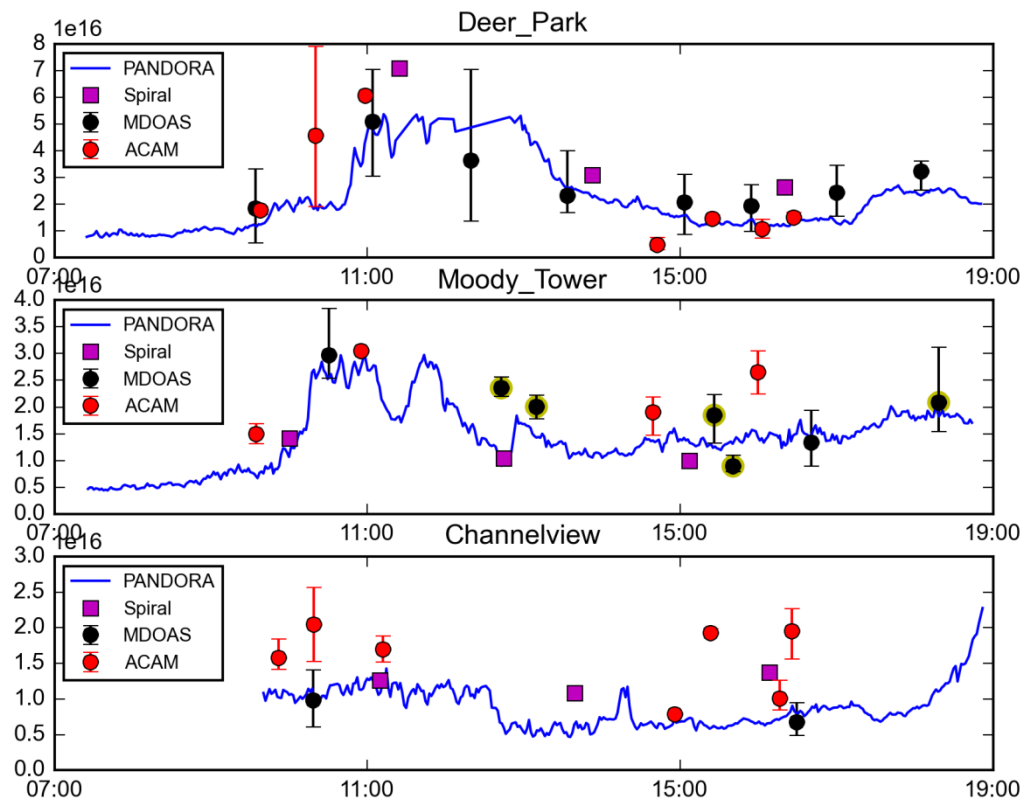
Figure 44 Comparison of NO_2 columns measured at three sites, Deer Park, Moody Tower and Channelview, at different times with different methods throughout September 25, 2013. ACAM columns are raw slant columns and have not been inverted to vertical columns. Error bars for Mobile DOAS and ACAM columns indicate the 5 to 95 percentile range of measurements during one pass, while the circles indicate the mean. Yellow circles around black Mobile DOAS circles indicate that the data point represents a slightly different section than marked in the map since a different route was driven.

Figure 45 shows a comparison of all the measurements of HCHO by the different methods at the three sites on September 25 plotted as a function of time. Unfortunately there are no PANDORA measurements of HCHO available and the ACAM measurements seem to be fairly unstable so this is mostly a comparison between the spirals and the HCHO measurements. Compared to the NO_2 measurements the variations in HCHO columns over the day seem to be small for both Mobile DOAS and the spirals. For the Deer Park site there seem to be quite good agreement between Mobile DOAS and the spirals, while for the Moody Tower site Mobile DOAS shows significantly higher columns, especially in the early part of the day. This could again be due to the fact that the Moody Tower site is further away from the Mobile DOAS measurement route than the other sites and concentration might be

expected to be higher closer to the Ship Channel. For the Channelview site, there are fewer passes with the Mobile DOAS, but the columns seem to agree slightly better than for the Moody Tower site, although not as good as for Deer Park.
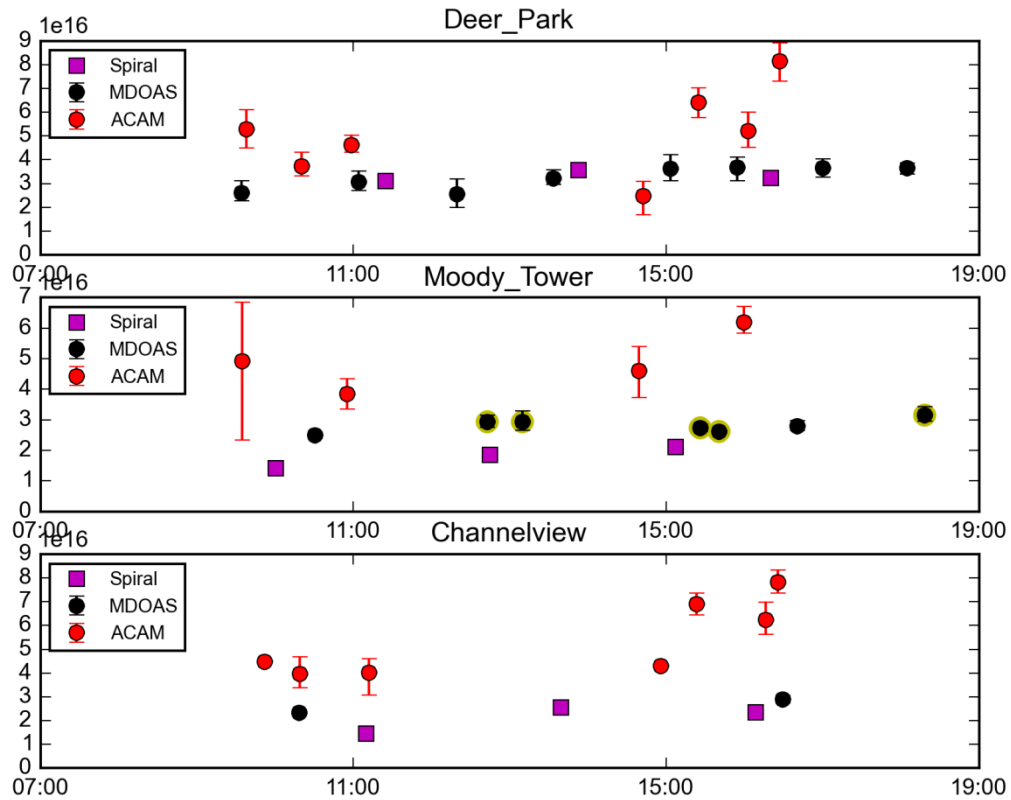
Figure 45 Comparison of HCHO columns measured at three sites, Deer Park, Moody Tower and Channelview, at different times with different methods throughout September 25, 2013. ACAM columns are raw slant columns and have not been inverted to vertical columns. Error bars for Mobile DOAS and ACAM columns indicate the 5 to 95 percentile range of measurements during one pass, while the circles indicate the mean. Yellow circles around black Mobile DOAS circles indicate that the data point represents a slightly different section than marked in the map since a different route was driven.

5.4 Emission measurements

5.4.1. Houston Ship Channel

Alkanes

Figure 46 shows and example of an alkane measurement south of Houston Ship Channel covering sectors 1-5. Unfortunately, due to the lack of northerly wind, this is the only alkane measurement traverse that allowed separation of all these sectors. Some measurement in easterly winds also gave the sum of emissions from sector 4 and 5. As seen in Table 4, which summarizes all alkane measurements in HSC processed, there is notable discrepancy between the few sector specific measurements and the measurements of total emissions. Since there are more total measurements, they should probably be considered as more reliable.
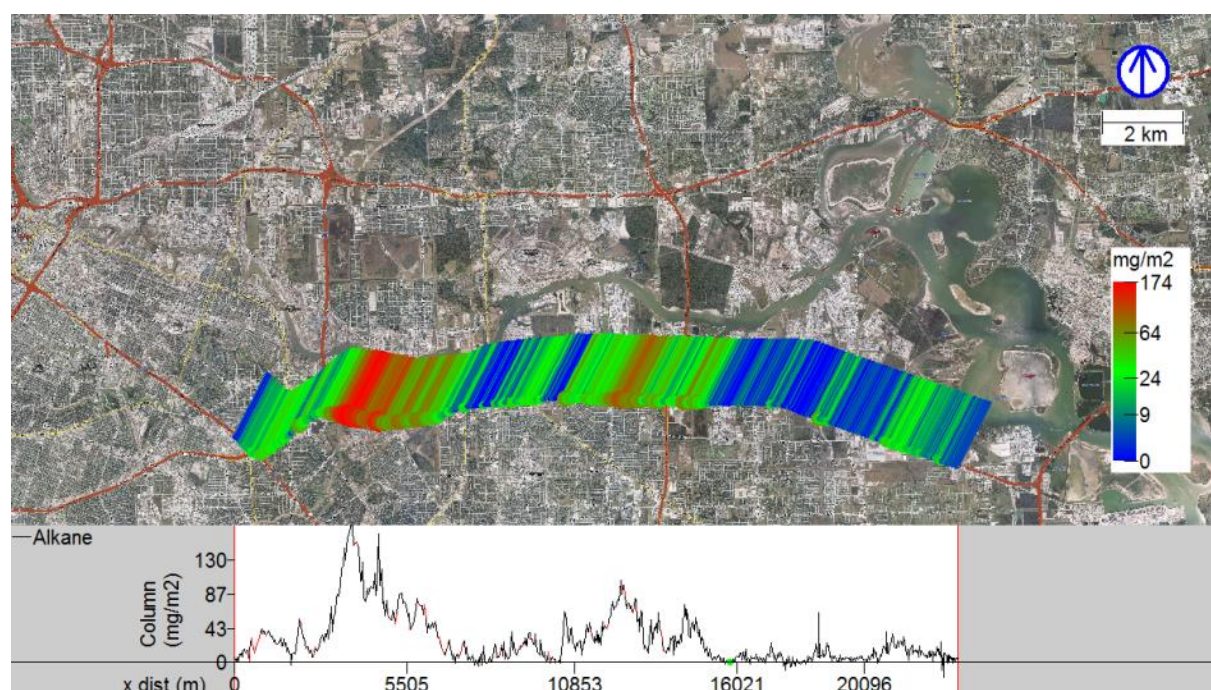
Figure 46 SOF measurement of alkanes south of the Houston Ship Channel on September 22, 2013, 09:40–10:15. Each measured spectrum is represented with a point, which color and size indicate the evaluated integrated vertical alkane column. The alkane column by distance driven through the plume is also shown in the lower part of the figure. A line from each point indicates the direction from which the wind is blowing.

Table 4 Summary of alkane emission transects in Houston Ship Channel. N is the number of measurement transects, Start and Stop are the start and stop times, Mean and SD are the average and standard deviations of the

measured emission fluxes, and WS and WD are the wind speed and wind directions given as an average and a range respectively.

Region	Day	N	Start	Stop	Mean (kg/h)	SD (kg/h)	WS (m/s)	Range WD (deg)	
HSC 1									
	130922	1	94229	95043	3227.9	-	10.1	62	62
Total		**1**	**94229**	**95043**	**3227.9**	**-**	**10.1**	**62**	**62**
HSC 2									
	130922	1	95041	95638	714.7	-	10.1	61	61
Total		**1**	**95041**	**95638**	**714.7**	**-**	**10.1**	**61**	**61**
HSC 3									
	130922	1	95635	100402	1693.7	-	10.0	60	60
Total		**1**	**95635**	**100402**	**1693.7**	**-**	**10.0**	**60**	**60**
HSC 4									
	130922	1	100359	100838	199.2	-	10.0	60	60
Total		**1**	**100359**	**100838**	**199.2**	**-**	**10.0**	**60**	**60**
HSC 5									
	130922	1	100835	101226	573.7	-	9.9	59	59
Total		**1**	**100835**	**101226**	**573.7**	**-**	**9.9**	**59**	**59**
HSC 7									
	130910	1	153524	154815	410.2	-	8.5	121	121
	130918	1	165320	170513	496.8	-	7.7	133	133
	130925	1	172944	173644	248.1	-	2.3	41	41
Total		**3**	**153524**	**173644**	**385.0**	**126.3**	**6.2**	**41**	**133**
HSC all									
	130909	1	142650	144859	17612.7	-	8.4	126	126
	130925	2	154156	171458	13822.2	7326.2	2.8	28	41
	130926	2	92900	180245	12206.2	1217.4	6.0	137	192
Total		**5**	**92900**	**180245**	**13933.9**	**4321.0**	**5.2**	**28**	**192**
HSC 4+5									
	130918	7	95826	115043	603.6	137.8	6.2	102	109
	130926	3	164237	170732	627.8	144.9	7.8	135	135
Total		**10**	**95826**	**170732**	**610.8**	**132.2**	**6.7**	**102**	**135**

Alkenes

For the alkenes, there were more HSC measurements that could be separated into sectors and the sum of the sector results generally showed better agreement with measurements of total emissions. Figure 47 and Figure 48 give examples of an ethene and a propene measurement in HSC. All ethene and propene emission transects in HSC are summarized in Table 5 and Table 6 respectively.
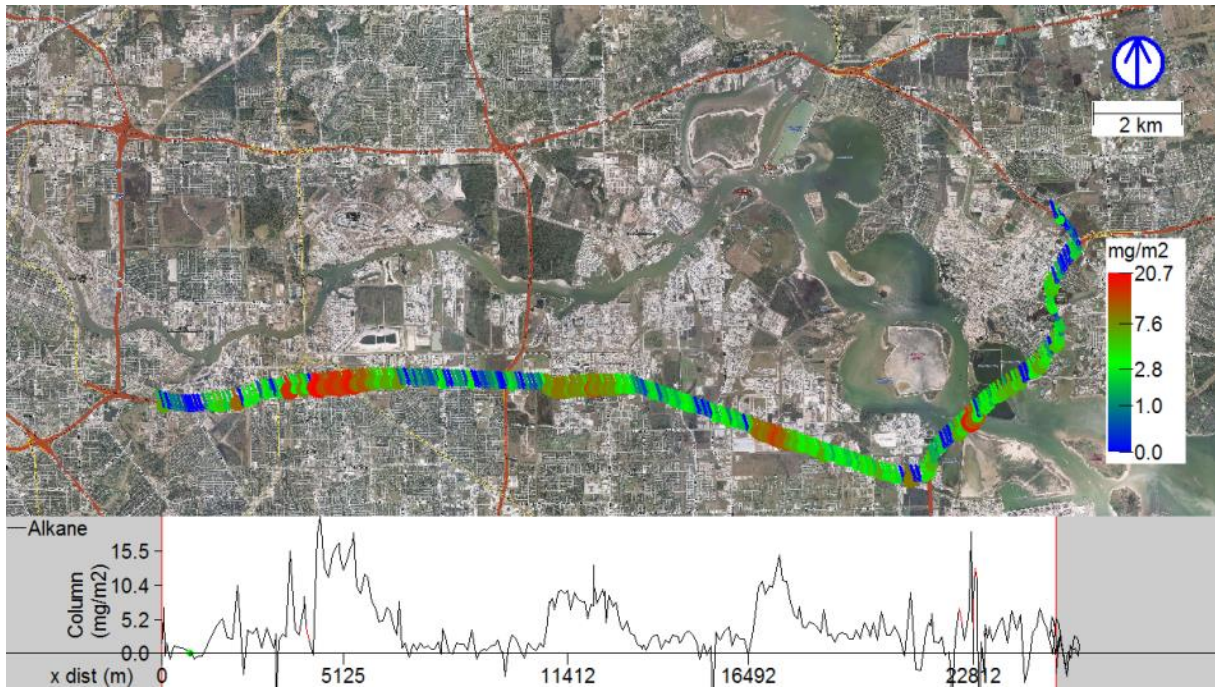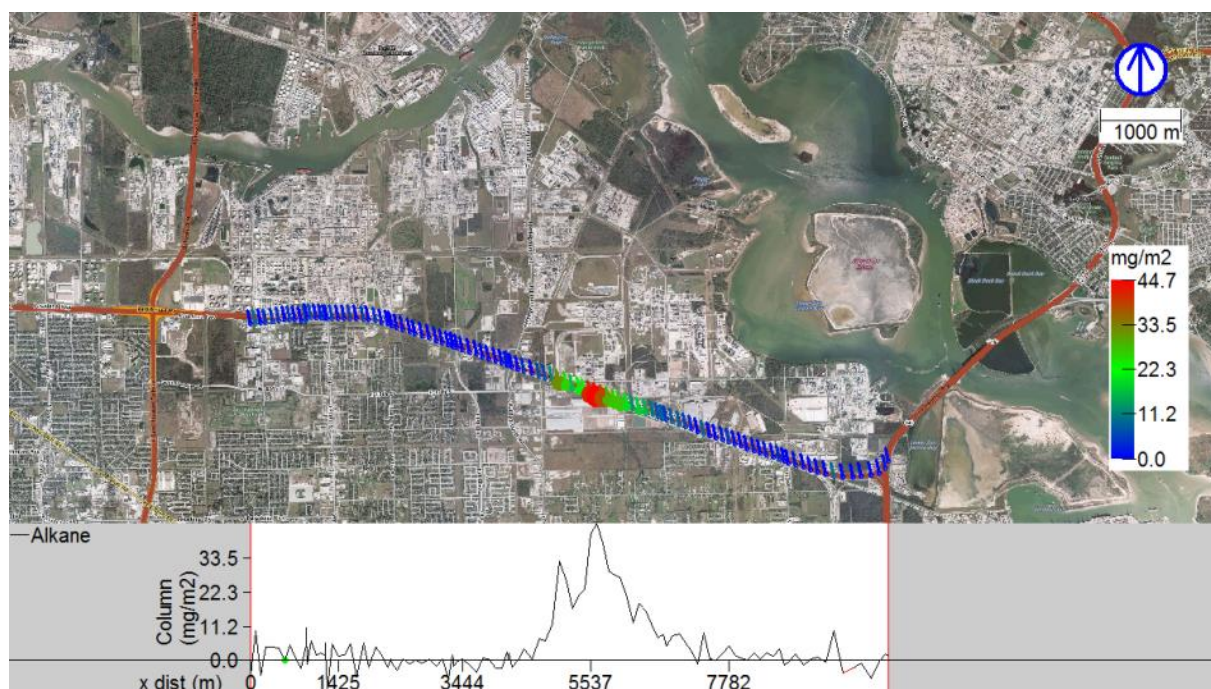
Figure 47 SOF measurement of ethene south of the Houston Ship Channel on September 25, 2013, 10:40–11:30. Each measured spectrum is represented with a point, which color and size indicate the evaluated integrated vertical ethene column. The ethene column by distance driven through the plume is also shown in the lower part of the figure. A line from each point indicates the direction from which the wind is blowing.

Table 5 Summary of ethene emission transects in Houston Ship Channel.

Region	Day	N	Start	Stop	Mean (kg/h)	SD (kg/h)	WS (m/s)	Range WD (deg)	
HSC 1									
	130924	3	163239	181009	48.3	4.3	6.0	8	17
	130925	3	104123	131645	62.1	20.3	1.7	40	346
Total		**6**	**104123**	**181009**	**55.2**	**15.1**	**3.8**	**8**	**346**
HSC 2									
	130924	4	151359	180259	109.9	23.1	5.6	3	355
	130925	4	104917	151805	137.7	27.2	2.1	28	346
Total		**8**	**104917**	**180259**	**123.8**	**27.7**	**3.8**	**3**	**355**
HSC 3									
	130913	1	91330	91515	83.3	-	5.3	30	30
	130924	5	141931	175201	143.8	88.0	5.7	4	360
	130925	4	105857	150843	77.3	12.4	2.1	28	346
Total		**10**	**91330**	**175201**	**111.2**	**68.4**	**4.2**	**4**	**360**
HSC 4									
	130924	5	140537	174324	80.6	53.3	5.9	2	357
	130925	4	110937	150014	47.0	5.4	2.1	28	346
Total		**9**	**110937**	**174324**	**65.6**	**41.8**	**4.2**	**2**	**357**
HSC 5									
	130924	5	135946	173927	91.8	54.7	6.0	4	358
	130925	3	111251	145559	93.5	59.7	2.4	28	343
Total		**8**	**111251**	**173927**	**92.4**	**52.2**	**4.7**	**4**	**358**
HSC 6									
	130924	4	154331	173455	56.0	28.4	6.1	5	359
	130925	4	111639	145202	44.9	38.1	2.1	28	346
Total		**8**	**111639**	**173455**	**50.4**	**31.7**	**4.1**	**5**	**359**
HSC 7									
	130903	1	152552	153328	157.5	-	5.6	182	182
	130913	2	110206	111532	89.5	42.6	3.8	55	55
	130924	2	130104	134412	121.7	45.7	6.4	14	18
	130925	3	111908	143355	55.6	9.7	1.7	40	346
	130926	1	111031	111723	89.2	-	4.5	153	153
Total		**9**	**110206**	**153328**	**92.9**	**42.0**	**4.0**	**14**	**346**
HSC all									
	130925	5	90955	152303	485.5	83.8	2.3	28	346
	130926	1	110430	114603	421.9	-	4.7	155	155
Total		**6**	**90955**	**152303**	**474.9**	**79.3**	**2.7**	**28**	**346**
HSC 4+5									
	130911	3	115233	142938	251.9	45.8	6.1	104	116
	130912	3	91558	164937	274.5	98.5	6.2	71	121
	130913	1	170023	170737	222.5	-	5.5	148	148
	130926	5	152822	162553	170.4	99.2	6.5	141	146
Total		**12**	**91558**	**170737**	**221.1**	**89.1**	**6.2**	**71**	**148**

Table 6 Summary of propene emission transects in Houston Ship Channel.

Region	Day	N	Start	Stop	Mean (kg/h)	SD (kg/h)	WS (m/s)	Range WD (deg)	
HSC 3									
	130913	1	101647	101820	48.8	-	3.9	38	38
	130924	4	142107	174923	81.8	16.2	5.6	0	356
	130925	2	93200	122258	27.7	17.5	2.1	322	346
Total		**7**	**93200**	**174923**	**61.6**	**29.4**	**4.3**	**0**	**356**
HSC 5									
	130912	5	91531	164705	393.5	395.5	6.4	71	123
	130913	1	101942	102052	123.2	-	3.9	39	39
	130924	4	140528	173953	109.2	38.0	5.8	3	358
	130925	5	94104	145701	151.4	19.4	2.0	40	346
	130926	5	152849	162553	212.8	40.2	6.5	141	147
Total		**20**	**91531**	**173953**	**217.4**	**214.1**	**5.1**	**3**	**358**
HSC 7									
	130913	2	110142	111445	350.6	4.2	3.8	55	55
	130924	2	130509	134125	132.4	24.3	6.4	14	18
	130925	2	115232	142923	68.8	1.3	1.8	40	346
	130926	2	111021	140543	153.2	60.3	5.3	141	153
Total		**8**	**110142**	**142923**	**176.2**	**115.3**	**4.3**	**14**	**346**

Figure 48 SOF measurement of propene form Area 5 in Houston Ship Channel on September 25, 2013, 11:00–11:20. Each measured spectrum is represented with a point, which color and size indicate the evaluated integrated vertical propene column. The propene column by distance driven through the plume is also shown in the lower part of the figure. A line from each point indicates the direction from which the wind is blowing.

Sulfur dioxide (SO$_2$)

All the measurements of the SO$_2$ in HSC are summarized in Table 7. The results labeled *HSC 0* refers to a small area just west of sector 1 which contains a large SO$_2$ source. One of the measurement transects the fluxes have been derived from is shown in Figure 49.
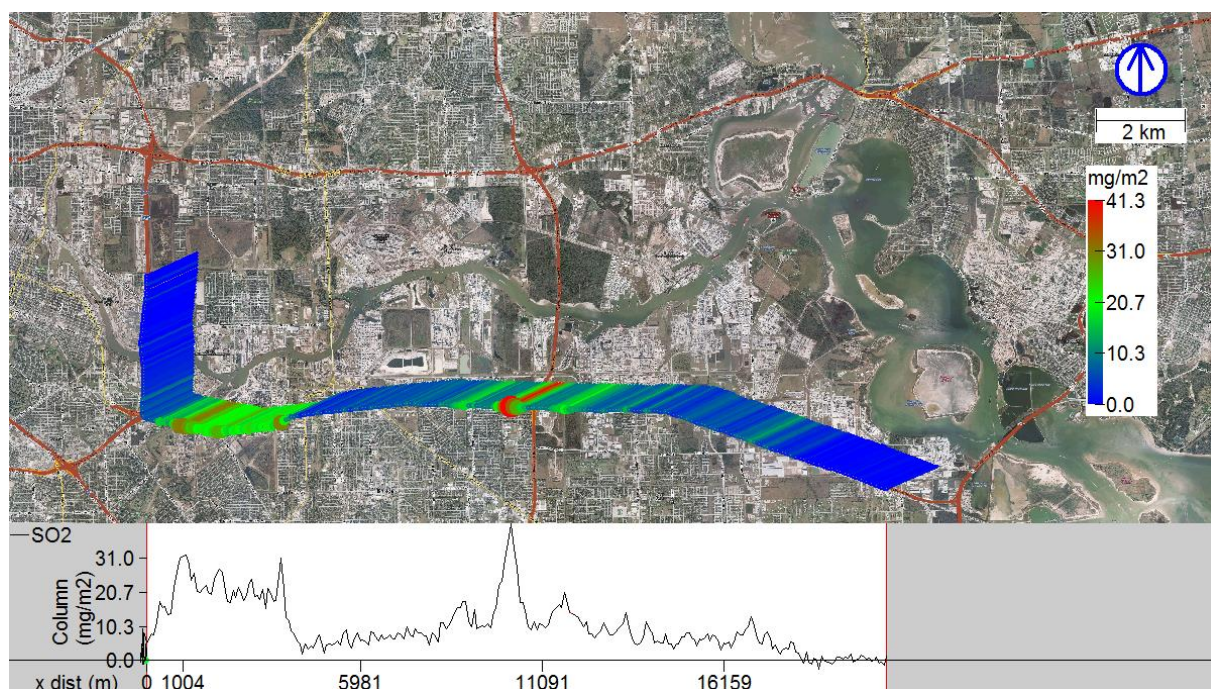
Figure 49 Mobile DOAS measurement of SO$_2$ south of Houston Ship Channel on September 12, 2013, 10:00–10:20. Each measured spectrum is represented with a point, which color and size indicate the evaluated integrated vertical SO$_2$ column. The SO$_2$ column by distance driven through the plume is also shown in the lower part of the figure. A line from each point indicates the direction from which the wind is blowing.

Table 7 Summary of SO$_2$ emission transects in Houston Ship Channel.

Region	Day	N	Start	Stop	Mean (kg/h)	SD (kg/h)	WS (m/s)	Range WD (deg)	
HSC 0									
	130903	1	134958	135226	309.4	-	2.6	204	204
	130904	1	100622	100734	1118.6	-	2.5	262	262
	130913	1	90132	90223	448.3	-	4.8	29	29
	130922	2	94209	163348	636.0	186.7	8.6	31	62
	130924	6	102443	164622	564.2	250.1	4.6	0	23
	130925	2	123952	154239	149.3	85.2	2.5	28	343
Total		13	90132	164622	525.5	299.4	4.6	0	343
HSC 1									
	130906	4	80636	180046	425.6	5.9	6.2	36	140
	130909	1	142826	143316	301.7	-	8.3	126	126
	130912	5	93601	170719	430.7	87.0	6.1	66	126
	130913	3	90335	121014	496.8	71.5	4.5	29	68
	130918	2	155726	173627	482.3	48.5	7.4	129	132
	130922	2	94701	162842	432.5	24.9	8.7	30	61
	130924	7	92223	165103	477.1	160.3	4.5	2	356
	130925	3	122713	165505	460.6	105.6	2.4	28	341
Total		27	80636	180046	451.8	100.2	5.5	2	356
HSC 3									
	130908	1	162336	162942	304.4	-	5.3	133	133
	130909	1	143412	144241	334.7	-	8.4	126	126
	130912	3	100756	143050	422.3	58.7	5.6	65	93
	130913	2	91331	102016	508.1	68.1	4.6	30	38
	130918	1	172523	173003	643.4	-	7.6	130	130
	130922	3	95749	162027	457.4	64.5	8.5	27	60
	130924	7	91227	171400	362.3	75.7	4.5	1	356
	130925	2	145540	155743	429.0	114.4	2.8	28	40
	130926	2	93649	113114	592.4	274.4	5.0	156	187
Total		22	91227	173003	432.6	122.0	5.4	1	356
HSC 6									
	130911	3	94250	135328	40.4	13.6	7.1	96	107
	130914	2	91620	104907	64.3	44.1	4.7	75	80
Total		5	91620	135328	50.0	27.4	6.1	75	107
HSC 7									
	130903	1	152457	152953	324.1	-	5.5	180	180
	130908	1	163210	163958	328.6	-	4.9	130	130
	130909	1	144553	145027	414.5	-	8.5	126	126
	130911	4	104520	173344	419.0	96.8	7.0	105	126
	130912	1	113724	114133	268.6	-	6.5	74	74
	130913	4	92151	111846	431.4	60.0	4.2	30	55
	130914	2	95756	101838	389.0	116.4	4.4	73	77
	130918	1	170011	170503	335.8	-	7.8	133	133
	130922	6	100901	161410	421.6	167.3	7.9	25	66
	130924	3	90250	135439	479.4	60.6	5.3	11	34

130925	3	95459	143319	398.1	112.4	2.6	291	324
130926	3	92833	140559	402.1	109.5	5.3	141	194
Total	**30**	**90250**	**173344**	**407.3**	**102.9**	**5.8**	**11**	**324**
HSC all								
130912	3	100052	112324	1820.0	294.0	6.0	66	73
130913	3	90247	121026	1712.2	134.2	4.4	30	62
130914	1	91436	93211	1694.1	-	5.2	74	74
130922	2	94701	162739	1460.4	277.1	8.7	29	60
130924	1	90250	93210	1618.3	-	3.0	20	20
Total	**10**	**90247**	**162739**	**1683.0**	**223.1**	**5.7**	**20**	**74**

Nitrogen dioxide (NO$_2$)

An example of an NO$_2$ measurement transect in HSC is shown in Figure 50. All NO$_2$ measurements in HSC are summarized in Table 8.
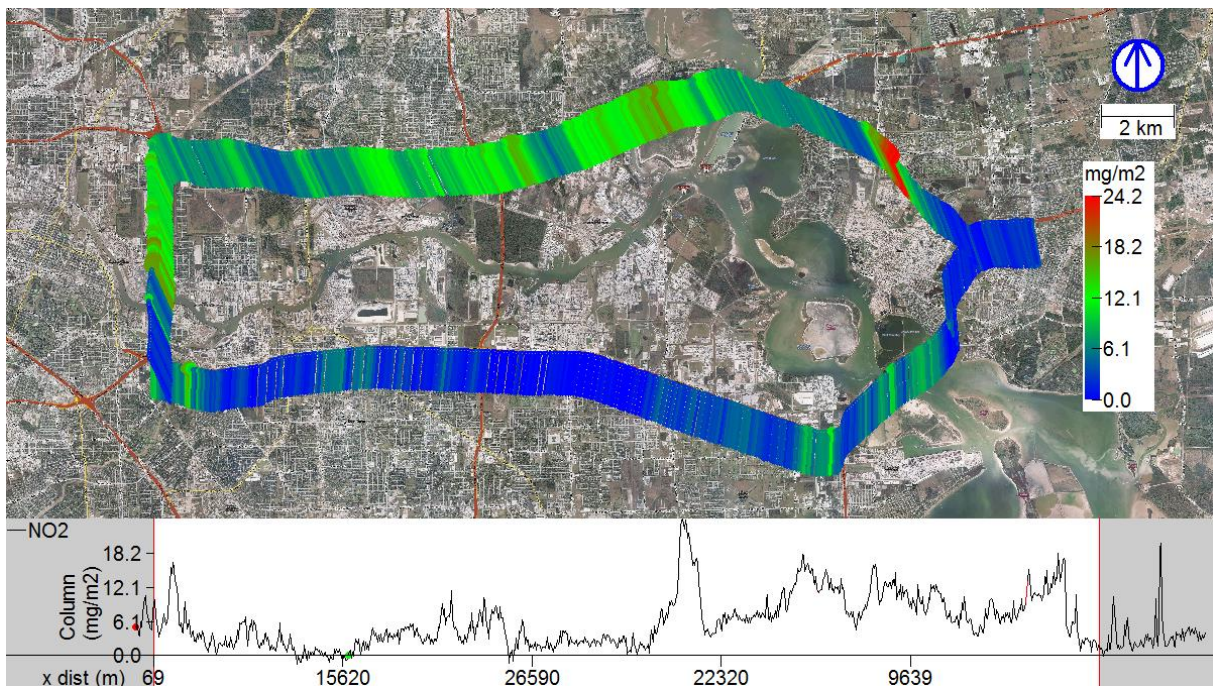
Figure 50 Mobile DOAS measurement of NO$_2$ south of Houston Ship Channel on September 26, 2013, 11:25–11:50. Each measured spectrum is represented with a point, which color and size indicate the evaluated integrated vertical NO$_2$ column. The NO$_2$ column by distance driven through the plume is also shown in the lower part of the figure. A line from each point indicates the direction from which the wind is blowing.

Table 8 Summary of NO₂ emission transects in Houston Ship Channel.

Region	Day	N	Start	Stop	Mean (kg/h)	SD (kg/h)	WS (m/s)	Range WD (deg)	
HSC 1									
	130906	2	164930	174623	250.3	11.3	6.3	129	137
	130922	1	94621	95221	252.5	-	10.1	61	61
	130924	3	150514	165146	459.6	73.7	5.2	9	359
Total		**6**	**94621**	**174623**	**355.3**	**123.5**	**6.4**	**9**	**359**
HSC 2									
	130924	3	151319	170348	250.3	42.2	5.0	2	356
Total		**3**	**151319**	**170348**	**250.3**	**42.2**	**5.0**	**2**	**356**
HSC 3									
	130922	2	95657	142319	362.3	76.6	9.0	27	60
	130924	4	152253	175348	522.4	172.0	5.7	0	356
Total		**6**	**95657**	**175348**	**469.1**	**160.5**	**6.8**	**0**	**356**
HSC 4+5									
	130911	2	115605	141123	270.3	22.2	6.1	102	112
	130912	3	141029	164852	400.8	66.2	6.3	84	123
	130913	1	165745	170812	309.7	-	5.5	148	148
	130918	5	95624	115118	208.7	13.2	6.1	102	108
	130924	5	135652	174152	486.7	218.8	6.1	5	359
	130926	5	152625	162850	370.9	112.9	6.5	141	147
	130927	2	121345	125016	533.6	58.8	8.8	125	130
Total		**23**	**95624**	**174152**	**367.5**	**155.8**	**6.4**	**5**	**359**
HSC 7									
	130906	1	154159	154659	289.0	-	6.4	119	119
	130911	2	165118	173352	340.3	50.8	7.3	123	126
	130912	1	113718	114333	297.2	-	6.5	74	74
	130913	2	105855	111846	405.8	36.8	3.8	55	55
	130914	2	95652	102020	344.4	7.6	4.4	73	77
	130918	1	165915	170735	391.6	-	7.8	133	133
	130922	4	104227	155935	296.8	81.9	7.6	25	66
	130924	1	133921	134626	235.1	-	6.5	14	14
	130925	2	115227	143407	210.8	15.4	2.3	297	346
	130926	1	135951	140537	201.5	-	6.0	141	141
Total		**17**	**95652**	**173352**	**306.1**	**75.7**	**5.8**	**14**	**346**
HSC all									
	130903	1	140158	145640	1793.3	-	2.1	210	210
	130909	1	142604	145121	2740.6	-	8.4	126	126
	130912	3	91525	175447	2462.8	700.7	6.2	66	128
	130913	3	90212	121445	2892.9	1281.4	4.4	31	63
	130914	3	85057	113945	2005.3	288.1	5.3	73	79
	130918	2	155534	173723	3018.6	648.2	7.6	131	133
	130922	1	161013	162924	1074.2	-	7.4	29	29
	130924	5	90059	172552	1667.5	296.4	4.0	0	19
	130925	4	91027	171232	2204.0	118.5	2.3	40	299
	130926	2	85213	114840	2420.4	88.3	4.5	166	198

		130927	1	93410	95322	2577.8	-	6.7	130	130
Total			**26**	**85057**	**175447**	**2242.3**	**683.8**	**4.8**	**0**	**299**

Formaldehyde (HCHO)

The formaldehyde measurements in the 2009 campaign discovered one distinct recurring formaldehyde source close to Jefferson Road in HSC. In 2011, this source was repeatedly detected again and another distinct source was found close to the Fred Hartman Bridge. The second source was not detected again during this study. The source at Jefferson Road was not detected as regularly as before during this study and when it was detected, the emissions were typically lower than before. Figure 51 shows on of the formaldehyde measurements at this source. All of the formaldehyde measurements at the Jefferson Road source are summarized in Table 9.
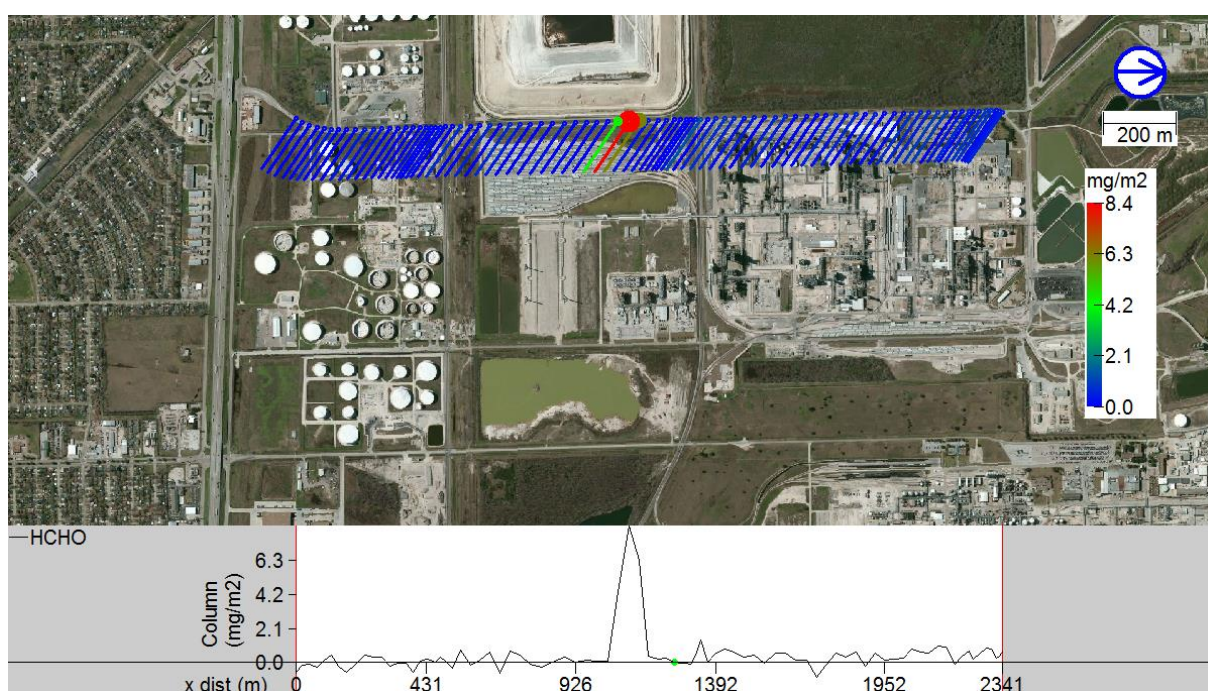

Figure 51 Mobile DOAS measurement of formaldehyde west of a source close to Jefferson Road in Houston Ship Channel on September 6, 2013, 16:10–16:15. Each measured spectrum is represented with a point, which color and size indicate the evaluated integrated vertical formaldehyde column. The formaldehyde column by distance driven through the plume is also shown in the lower part of the figure. A line from each point indicates the direction from which the wind is blowing.

Table 9 Summary of formaldehyde emission transects at Jefferson Road in Houston Ship Channel.

Region	Day	N	Start	Stop	Mean (kg/h)	SD (kg/h)	WS (m/s)	Range WD (deg)	
Jefferson									
	130906	2	161024	161457	10.4	1.5	6.1	123	124
	130908	1	160039	160119	5.4	-	5.5	134	134
	130924	5	92155	165902	27.2	17.8	4.2	7	30
	130925	3	151435	165437	25.3	14.5	3.0	28	41
Total		**11**	**92155**	**165902**	**21.7**	**15.5**	**4.3**	**7**	**134**

5.4.2 Mont Belvieu

Due to the possibilities for comparisons with flight data from the DISCOVER-AQ aircrafts, the main focus of the campaign was measurement in Houston Ship Channel, especially on flight days. During the periods between the flight days, measurements were also made in other areas, like Mont Belvieu. Due to the prevailing winds and lack of good measurement roads, it was not possible to make good measurements downwind encompassing all sites in Mont Belvieu. Instead measurements of different parts of Mont Belvieu are described below.

Alkanes

Figure 52 shows one of the measurements of alkanes from the northern part of Mont Belvieu. The results of all alkane measurements at this sub-area are summarized in Table 10. Unfortunately, only three measurements on a single day were available, showing large but variable emissions. This might suggest that they represent untypical emissions.
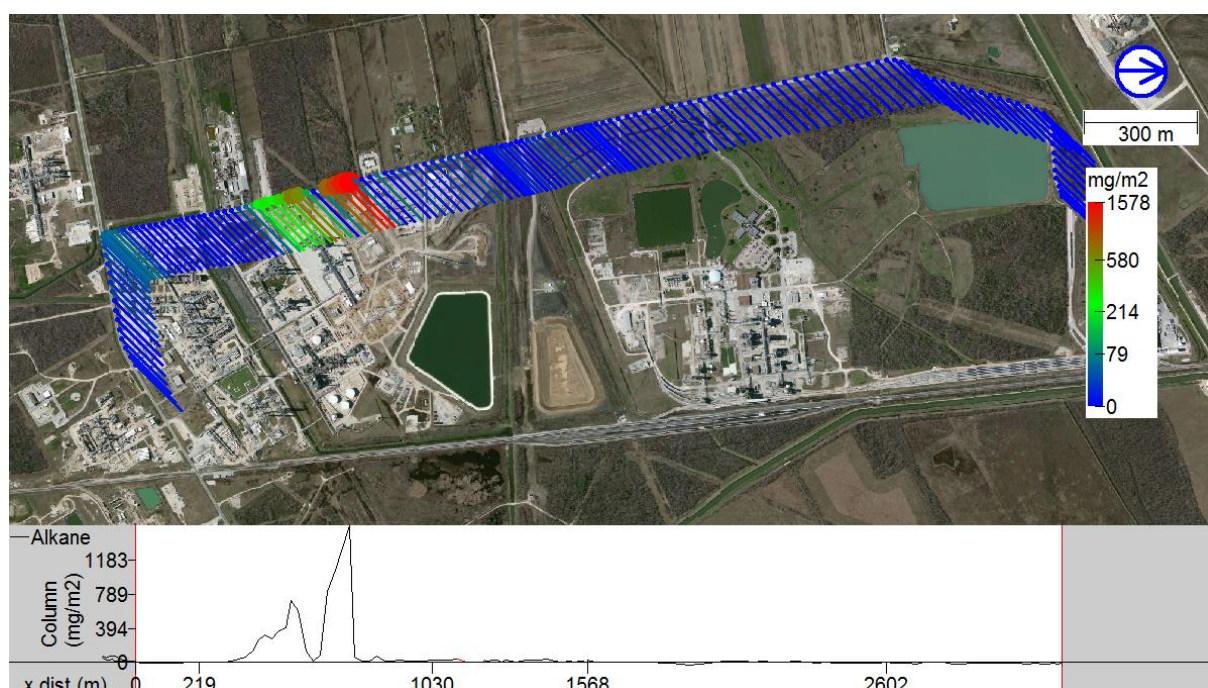

Figure 52 SOF measurement of alkanes west of the northern part of Mont Belvieu on September 22, 2013, 12:30–12:40. Each measured spectrum is represented with a point, which color and size indicate the evaluated integrated vertical alkane column. The alkane column by distance driven through the plume is also shown in the lower part of the figure. A line from each point indicates the direction from which the wind is blowing.

Table 10 Summary of alkane emission transects in the northern part of Mont Belvieu.

Region	Day	N	Start	Stop	Mean (kg/h)	SD (kg/h)	WS (m/s)	Range WD (deg)	
MB north									
	130922	3	121509	125247	2853.7	1212.1	6.5	41	47
Total		**3**	**121509**	**125247**	**2853.7**	**1212.1**	**6.5**	**41**	**47**

Alkenes

Example measurements of ethene and propene from the northern part of Mont Belvieu are shown in Figure 53 and Figure 54. Table 11 and Table 12 summarize all alkene measurements from this area. Additionally a significant propene emission source was detected in the eastern part of Mont Belvieu. One of these measurements is shown in Figure 55 and the measurements are summarized in Table 13.
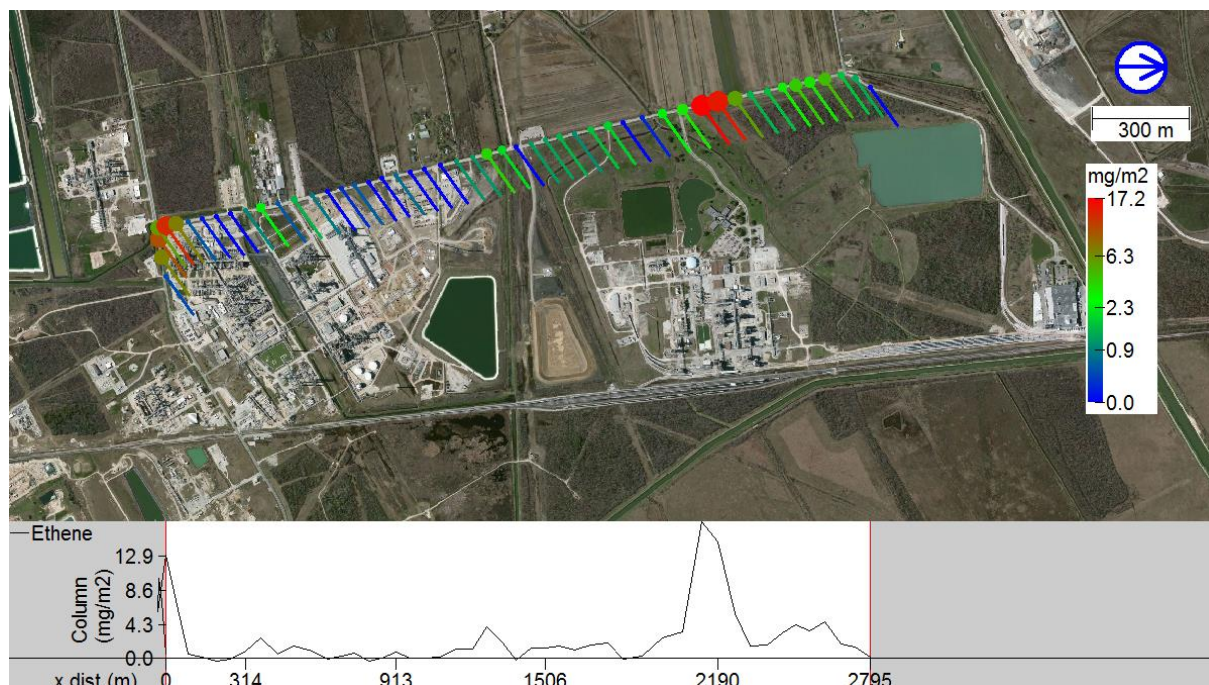

Figure 53 SOF measurement of ethene west of the northern part of Mont Belvieu on September 23, 2013, 13:05–13:15. Each measured spectrum is represented with a point, which color and size indicate the evaluated integrated vertical ethene column. The ethene column by distance driven through the plume is also shown in the lower part of the figure. A line from each point indicates the direction from which the wind is blowing.

Table 11 Summary of ethene emission transects in the northern part of Mont Belvieu.

Region	Day	N	Start	Stop	Mean (kg/h)	SD (kg/h)	WS (m/s)	Range WD (deg)	
MB north									
	130913	1	142310	142849	63.2	-	4.3	77	77
	130923	6	130623	160508	110.5	22.8	4.8	54	81
Total		**7**	**130623**	**160508**	**103.7**	**27.4**	**4.7**	**54**	**81**

Table 12 Summary of the propene emission transects in the northern part of Mont Belvieu.

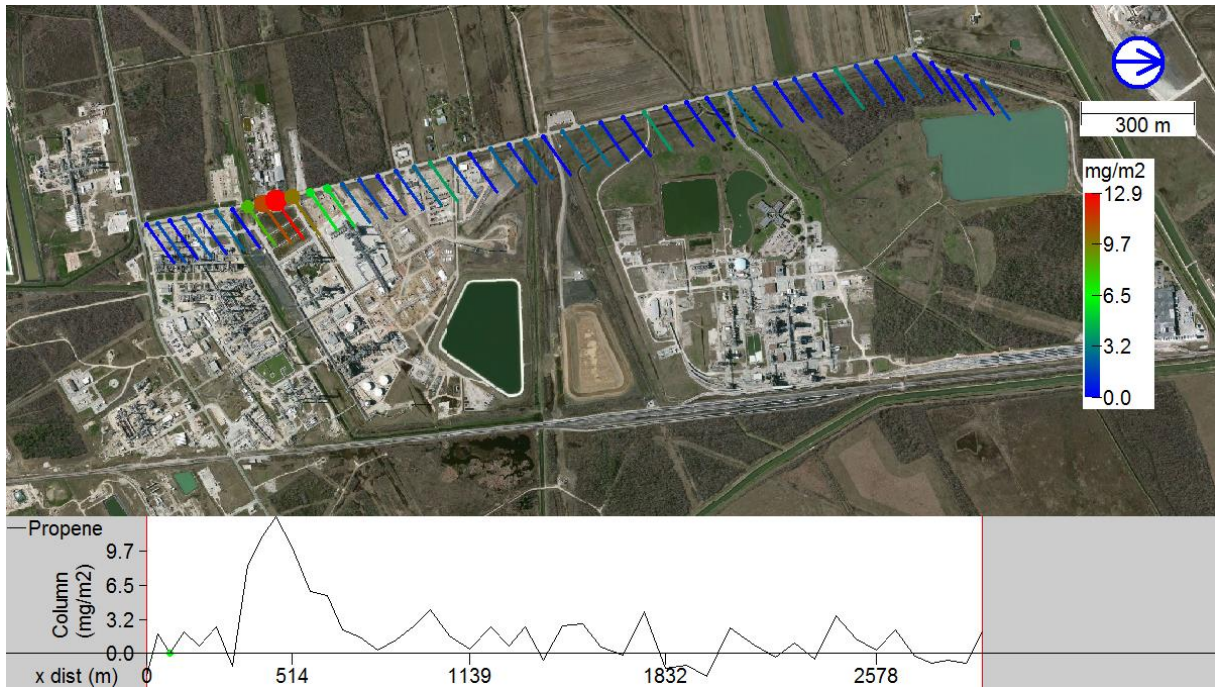| Region	Day	N	Start	Stop	Mean (kg/h)	SD (kg/h)	WS (m/s)	Range WD (deg)	
MB north									
	130913	1	142652	142826	93.6	-	4.3	75	75
	130923	6	130809	151221	105.2	111.9	4.9	54	79
Total		**7**	**130809**	**151221**	**103.5**	**102.3**	**4.8**	**54**	**79**

Figure 54 SOF measurement of propene west of the northern part of Mont Belvieu on September 23, 2013, 13:50–14:00. Each measured spectrum is represented with a point, which color and size indicate the evaluated integrated vertical propene column. The propene column by distance driven through the plume is also shown in the lower part of the figure. A line from each point indicates the direction from which the wind is blowing.

Table 13 Summary of propene emission transects from the eastern part of Mont Belvieu.

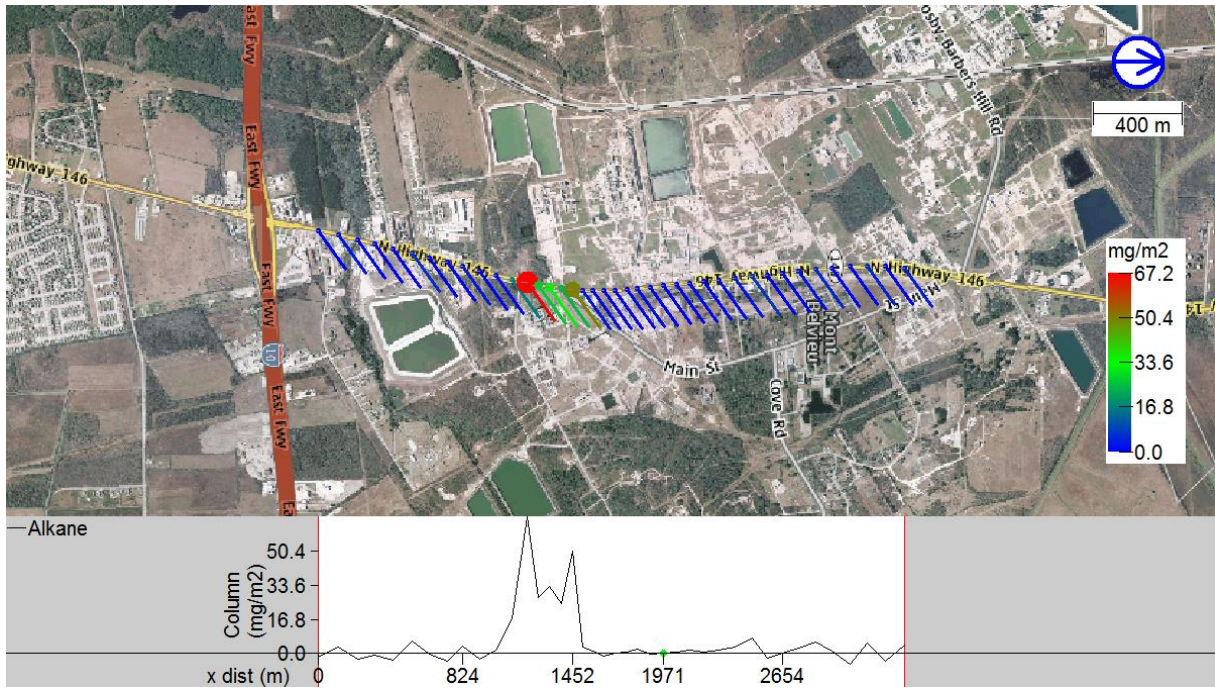| Region	Day	N	Start	Stop	Mean (kg/h)	SD (kg/h)	WS (m/s)	Range WD (deg)	
MB east									
	130923	2	125542	134523	116.8	53.4	4.8	54	54
Total		**2**	**125542**	**134523**	**116.8**	**53.4**	**4.8**	**54**	**54**

Figure 55 SOF measurement of propene west of the eastern part of Mont Belvieu on September 23, 2013, 12:55–13:00. Each measured spectrum is represented with a point, which color and size indicate the evaluated integrated vertical propene column. The propene column by distance driven through the plume is also shown in the lower part of the figure. A line from each point indicates the direction from which the wind is blowing.

On September 3, southerly winds allowed alkene emissions from the southern part of Mont Belvieu to be measured. One such measurement is shown in Figure 56. All the measurements are summarized in Table 14.

Table 14 Summary of the ethene emission transects in the southern part of Mont Belvieu.

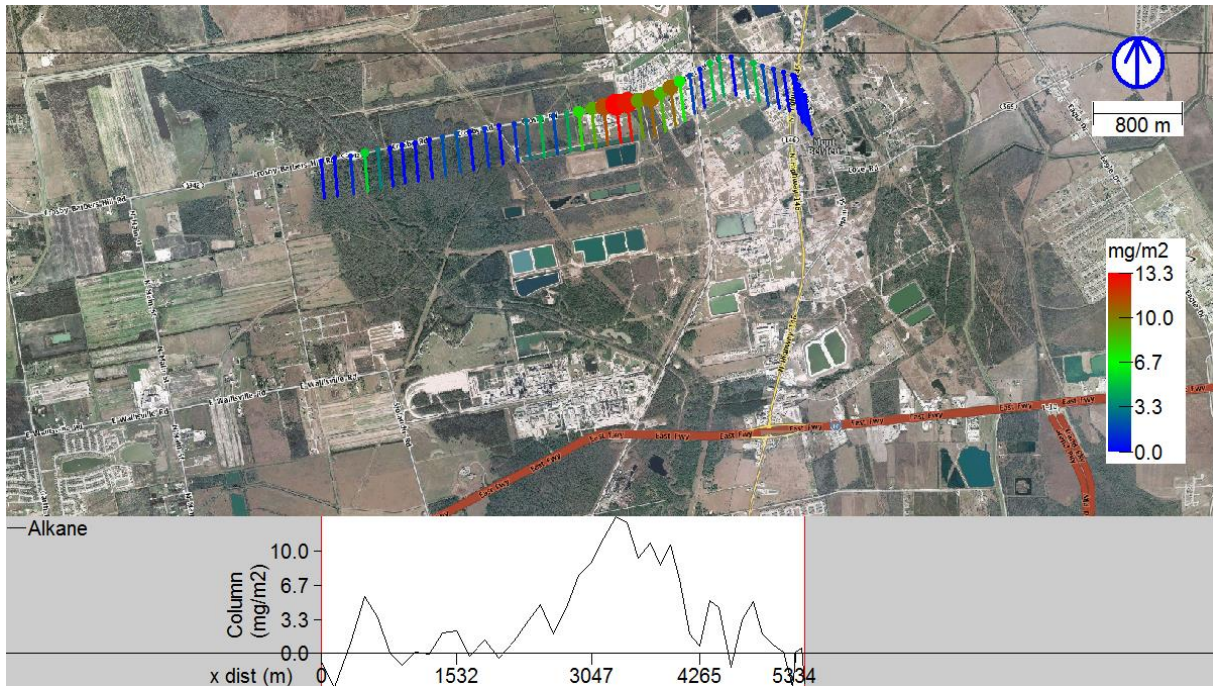| Region	Day	N	Start	Stop	Mean (kg/h)	SD (kg/h)	WS (m/s)	Range WD (deg)	
MB south	130903	3	161248	171447	167.3	18.0	3.6	172	194
Total		3	161248	171447	167.3	18.0	3.6	172	194

Figure 56 SOF measurement of ethene north of the southern part of Mont Belvieu on September 3, 2013, 16:25–16:35. Each measured spectrum is represented with a point, which color and size indicate the evaluated integrated vertical ethene column. The ethene column by distance driven through the plume is also shown in the lower part of the figure. A line from each point indicates the direction from which the wind is blowing.

Sulfur dioxide (SO$_2$)

No significant sulfur dioxide emissions were detected in Mont Belvieu.

Nitrogen dioxide (NO$_2$)

Figure 57 shows an NO$_2$ measurement in the northern part of Mont Belvieu. All NO$_2$ measurements at this site are summarized in Table 15.
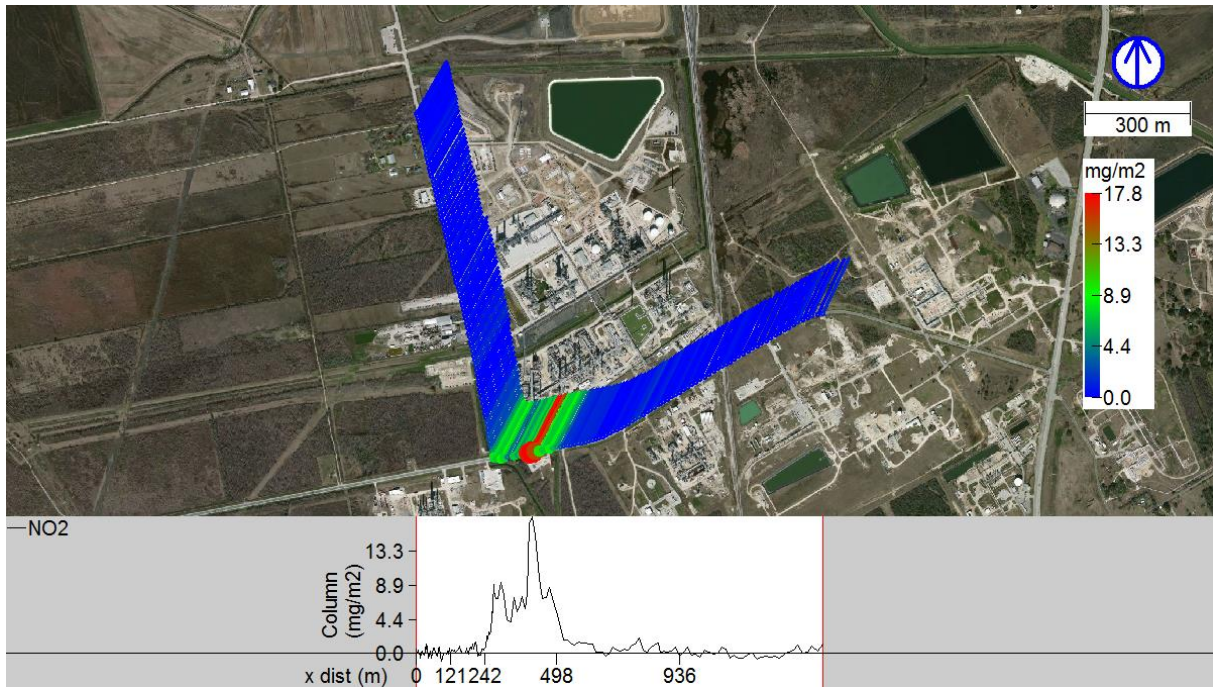
Figure 57 Mobile DOAS measurement of NO_2 south of the northern facilities in Mont Belvieu on September 22, 2013, 12:50–12:55. Each measured spectrum is represented with a point, which color and size indicate the evaluated integrated vertical NO_2 column. The NO_2 column by distance driven through the plume is also shown in the lower part of the figure. A line from each point indicates the direction from which the wind is blowing.

Table 15 Summary of NO_2 emission transects from the northern part of Mont Belvieu.

Region	Day	N	Start	Stop	Mean (kg/h)	SD (kg/h)	WS (m/s)	Range WD (deg)	
MB north									
	130909	2	150848	152159	75.2	17.3	8.8	128	129
	130913	4	141626	145746	95.2	22.6	4.0	56	74
	130922	3	121754	125235	64.5	17.9	6.5	28	36
	130923	9	130620	161307	74.7	19.4	4.2	43	73
	130927	1	142040	142322	131.9	-	8.4	132	132
Total		**19**	**121754**	**161307**	**80.5**	**23.7**	**5.2**	**28**	**132**

NO_2 emissions from southern part of Mont Belvieu were also measured on September 3. One such measurement is shown in Figure 58 and all of the measurements are summarized in Table 16.
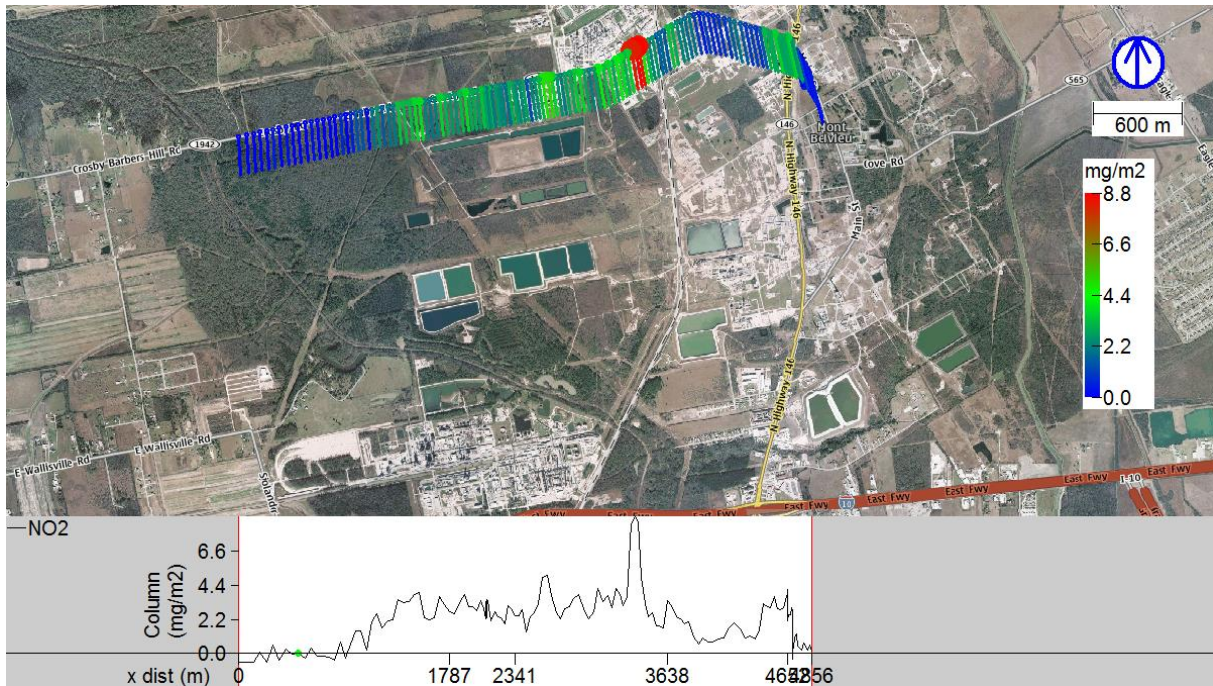
Figure 58 Mobile DOAS measurement of NO$_2$ north of the southern part of Mont Belvieu on September 3, 2013, 16:50–17:00. Each measured spectrum is represented with a point, which color and size indicate the evaluated integrated vertical NO$_2$ column. The NO$_2$ column by distance driven through the plume is also shown in the lower part of the figure. A line from each point indicates the direction from which the wind is blowing.

Table 16 Summary of NO$_2$ emission transects from the southern part of Mont Belvieu.

Region	Day	N	Start	Stop	Mean (kg/h)	SD (kg/h)	WS (m/s)	Range WD (deg)	
MB south									
	130903	3	162822	171438	227.2	71.3	3.8	170	193
	130909	1	152421	152637	88.5	-	8.9	130	130
	130927	1	141715	141922	54.9	-	8.4	132	132
Total		**5**	**141715**	**171438**	**165.0**	**99.7**	**5.7**	**130**	**193**

Formaldehyde (HCHO)

The formaldehyde measurements in 2009 found two distinct formaldehyde sources in the northern part of Mont Belvieu. One of them, the one furthest to the north, was only detected sporadically in this study, and showed emissions of less than 5 kg/h at those times. The other source, however, was detected almost every time it was passed and showed fairly stable emissions. Figure 59 shows a measurement on west side of both of these sources where they are both detected. The more southern source is clearly more distinct and easier to separate from the noise. All formaldehyde measurements at this source are summarized in Table 17.
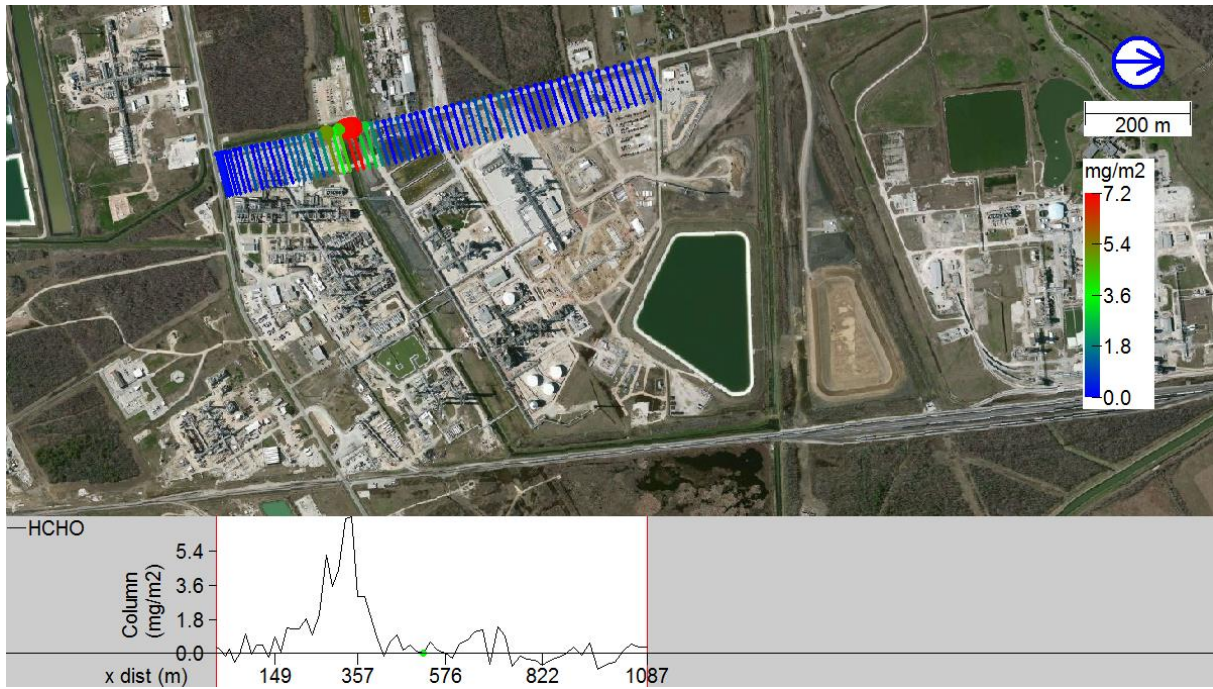
Figure 59 Mobile DOAS measurement of formaldehyde west of the northern part of Mont Belvieu on September 23, 2013, 15:10–15:15. Each measured spectrum is represented with a point, which color and size indicate the evaluated integrated vertical formaldehyde column. The formaldehyde column by distance driven through the plume is also shown in the lower part of the figure. A line from each point indicates the direction from which the wind is blowing.

Table 17 Summary of the formaldehyde emission transects in the northern part of Mont Belvieu.

Region	Day	N	Start	Stop	Mean (kg/h)	SD (kg/h)	WS (m/s)	Range WD (deg)	
MB north									
	130909	2	150902	152137	7.1	3.7	7.6	141	145
	130913	4	141718	145658	13.2	6.3	4.3	32	110
	130922	3	121834	125155	9.0	3.1	6.5	28	36
	130923	5	130800	161137	8.2	3.0	4.3	42	74
Total		**14**	**121834**	**161137**	**9.7**	**4.5**	**5.2**	**28**	**145**

5.4.3 Texas City

Emission measurements in Texas City were attempted on several days, but persistent clouds made SOF measurement very difficult. For this reason no successful alkene measurements were made in Texas City and only one day gave good measurements of alkanes. Mobile DOAS measurements of SO_2 and NO_2 were possible on two additional days since they are not as sensitive to clouds.

Alkanes

Figure 60 shows an example of an alkane measurement on the east side of Texas City. All alkane measurements in Texas City are summarized in Table 18.

Figure 60 SOF measurement of alkanes west of Texas City on September 9, 2013, 11:25–11:35. Each measured spectrum is represented with a point, which color and size indicate the evaluated integrated vertical alkane column. The alkane column by distance driven through the plume is also shown in the lower part of the figure. A line from each point indicates the direction from which the wind is blowing.

Table 18 Summary of alkane emission transects in Texas City.

Region	Day	N	Start	Stop	Mean (kg/h)	SD (kg/h)	WS (m/s)	Range WD (deg)	
TC									
	130909	3	112635	131708	1339.7	139.5	6.3	96	104
Total		**3**	**112635**	**131708**	**1339.7**	**139.5**	**6.3**	**96**	**104**

Sulfur dioxide (SO₂)

A measurement of SO_2 emissions from the industries in Texas City is shown in Figure 61. Table 19 gives a summary of all SO_2 measurements in Texas City.
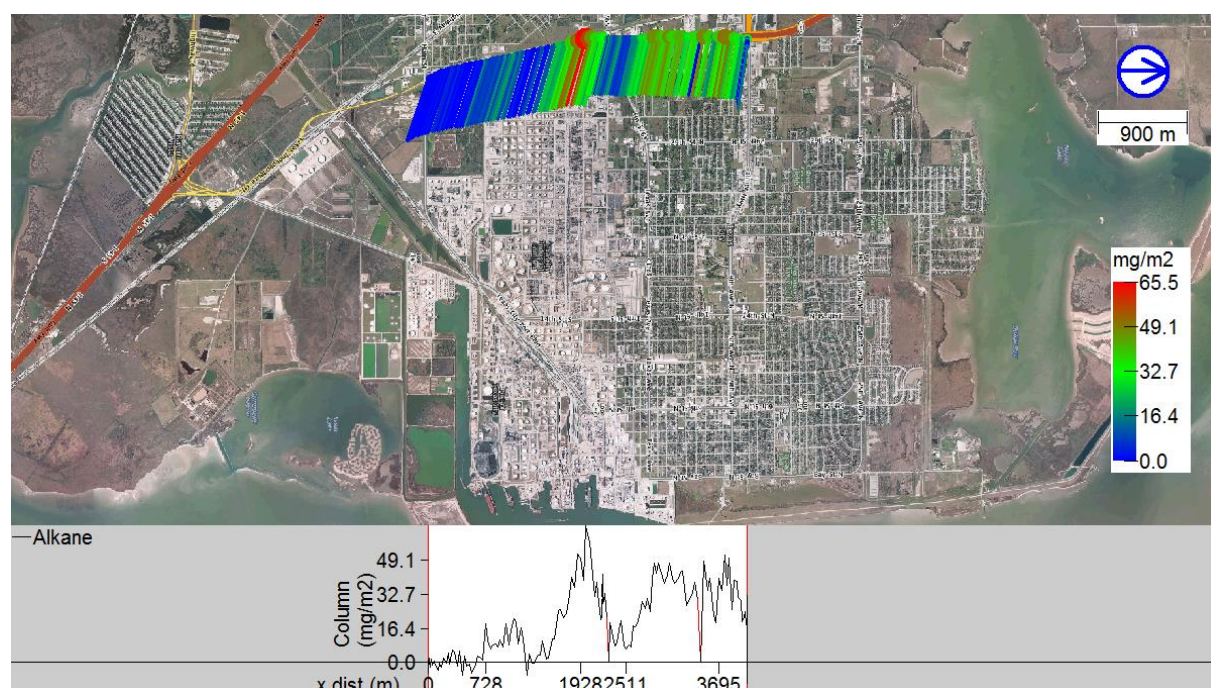

Figure 61 Mobile DOAS measurement of SO_2 northwest of Texas City on September 4, 2013, 16:35–16:45. Each measured spectrum is represented with a point, which color and size indicate the evaluated integrated vertical SO_2 column. The SO_2 column by distance driven through the plume is also shown in the lower part of the figure. A line from each point indicates the direction from which the wind is blowing.

Table 19 Summary of SO_2 emission transects in Texas City.

Region	Day	N	Start	Stop	Mean (kg/h)	SD (kg/h)	WS (m/s)	Range WD (deg)	
TC									
	130904	3	160934	165436	259.6	46.3	4.2	101	109
	130909	5	122702	131443	515.9	164.1	8.0	108	115
	130918	1	131531	131921	370.0	-	7.3	98	98
Total		9	122702	165436	414.3	172.3	6.7	98	115

Nitrogen dioxide (NO_2)

Figure 62 shows an NO_2 measurement transect northwest of Texas City. All NO_2 measurements in Texas City are summarized in Table 20.
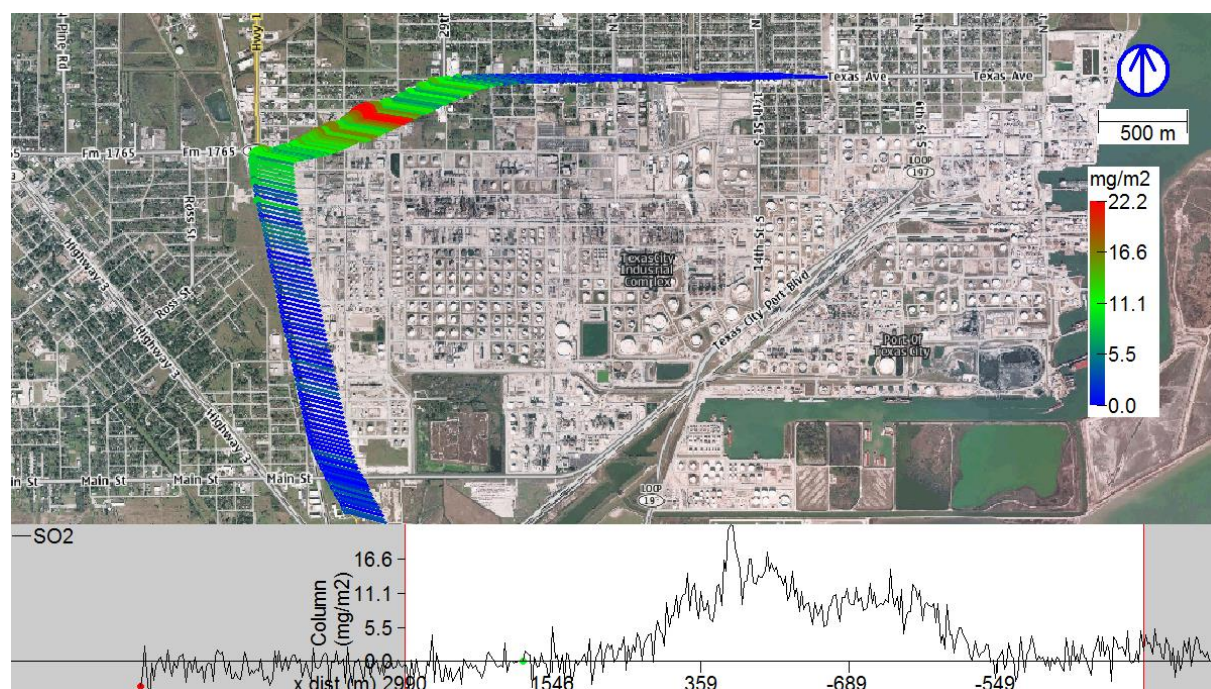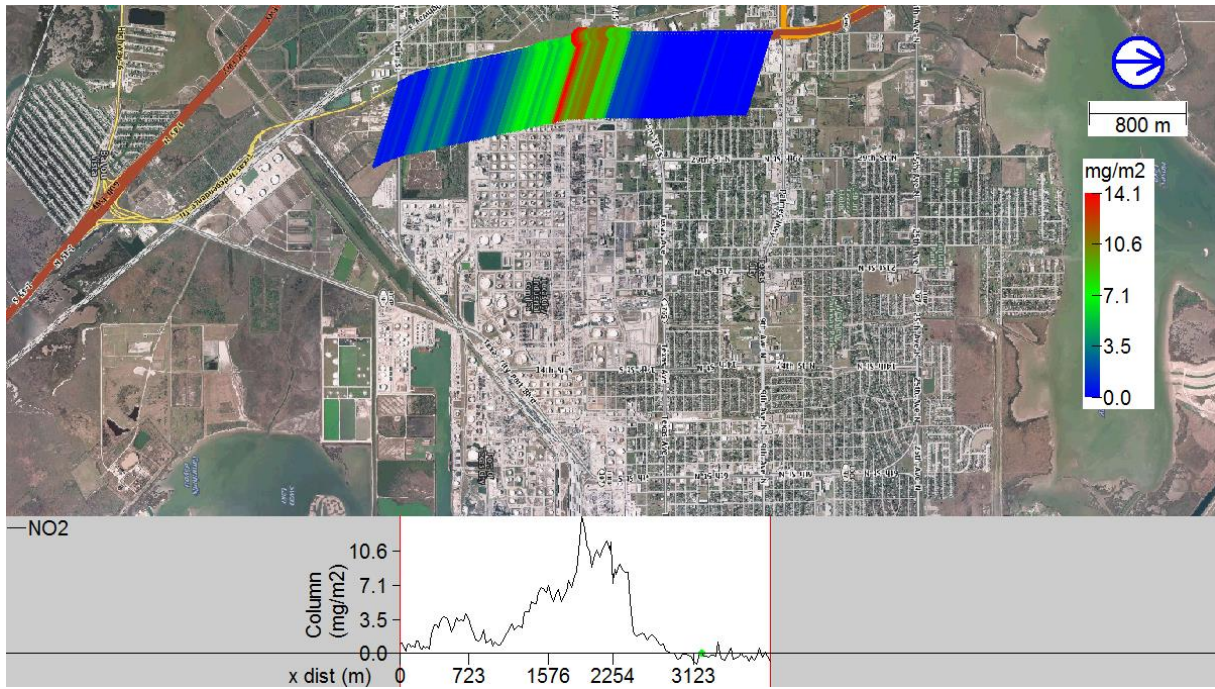
Figure 62 Mobile DOAS measurement of NO₂ northwest of Texas City on September 18, 2013, 13:15–13:20. Each measured spectrum is represented with a point, which color and size indicate the evaluated integrated vertical NO₂ column. The NO₂ column by distance driven through the plume is also shown in the lower part of the figure. A line from each point indicates the direction from which the wind is blowing.

Table 20 Summary of NO₂ emission transects in Texas City.

Region	Day	N	Start	Stop	Mean (kg/h)	SD (kg/h)	WS (m/s)	Range WD (deg)	
TC									
	130904	4	155613	165434	395.4	59.3	4.2	92	109
	130909	5	122710	131457	431.8	122.2	8.0	107	116
	130918	1	131525	131939	341.9	-	8.7	107	107
Total		**10**	**122710**	**165434**	**408.3**	**93.1**	**6.5**	**92**	**116**

5.4.4 Special episodes

HSC sector 6, September 12

On September 12, large ethene emissions were repeatedly detected from Sector 6 in HSC, where we have never before seen ethene emissions of similar magnitude. Because of the temporary nature of these emissions, they were considered to be non-routine emissions. The emissions were tracked with the measurement vehicle and the source was pinpointed to site for storing large amounts of various small gas cylinders. Except for the gas cylinders the site also contained a large tank marked with the text *Ethylene*. This tank was suspected to be the source of the non-routine ethene emissions. One of the ethene measurements in sector 6 is shown in Figure 63. All of these measurements are summarized in Table 21.

Figure 63 SOF measurement of ethene southwest of sector 6 in HSC on September 12, 2013, 13:10–13:15. Each measured spectrum is represented with a point, which color and size indicate the evaluated integrated vertical ethene column. The ethene column by distance driven through the plume is also shown in the lower part of the figure. A line from each point indicates the direction from which the wind is blowing.

Table 21 Summary of ethene emission transects in Sector 6 in Houston Ship Channel on September 12, 2013.

Region	Day	N	Start	Stop	Mean (kg/h)	SD (kg/h)	WS (m/s)	Range (deg)	WD
HSC 6									
	130912	8	130441	162022	286.5	226.4	6.4	82	127
Total		**8**	**130441**	**162022**	**286.5**	**226.4**	**6.4**	**82**	**127**

Bayport, September 26

SOF measurements were made at Bayport during the SOF measurement study in 2006 but it was not one of the largest emission source in that study. On September 26 the wind turned southerly and a significant alkene plume was detected in SOF measurements upwind from

HSC and Bayport seemed to be the most likely source. A few measurements were also made closer to the site, confirming this. Figure 64 and Figure 65 shows ethene and propene plumes measured upwind from HSC. The measurements of this plume is summarized in Table 22 and Table 23. The propene emissions from this area were especially high.
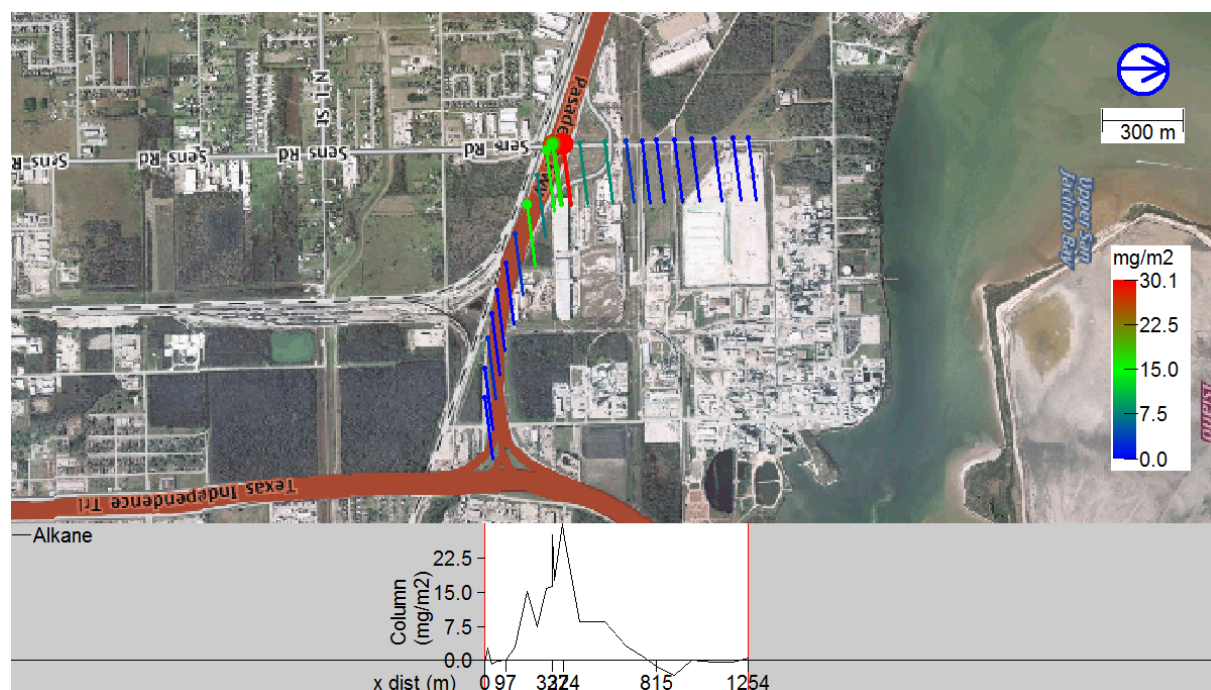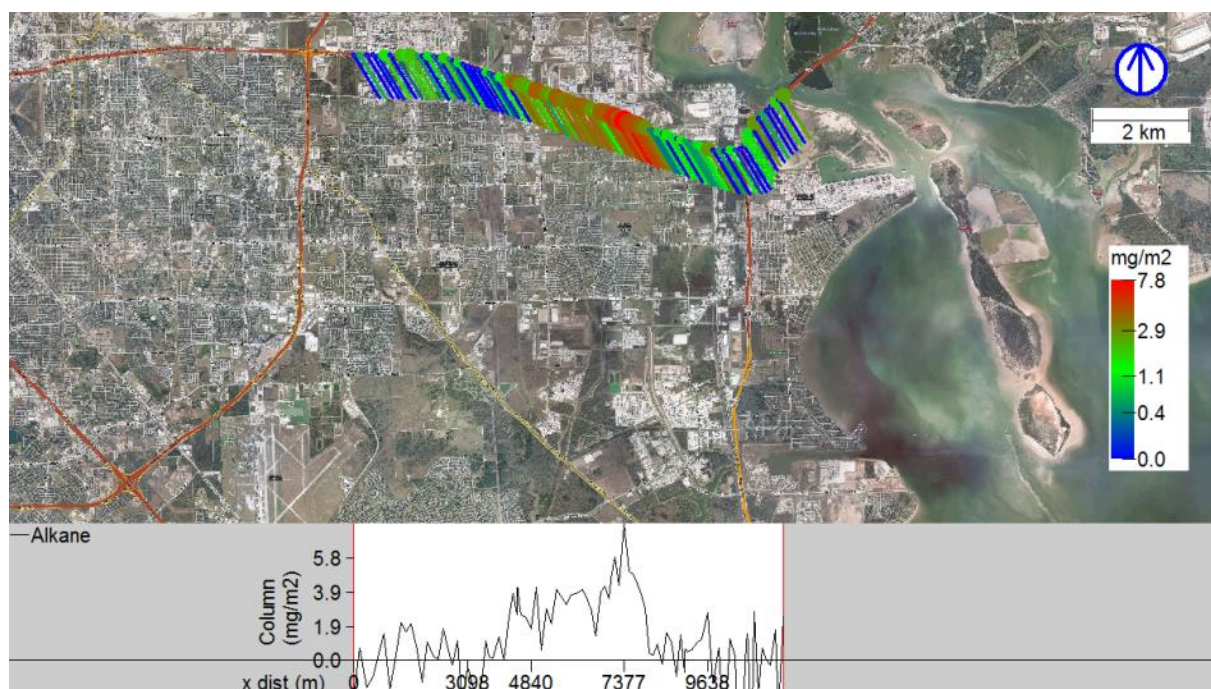

Figure 64 SOF measurement of ethene north of Bayport on September 26, 2013, 10:40–10:55. Each measured spectrum is represented with a point, which color and size indicate the evaluated integrated vertical ethene column. The ethene column by distance driven through the plume is also shown in the lower part of the figure. A line from each point indicates the direction from which the wind is blowing.

Table 22 Summary of ethene emission transects in Bayport.

| Region	Day	N	Start	Stop	Mean (kg/h)	SD (kg/h)	WS (m/s)	Range WD (deg)	
Bayport									
	130926	3	104223	131855	95.9	58.6	5.1	147	189
Total		3	104223	131855	95.9	58.6	5.1	147	189
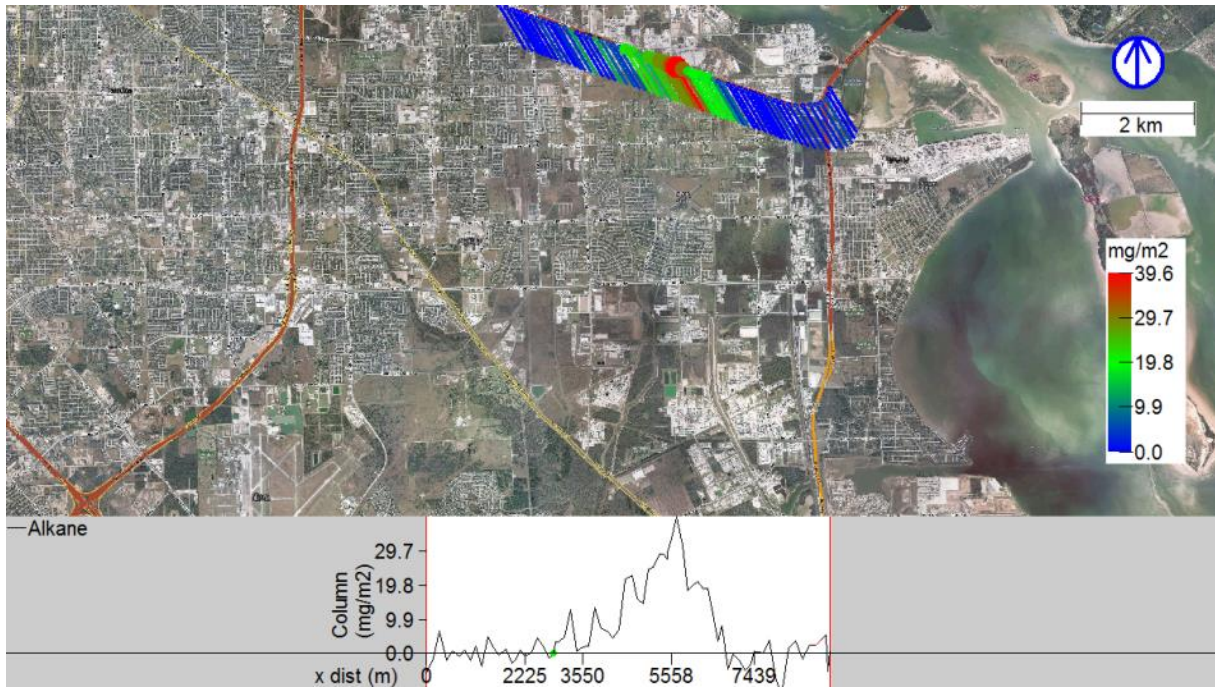
Figure 65 SOF measurement of propene north of Bayport on September 26, 2013, 10:40−10:55. Each measured spectrum is represented with a point, which color and size indicate the evaluated integrated vertical propene column. The propene column by distance driven through the plume is also shown in the lower part of the figure. A line from each point indicates the direction from which the wind is blowing.

Table 23 Summary of propene emission transects in Bayport.

Region	Day	N	Start	Stop	Mean (kg/h)	SD (kg/h)	WS (m/s)	Range WD (deg)	
Bayport									
	130926	5	104156	132014	624.0	213.1	4.9	147	188
Total		**5**	**104156**	**132014**	**624.0**	**213.1**	**4.9**	**147**	**188**

The measurements closer to Bayport also showed significant amounts of NO_2 emissions. One of these measurements is shown in Figure 66. The results from both of the measurements are summarized in Table 24.
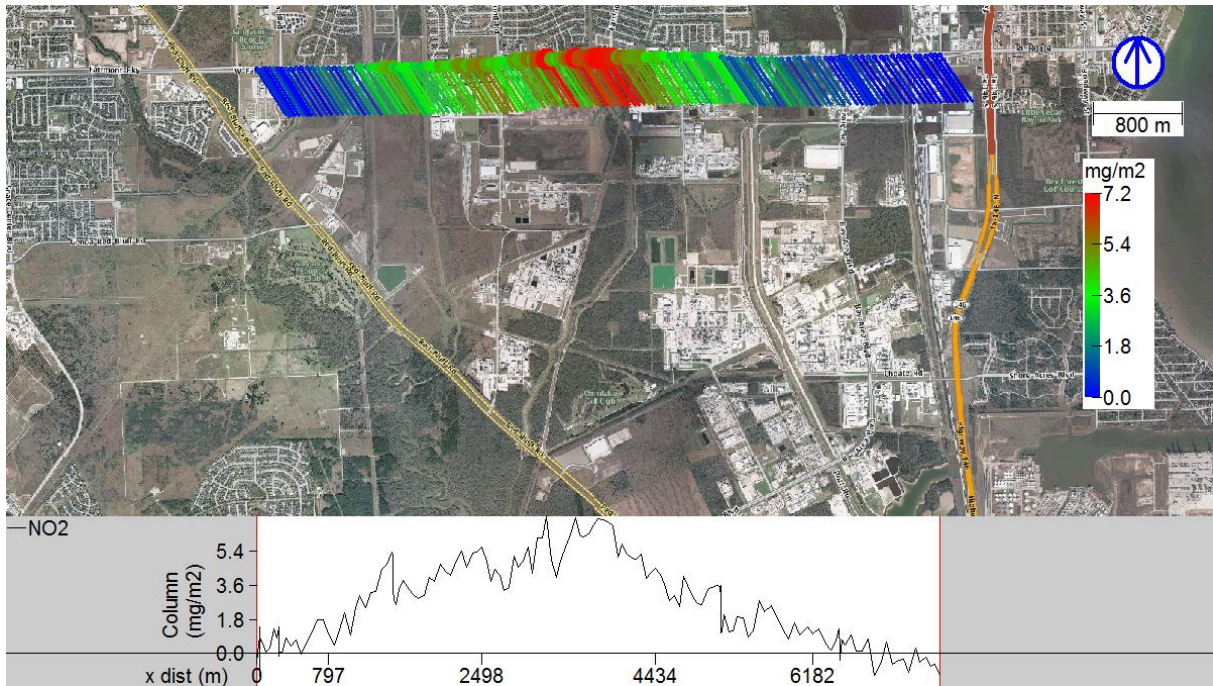
Figure 66 Mobile DOAS measurement of NO_2 north of Bayport on September 26, 2013, 13:10–13:20. Each measured spectrum is represented with a point, which color and size indicate the evaluated integrated vertical NO_2 column. The NO_2 column by distance driven through the plume is also shown in the lower part of the figure. A line from each point indicates the direction from which the wind is blowing.

Table 24 Summary of NO_2 emission transects in Bayport.

Region	Day	N	Start	Stop	Mean (kg/h)	SD (kg/h)	WS (m/s)	Range WD (deg)	
Bayport									
	130926	2	125701	132140	295.0	90.6	5.5	146	148
Total		**2**	**125701**	**132140**	**295.0**	**90.6**	**5.5**	**146**	**148**

6. Mapping of Aromatics and alkanes

This section summarizes the results of the measurements with the MW-DOAS instrument and the MeFTIR system. The measurements were mainly concentrated to three areas: Channelview, Baytown and Texas City. Some measurements were also performed in Mont Belvieu and in the Deer Park/Battleground area. During all measurements the wind was predominately easterly or southeasterly. Most measurements were performed during late evening and nights when the air was more stable and the emission plumes remained close to ground, in contrast to daytime. The measurements were performed while driving slowly, 15-25 mph, on public roads close to oil refineries, oil storage tanks and chemical processing plants. Figure 67 to Figure 69 show examples of aromatic VOC measurements with the MW-DOAS in different industrial areas.
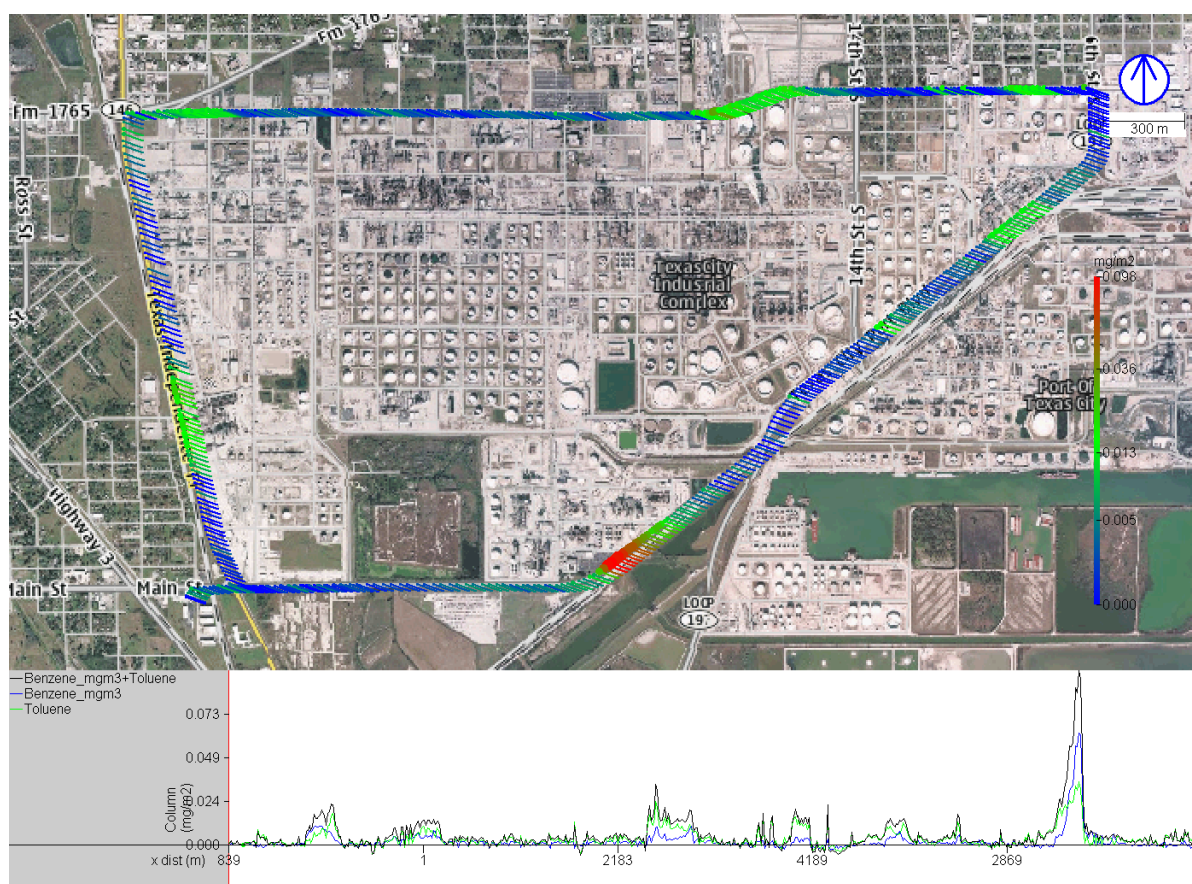
Figure 67 Example of a box measurement of aromatics and in southeasterly wind with the MW-DOAS in Texas City.
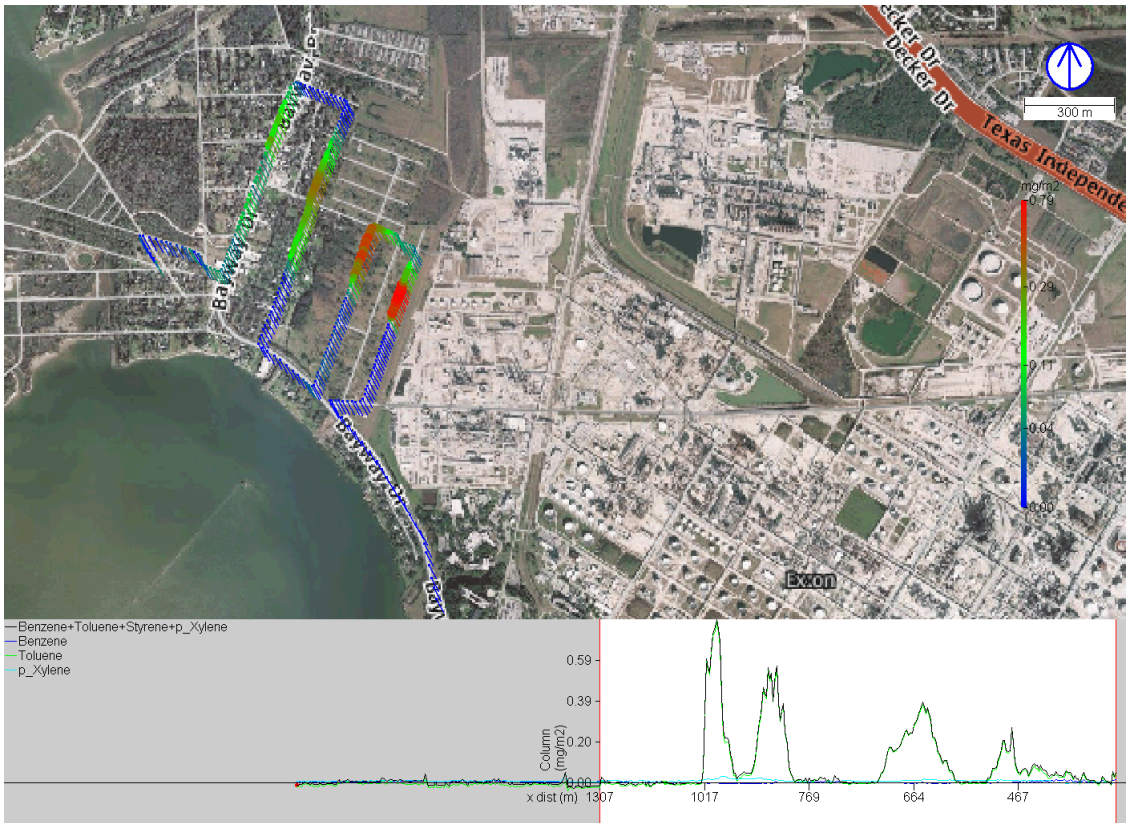
Figure 68 Toluene concentration measurements downwind of a refinery in Baytown, HSC.
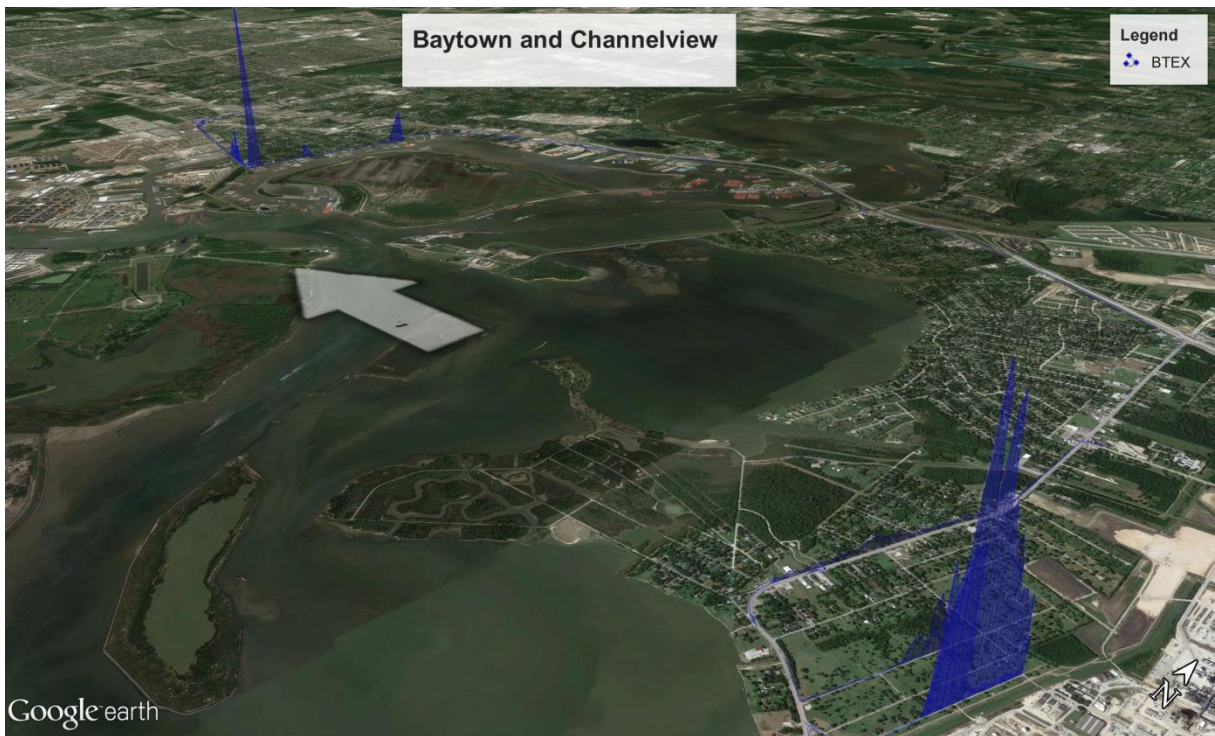
Figure 69 Aromatics VOC concentration measurements along HSC between Baytown and Channelview.

6.1 Intercomparison

As described in section 3.4 an intercomparison exercise was carried out on September 17, 2013 comparing the MW-DOAS on the SOF van with a PTR-MS instrument operated by Berk Knighton, (University of Montana) and installed in a van run by the research company Aerodyne. The two measurement vehicles drove at a distance of 20 to 200 m apart, at a speed of 15-30 km/h. In Figure 70 peaks from several sources detected during September 17 have been combined into single plots for each species in order to give a comparable view. The time shift between plume interception for the two vehicles caused by their spatial separation has been manually corrected for as far as possible. The plumes will nevertheless not be identical in many cases as turbulence may alter the shape of the plumes during the time between passages. The distance between the two cars is also shown in the plots of Figure 70. It is clearly visible, particularly for toluene, that the correlation between peaks tend to be smaller when this distance is larger than 100 m.
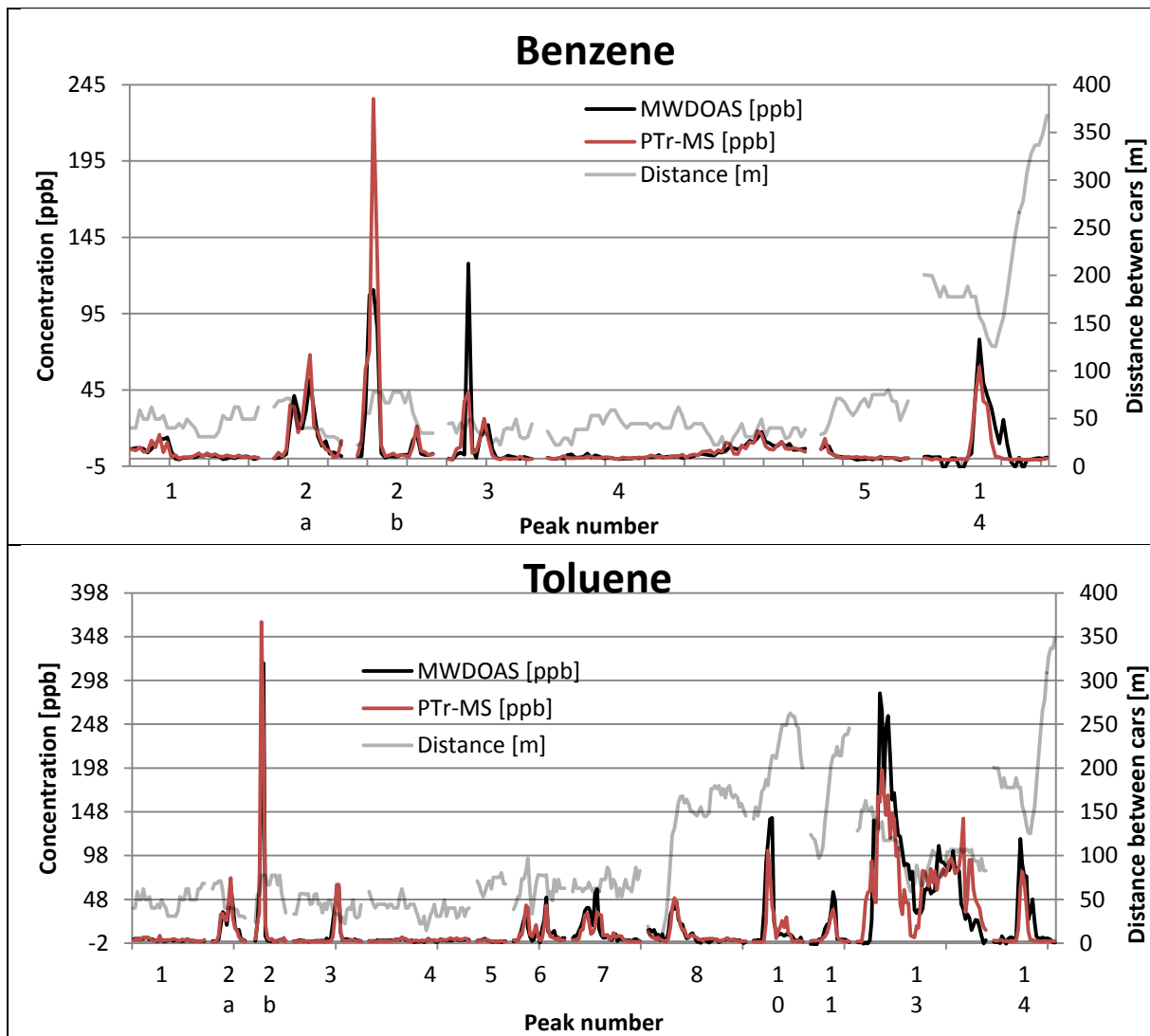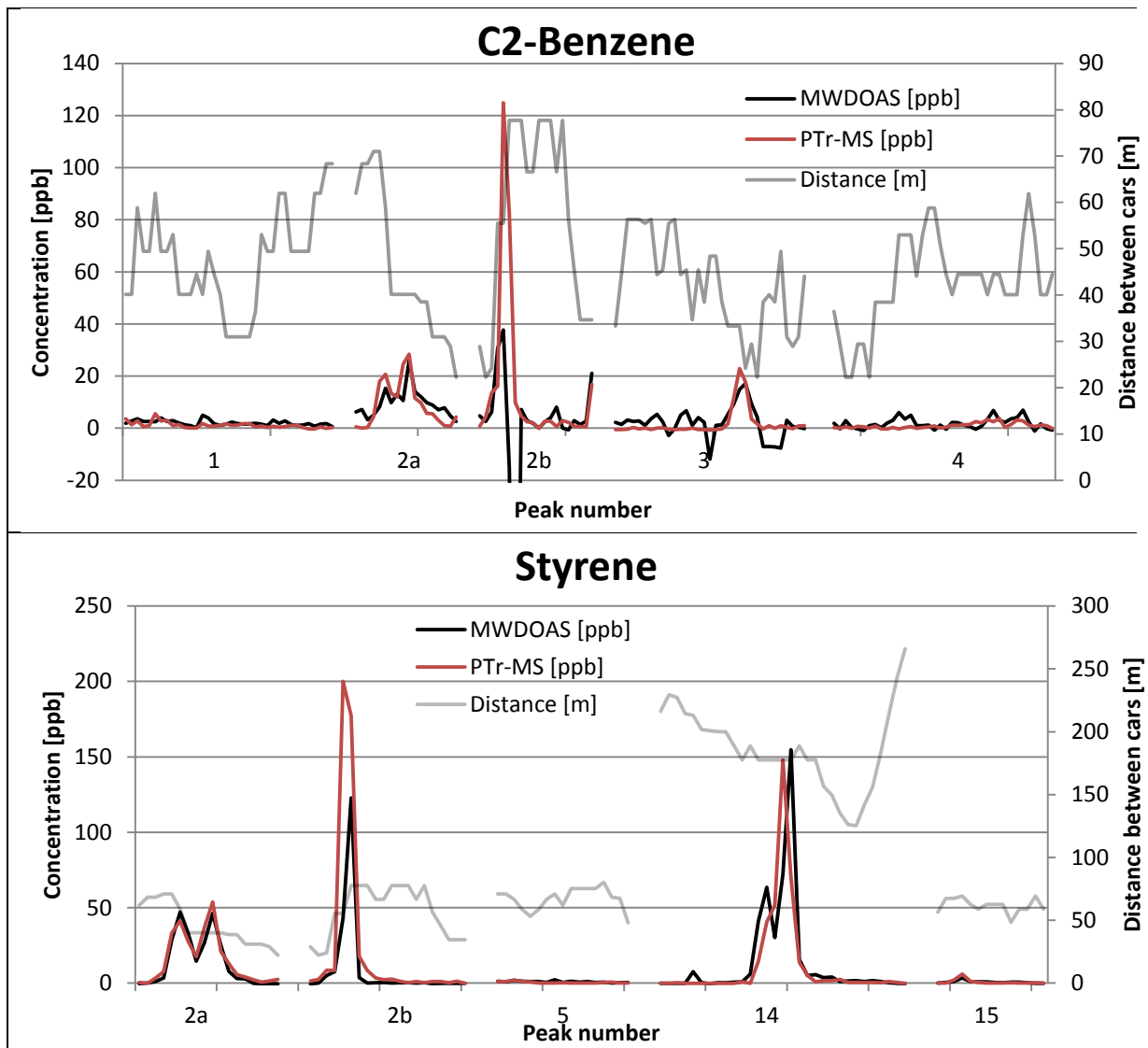
Figure 70 Concentration measurements of benzene, toluene, C2-benzenes (xylene + Ethylbenzene) and styrene in Channelview, HSC, by PTR-MS and MW-DOAS.

For each of the four measured species and for each peak, the ratio between the areas under the peak for MWDOAS and PTR-MS respectively was calculated. In this calculation the peak 2b for C2-Benzenes was removed due to strong negative interference in the MWDOAS measurements, as seen in Figure 70. Since several of the peaks contained high concentrations of the four species it is difficult to see the correlation for lower concentrations in the figures above. Zoomed-in plots of low level peaks for benzene and toluene are therefore shown in Figure 71.
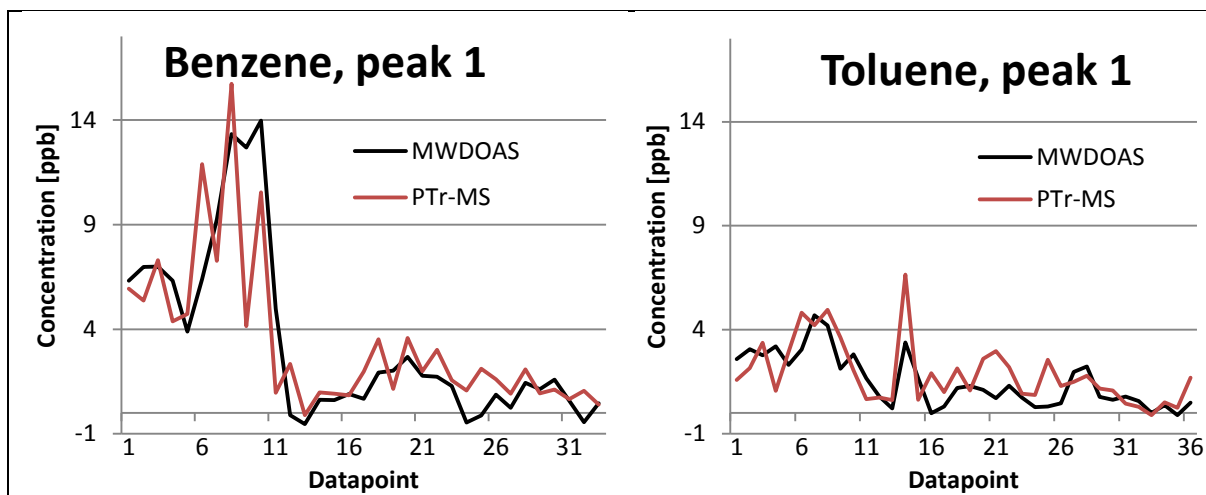
Figure 71 Peak 1 for Benzene and Toluene showed on a scale for lower concentration plumes.

Table 25. MWDOAS/PT-TMS ratios for mean concentrations under the peaks in Figure 70.

Species	Ratio for sum of peak concentrations (Standard deviation)	Plumes not used in average
Benzene	1.00 (0.24)	
Toluene	1.12 (0.36)	
C2-Benzene	1.42 (0.41)	2b
Styrene	1.05 (0.55)	

The comparison between PTR-MS and MWDOAS good agreement between the two methods. Since the vehicles were sampling the plumes at different times the ratios show a rather high variation. Benzene measurements agree fully with a standard deviation of 24%, Toluene concentrations were 12% higher on average for MWDOAS but still agree well within the variation. The exception is C2-Benzene where MWDOAS was measuring a 42% higher concentration than PTR-MS on average.

6.2 Aromatic to alkane ratios

Simultaneous measurements by the MW-DOAS and the MeFTIR systems were carried out during the campaign. A sample inlet to the MeFTIR was placed in close proximity to the open White cell positioned on the roof. Concentration levels of methane, propane, butane and octane where measured with the MeFTIR system at a time resolution of about 15 s. The purpose of these measurements is to calculate ratios of aromatics to alkanes and use this to estimate aromatic fluxes based from alkane fluxes measured with SOF. As an example of this we compared the amount of alkanes and aromatic in the refinery area in Texas City TX (Figure 72). The measurement vehicle was driven on public roads outside and through the refinery area and data from both systems were recorded simultaneous together with wind and GPS data. As the two systems have different time resolution the data from the MeFTIR system was interpolated in time to match the MWDOAS data. The results were then combined into a single dataset that can be plotted in a custom computer program. The ratio of aromatics to alkanes can be directly seen in the computer program and relevant sections of the

measurement transects are made. An example of a typical plume measurement is shown in Figure 73.
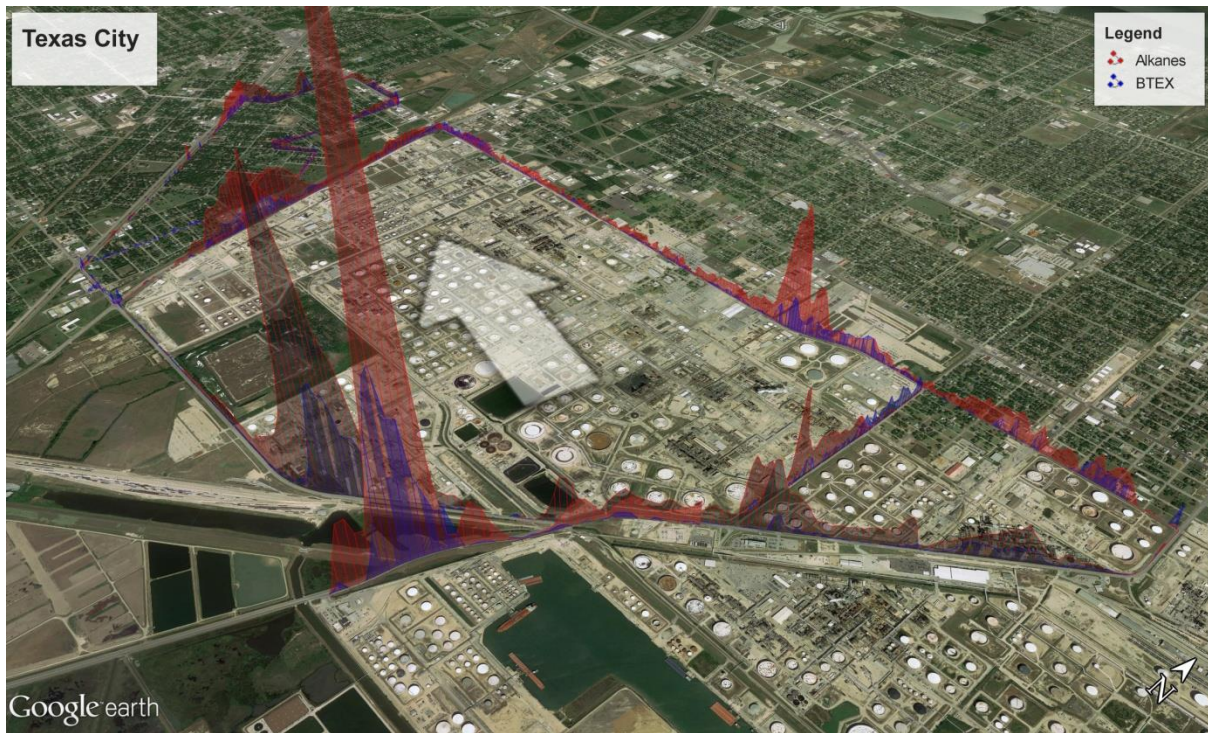
Figure 72 The Refinery area at Texas City. A major plume can be seen originating from the Oil Tanking area in the south east corner. Smaller plumes, can be seen from the east area. The arrow represent the wind direction. Data from several runs have been combined and presented in Google earth. The BTEX data is multiplied by a factor of 10 for visibility.
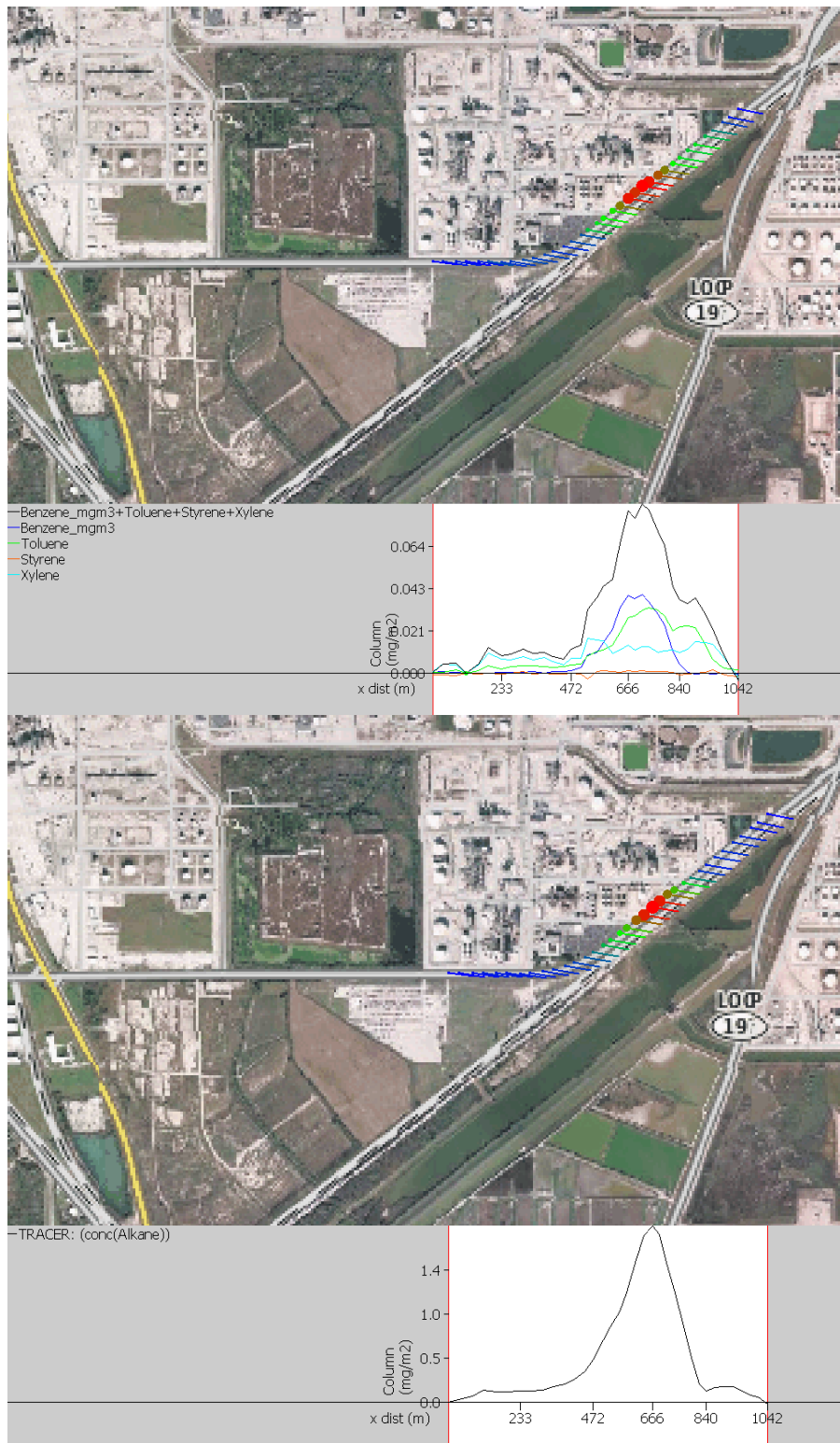
Figure 73. The plume from the Oil Tanking area, TXC. The lower plot shows the total Alkanes measured by the MeFTIR. There is a slight time difference (The vehicle is driving towards left side of the picture) as the MWDOAS is open while the MeFTIR is a closed cell sampling ambient air through a pump. The units are mg/m^3 , the bars indicates the wind direction (ESE) and their lengths the wind speed (~5 m/s). The BTEX to alkane ratio was 0.05 in this case.

The average alkane emissions from Texas City during the campaign, as measured with SOF and presented in section 5.4.3, was approximately 1340 kg/h. The total BTEX to alkene ratio downwind the facility was measured with the MWDOAS and MeFTIR systems on the night of September 15, 2013. The results of four measurement traverses downwind of Texas City are presented in Table 26. The total BTEX flux from Texas City was estimated to be 134 ± 5 kg/h based on these results.

Table 26. The BTEX to alkane ratios measured downwind Texas City on the night of September 15, 2013.

Time period	Ratio
204159-210409	0.09
192851-195211	0.08
200957-202422	0.16
224658-230751	0.06
Average	**0.10±0.04**

Apart from the total emission, a few "hotspots" can be pointed out as probable main sources of aromatics.

- The tank area has a fairly low BTEX to alkane ratio (5%) but the high concentrations and the high benzene content makes this an interesting source.
- A distinct plume from four large tanks between 14:th and 21:th, shown in Figure 74, was shown to have a ~7% BTEX to alkane ratio.
- Emissions of variable ratios coming from the tanks in the eastern part of the area and the port of Texas City.
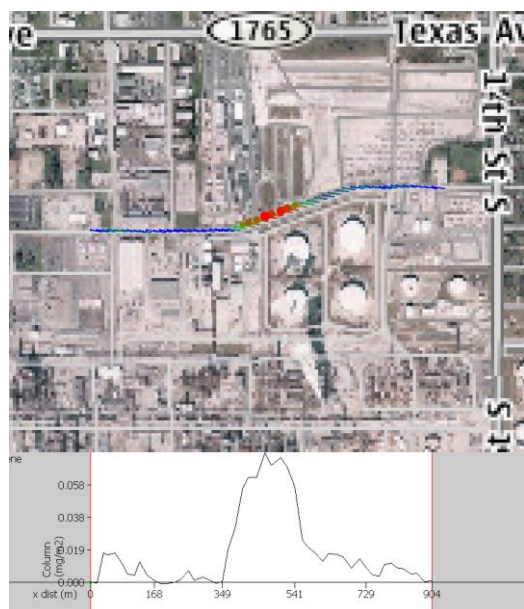
Figure 74. The total BTEX plume from the four large tanks between 14:th and 21:th street.

7. Acknowledgements

8. References

Allen, D.T. and V.M. Torres, 2010 TCEQ Flare Study Project, Final Report. 2011.

Arnold S.R., Methven J., Evans M.J., Chipperfield M.P., Lewis A.C., Hopkins J., McQuaid J.B., Watson N., Purvis R.M., Lee J.D., Atlas E.L., Blake D.R., Rappenglück B. (2007): Statistical inference of OH concentrations and air mass dilution rates from successive observations of nonmethane hydrocarbons in single air masses, *J. Geophys. Res.*, 112, D10S40, doi:10.1029/2006JD007594

Bogumil, K. et al., 2003, Measurements of Molecular Absorption Spectra with the SCIAMACHY PreFlight Model: Instrument Caracterization and Reference Data for Atmospheric Remote-Sensing in the 230–2380 nm Region, J. Photoch. Photobio. A, 157, 167–184

Buhr, M., Alvarez, S., Kauffmann, L., Shauck, M., Zanin, G., Alkene/NOy Emission Ratios observed from the Baylor Aztec during the 2006 TexAQS II study and Comparison with results obtained during 2001–2002, Rapid science synthesis workshop, Austin, october 12, 2006

Burrows, J.P et al., 1999, Atmospheric Remote-Sensing Reference Data from GOME: 2. Temperature-Dependent Absorption Cross Sections of O3 in the 231–794 nm Range, Journal of Quantitative Spectroscopy and Radiative Transfer 61, 509–517

Börjesson, G., J. Samuelsson, J. Chanton, R. Adolfsson, B. Galle, and B.H. Svensson. 2009. A national landfill methane budget for Sweden based on field measurements, and an evaluation of IPCC models. Tellus, 61B: 424–435.

Cantrell CA, Davidson JA, McDaniel AH, Shetter RE, Calvert JG. 1990, Temperature dependent formaldehyde cross sections in the near-ultraviolet spectral region. J Phys Chem, 94:3902–8.

De Gouw, J.A., et. al. (2009), Airborne Measurements of Ethene from Industrial Sources Using Laser Photo-Acoustic Spectroscopy, Environmental Science and Technology, 43, 2437–2442.

Doussin J. F.;Dominique R.; Patrick C., Applied Optics, **38** 4145 (1999)

ERG, Forth Natural gas Air Quality Study Final Report, 2011, www.forthworthgov.org

Etzkorn, T., B. Klotz, S. Sørensen, I.V. Patroescu, I. Barnes, K.H. Becker, and U. Platt, "Gas-phase absorption cross sections of 24 monocyclic aromatic hydrocarbons in the UV and IR spectral ranges," Atmos. Environ. 33, 525-540 (1999).

Fally, S., M. Carleer, and A. C. Vandaele, "UV Fourier transform absorption cross sections of benzene, toluene, meta-, ortho-, and para-xylene", J. Quant. Spectrosc. Radiat. Transfer 110, 766-782 (2009).

Fayt, C. and Van Roozendael, M., 2001. QDOAS 1.00 Software User Manual, BIRA-IASB.

Fish, D.J. and Jones, R.L., 1995. Rotational Raman scattering and the ring effect in Zenith-sky spectra. Geophysical Research Letters, 22(7): 811–814.

Galle, B.; Mellqvist, J., et al., Ground Based FTIR Measurements of Stratospheric Trace Species from Harestua, Norway during Sesame and Comparison with a 3-D Model, JAC, 1999, 32, no. 1, 147–164.

Galle, B., J. Samuelsson, B.H. Svensson, G. Börjesson, "Measurements of methane emissions from landfills using a time correlation tracer method based on FTIR absorption spectroscopy." Environ. Sci. Technol. 35: 21–25. 2001.

Galle, B., Oppenheimer, C., Geyer, A., McGonigle, A.J.S., Edmonds, M. and Horrocks, L., (2002), A miniaturised ultraviolet spectrometer for remote sensing of SO_2 fluxes: A new tool for volcano surveillance, Journal of Volcanology and Geothermal Research, 119 241–254

Gratien, A. et al (2007), UV and IR Absorption Cross-sections of HCHO, HCDO, and DCDO, J. Phys. Chem. A, 111, 11506–11513

Grenfell R.J.P., Milton M.J.T., Harling A.M., Vargha G.M., Brookes C., Quincey P.G., Woods P.T. (2010): Standard mixtures of ambient volatile organic compounds in synthetic and whole air with stable reference values, *J. Geophys. Res*, 115, D14302, doi:10.1029/2009JD012933

Griffith D.W.T., Synthetic calibration and quantitative analysis of gas-phase FT-IR spectra. Applied Spectroscopy, 1996. 50(1): p. 59–70.

Heckel, A., A. Richter, T. Tarsu, F. Wittrock, C. Hak, I. Pundt, W. Junkermann, and J.P. Burrows, MAX-DOAS measurements of formaldehyde in the Po-Valley, Atmospheric Chemistry and Physics, 5, 909–918, 2005.

Hermans, C.et al., Absorption cross-sections of atmospheric constituents: NO_2, O_2, and H_2O, Environ. Sci. Pollut. R. , 6, 151–158, 1999.

Hurley, P.J., Physick W.L., and Luhar A.K., TAPM: A practical approach to prognostic meteorological and air pollution modelling. Environmental Modelling and Software, 2005. 20(6): p. 737.

Johansson, M., C. et al, 2009, Mobile mini-DOAS measurement of the outflow of NO_2 and HCHO from Mexico City, Atmos. Chem. Phys., 9, 5647–5653

Johansson, J., et al., 2014a, Quantitative measurements and modeling of industrial formaldehyde emissions in the Greater Houston area during campaigns in 2009 and 2011, *J. Geophys. Res. Atmos.*, 119, doi:10.1002/2013JD020159.

Johansson, J., et al., 2014b, Emission measurements of alkenes, alkanes, SO_2, and NO_2 from stationary sources in Southeast Texas over a 5 year period using SOF and mobile DOAS, *J. Geophys. Res. Atmos.*, 119, doi:10.1002/2013JD020485.

Kihlman, M. (2005a), Application of solar FTIR spectroscopy for quantifying gas emissions, Technical report No. 4L, ISSN 1652-9103, Department of Radio and Space Science, Chalmers University of Technology, Gothenburg, Sweden.

Kihlman, M., J. Mellqvist, and J. Samuelsson (2005b), Monitoring of VOC emissions from three refineries in Sweden and the Oil harbor of Göteborg using the Solar Occultation Flux method, Technical report, ISSN 1653 333X, Department of Radio and Space, Chalmers University of Technology, Gothenburg, Sweden.

Koppmann R., Johnen F.J., Khedim A., Rudolph J., Wedel A., Wiards B. (1995): The influence of ozone on light nonmethane hydrocarbons during cryogenic preconcentration, *J. Geophys. Res.*, **100**, 11383–11391.

Leuchner M., Rappenglück B. (2010): VOC Source-Receptor Relationships in Houston during TexAQS-II, *Atmos. Environ.*, **44**, 4056–4067, doi:10.1016/j.atmosenv.2009.02.029

Mellqvist, J., Application of infrared and UV-visible remote sensing techniques for studying the stratosphere and for estimating anthropogenic emissions, doktorsavhandling, Chalmers tekniska högskola, Göteborg, Sweden, 1999a

Mellqvist, J och Galle, B., Utveckling av ett IR absorptionssystem användande solljus för mätning av diffusa kolväteemissioner, Rapport till Preems miljöstiftelse juli 1999b.

Mellqvist, J., Arlander, D. W., Galle, B. and Bergqvist, B., Measurements of Industrial Fugitive Emissions by the FTIR-Tracer Method (FTM), IVL report, 1995, B 1214.

Mellqvist, J., Flare testing using the SOF method at Borealis Polyethylene in the summer of 2000. 2001, Chalmers University of Technology. (Available at www.fluxsense.se)

Mellqvist, J., J. Samuelsson, C. Rivera, B. Lefer, and M. Patel (2007), Measurements of industrial emissions of VOCs, NH_3, NO_2 and SO_2 in Texas using the Solar Occultation Flux method and mobile DOAS, Project H053.2005, Texas Environmental Research Consortium., Texas. (http://www.harc.edu/projects/airquality/Projects/Projects/H053.2005)

Mellqvist, J.,Berg N. and Dan Ohlsson, 2008a, Remote surveillance of the sulfur content and NOx emissions of ships, Second international conference on Harbours, Air Quality and Climate Change (HAQCC), Rotterdam.

Mellqvist, J., Johansson, J.,Samuelsson, J., Rivera, C., Lefer, B. and S. Alvarez (2008b), Comparison of Solar Occultation Flux Measurements to the 2006 TCEQ Emission Inventory and Airborne Measurements for the TexAQS II, Project No. 582-5-64594-FY08-06 , TCEQ report., Texas. (available at http://www.tceq.state.tx.us/assets/public/implementation/air/am/contracts/reports/da/20081108-comparison_solar_occultation_flux_measurements.pdf)

Mellqvist, J., et al. (2009a), Emission Measurements of Volatile Organic Compounds with the SOF method in the Rotterdam Harbor 2008, available at www.fluxsense.se

Mellqvist, J., J. Samuelsson, J. Johansson, C. Rivera, B. Lefer, S. Alvarez, and J. Jolly (2010), Measurements of industrial emissions of alkenes in Texas using the solar occultation flux method, *J. Geophys. Res.*, 115, D00F17, doi:10.1029/2008JD011682.

Methven J., Arnold S.R., Stohl A., Evans M.J., Avery M., Law K., Lewis A.C., Monks P.S., Parrish D., Reeves C., Schlager H., Atlas E., Blake D., Coe H., Cohen R.C., Crosier J., Flocke F., Holloway J.S., Hopkins J.R., Hübler G., Lee J.D., Purvis R., Rappenglück B., Ryerson T.B., Sachse G.W., Singh H., Watson N., Whalley L., Williams P. (2006): Establishing Lagrangian connections between observations within air masses crossing the Atlantic during the International Consortium for Atmospheric Research on Transport and Transformation experiment, *J. Geophys. Res.*, 111, D23S62, doi:10.1029/2006JD007540

Plass-Dülmer C., Schmidbauer N., Slemr J., Slemr F., D'Souza H. (2006): The European Hydrocarbon Intercomparison Experiment AMOHA Part 4: Canister Sampling of Ambient Air, *J. Geophys. Res.*, 111, D4, D04306, doi:10.1029/2005JD006351

Platt, U., D. Perner, and H.W. Pätz, Simultaneous Measurement of Atmospheric CH_2O, O_3 and NO_2 by Differential Optical Absorption, Journal of Geophysical Research, 84 (C10), 6329–6335, 1979.

Rappenglück B., Schmitz R., Bauerfeind M., Cereceda-Balic F., v. Baer D., Jorquera H., Silva Y., Oyola P. (2005): An urban photochemistry study in Santiago de Chile, *Atmos. Environ.*, 39, 2913–2931, doi:10.1016/j.atmosenv.2004.12.049

Rappenglück B., Apel E., Bauerfeind M., Bottenheim J., Brickell P., Čavolka P., Cech J., Gatti L., Hakola H., Honzak J., Junek R., Martin D., Noone C., Plass-Dülmer Ch., Travers D., Wang T (2006): The first VOC intercalibration exercise within the Global Atmosphere Watch (GAW), *Atmos. Environ.*, 39, 2913–2931, doi:10.1016/j.atmosenv.2004.12.049

Rappengluck, B. et al, 2008a, Analysis of Primary vs. Secondary Fraction of Formaldehyde Houston Area During TexAQS-II, 10th Conference on Atmospheric Chemistry conference, The 88th Annual Meeting (20–24 January 2008), AMS,

Rappenglück, B et al, (2008b): In‐Situ Ground‐Based and Airborne Formaldehyde Measurements during the TRAMP Study; Atmos.Environ., submitted.

Rinsland, C. P., R. Zander, and P. Demoulin (1991), Ground-based infrared measurements of HNO3 total column abundances: long-term trend and variability, *J. Geophys. Res.*, *96*, 9379–9389.

Rivera, C. et al., (2010), Quantification of NO_2 and SO_2 emissions from the Houston Ship Channel and Texas City during the 2006 Texas Air Quality Study, J. Geophys. Res., 115, D08301, doi:10.1029/2009JD012675

Rivera , C., Application of Passive DOAS using Scattered Sunlight for quantification of gas emission from anthropogenic and volcanic sources (2009a), Doctoral Thesis, ISBN 978-91-7385-317-0, ISSN 0346

Rivera, C., J.A. Garcia, B. Galle, L. Alonso, Y. Zhang, M. Johansson, M. Matabuena, and G. Gangoiti (2009b), Validation of optical remote sensing measurement strategies applied to industrial gas emissions, Int. J. Remote Sens., vol 30, no 12, p3191–3204.

Rivera, C., et al. (2009c),Tula industrial complex (Mexico) emissions of SO_2 and NO_2 during the MCMA 2006 field campaign using a mobile mini_DOAS system, Atmos. Chem. Phys., 9, 6351–6361, 2009.

Rogers T.M. *et al.;*International Journal of mass Spectroscopy **252** 26-37 (2006)

Rothman et al. (2003), HITRAN 2000, Journal of Quantitative Spectroscopy and Radiative Transfer, vol. 82, pp. 5–44.

Ryerson, T. B., et al. (2003), Effect of petrochemical industrial emissions of reactive alkenes and NOx on tropospheric ozone formation in Houston, Texas, J. Geophys. Res., 108(D8), 549 4249, doi:10.1029/2002JD003070.

Samuelsson, J., Börjesson, G., Svensson, B., Galle, B., Metan från avfallsupplag i Sverige (Methane from landfills in Sweden), final report to the Swedish Energy Agency, projekt nr P10856-4, December 2005a. In Swedish (www.stem.se), can be ordered from Studsviksbiblioteket, 611 82 Nyköping, Sweden, www.lib.kth.se/SB/service/stemavf.html.

Samuelsson, J., et. al., VOC measurements of VOCs at Nynäshamn Refinery in Nynäshamn 2005b *(Utsläppsmätningar av flyktiga organiska kolväten vid Nynas Raffinaderi i Nynäshamn 2005, in Swedish)*, Bitumen refinery official report to provincial government 2005, Available at: http://www.fluxsense.se

Schürmann G., Schäfer K., Jahn C., Hoffmann H., Bauerfeind M., Fleuti E., Rappenglück B. (2007): The Impact of NO_x, CO and VOC Emissions on the Air Quality of the Airport Zurich, *Atmos. Environ.*, 41, 103–118, doi:10.1016/j.atmosenv.2006.07.030

Sharpe, S., et al. (2004), Gas-Phase Databases for Quantitative Infrared Spectroscopy, *Applied Optics*, *58*(12).

Slemr J., Slemr F., Partridge R., D´Souza H., Schmidbauer N. (2002): Accurate measurements of hydrocarbons in the atmosphere (AMOHA): three European intercomparisons, *J. Geophys. Res.*, 107, D19, 4409, doi:10.1029/2001JD001357

STARS, Emission inventory data extracted by John Jolly of the Texas Commission on Environmental Quality (TCEQ) from the TCEQ's State of Texas Air Reporting System (STARS) database, on Sept 28, Oct 3, and Oct 4, 2011.

Sullivan, D., et al, Oil and Gas Emissions in the DFW Region, University of Austin report , TCEQ Grant Activities No. 582-8-86245-FY09-03 , Jan , 2010

Taylor, B., and C. Kuyatt, 1994. "Guidelines for Evaluating and Expressing the Uncertainty of NIST Measurement Results." NIST Technical Note 1297 1994 edition. Gaithersburg, MD.

Thoma, E. et al. (2009), Development of EPA OTM 10 for Landfill Applications, in print, Journal of Environmental Engineering

Tucker, S., Marine boundary Layer dynamics and heights during TexAQS 2006: HRDL measurements from the RV Brown, Principal Findings Data Analysis Workshop TexAQS II, Austin, May 29–June 01, 2007. (available at www.tceq.state.tx.us)

URS Corporation, 2004. Passive FTIR Phase I Testing of Simulated and Controlled Flare Systems. Final report prepared for the Texas Commision on Environmental quality (TCEQ), 12100 Park 35 Circle, Austin, TX 78753

Vandaele A.C., C. Hermans, P.C. Simon, M. Carleer, R. Colin, S. Fally, M.F. Mérienne, A. Jenouvrier, and B. Coquart, Measurements of the NO_2 absorption cross-section from 42000 cm-1 to 10000 cm-1 (238–1000 nm) at 220 K and 294 K, J.Q.S.R.T., 59, 171–184 (1998)

Veillerot M., Locoge N., Galloo J.C., Guillermo R. (1998): Multidimensional capillary gas chromatography for the monitoring of individual non-methane hydrocarbons in air, *Analysis Magazine*, **26**, M38–M43.

Wagner, T., Apituley, A., Beirle, S., Dörner, S., Friess, U., Remmers, J., and Shaiganfar, R., Cloud detection and classification based on MAX-DOAS observations, Atmos. Meas. Tech., 7, 1289-1320, doi:10.5194/amt-7-1289-2014, 2014.

Walmsley, H. L., and S. J. O'Connor (1998), The accuracy and sensitivity of infrared differential absorption lidar measurements of hydrocarbon emissions from process units. *Pure Appl. Opt.*, *7*, 907–925.

Wert, B. P., et al. (2003), Signatures of terminal alkene oxidation in airborne formaldehyde 571 measurements during TexAQS 2000, J. Geophys. Res., 108(D3), 4104, doi:10.1029/2002JD002502, 2003.

Winkler J., Blank P., Glaser K., Habram M., Jambert C., Jaeschke W., Konrad S., Kurtenbach R., Lenschow P., Perros P., Pesch M., Prümke H.-J., Rappenglück B., Schmitz T., Slemr F., Volz-Thomas A. and Wickert B. (2002): Nonmethane hydrocarbon measurements in BERLIOZ: Characterization of the ground-based measurement sites and emission ratios derived from airborne measurements, *J. Atmos. Chem.*, 42, 465–492